Femtosecond laser induced periodic surface structures on metals and graphite: Fabrication of low reflective surface and SERS substrates

Thesis to be submitted for the degree of

DOCTOR OF PHILOSOPHY

BY

MUDASIR HASSAN DAR

13PHPH16

Under the joint supervision of

PROF. D. NARAYANA RAO

AND

DR. V. S. ASHOKA

School of Physics
University of Hyderabad
Hyderabad-500046, INDIA

February 2019

DECLARATION

I hereby declare that, this thesis titled "***Femtosecond laser induced periodic surface structures on metals and graphite: Fabrication of low reflective surface and SERS substrates***" is the result of investigation carried out by me in the school of physics, University of Hyderabad, India, under direct guidance and supervision of Prof. D. Narayana Rao and Dr. V. S. Ashoka. I also declare that it has not been submitted previously, in part or in full to this University or any other university or institution, for the award of any degree or diploma. I hereby agree that my thesis can be deposited in Shodhganga/INFLIBNET.

A report on plagiarism statistics from the University Librarian is enclosed.

Place: Hyderabad

Date:

Mudasir Hassan Dar
Reg. No.: 13PHPH16

CERTIFICATE

This is to certify that the thesis entitled "***Femtosecond laser induced periodic surface structures on metals and graphite: Fabrication of low reflective surface and SERS substrates***" submitted by Mudasir Hassan Dar, bearing registration number 13PHPH16, in partial fulfilment of the requirements for the award of Doctor of Philosophy in the School of Physics, is a bonafide work carried out by him under our supervision and guidance.

This thesis is free from plagiarism and has not been submitted previously in part or in full to this or any other University or Institution for award of any degree or diploma.

Further, the student has the following publications before the submission of the thesis for adjudication.

1. "Femtosecond laser nanostructuring of titanium metal towards fabrication of low-reflective surfaces over broad wavelength range", **Mudasir H. Dar**, R. Kuladeep, V. Saikiran, Narayana Rao D, Applied Surface Science 371 (2016) 479–487. (ISSN No: 0169-4332 (online)), Chapter-3.
2. "Ultrafast laser induced reproducible nano-gratings on molybdenum surface", **Mudasir H Dar**, Nabil A Saad, Chakradhar Sahoo, Sri Ram G Naraharisetty and Narayana Rao Desai, Laser Phys. Lett. 14 (2017) 026101. (ISSN print: 1612-2011, ISSN electronic: 1612-202X), Chapter-4.
3. "Femtosecond laser induced nanostructuring of graphite for the fabrication of quasi-periodic nanogratings and novel carbon nanostructures", V. Saikiran, **Mudasir H. Dar**, D. Narayana Rao, Applied Surface Science 428 (2018) 177–185. (ISSN No: 0169-4332 (online)), Chapter-6
4. "Ultrafast laser induced periodic sub-wavelength aluminum surface structures and nanoparticles in air and liquids", Rajamudili Kuladeep, **Mudasir H. Dar**, K. L. N. Deepak, and D. Narayana Rao, Journal of Applied Physics 116, 113107 (2014). (ISSN No: 1089-7550 (online)).

Further, the student has passed the following courses towards fulfilment of coursework requirement for Ph.D:

Course Code	Name of the Course	Credits	Pass/Fail
PY801	Advanced Quantum Mechanics	4	Pass
PY803	Advanced Statistical Mechanics	4	Pass
PY804	Advanced Electromagnetic Theory	4	Pass
PY821	Research Methodology	4	Pass

Prof. D. Narayana Rao
Thesis Supervisor
School of Physics
University of Hyderabad

Bindu A. Bambah
Dean
School of Physics
University of Hyderabad

Dr. V. S. Ashoka
Co-Supervisor
School of Physics
University of Hyderabad

Date:

Acknowledgements

First of all, thanks to Allah for showering his countless blessing on me throughout my life. I take this opportunity to thank my thesis supervisor Prof. D. Narayana Rao for allowing me to work in his research group. His constant support, encouragement and invaluable suggestions have helped me to grow in research. He is an inspiration for me. I would like to thank my thesis co-supervisor Dr. V. S. Ashoka for his help during my research years.

I thank the Dean, school of physics, for providing different facilities in the school. I would like to thank my DRC members for their valuable suggestions in DRC meetings. The support provided by the non-teaching staff in the school is highly appreciable. Thanks are due to Sunitha for her help in characterization of the samples.

Financial assistance, in the form of Junior Research Fellowship from Department of science and technology (DST) through ITPAR project is greatly acknowledged.

I would like to thank all my lab seniors Dr. Jhoti, Dr. Kuladeep, Dr. Saikiran, Dr. Sreeramulu, Dr. Ramya for their constant support and helpful discussions. Special thanks to my present lab members Nabil, Sahoo, Shihab, Tahir, and others for maintaining healthy atmosphere in the lab. I am grateful to my friends Waseem, Mushtaq, Srinivas, Suadat, Abid, Shivarama, Robertson, Bilal, Amin. I thank my colleagues Muzamil, Dr. Riyaz, Gazanfar, Dr. Firdous, Prof. Shakeel, Prof. Jala-ud-din.

I am grateful to all my teachers, who build my carrier, High school teachers Mr. Lokinder garu, Mr. Fakhre-Alam garu, Mr. Prasad garu, Mr. Anwar garu, Mr. Zaidi garu. B.Sc teachers- Prof. Mohd. Aslam Baba, Prof. Maqsood Ahmad. M. Phil Teachers Dr. Alok Sharan, Dr. S.V.M. Sathyanarayana.

The most important, I would like to thank all my family members and relatives for their support and guidance throughout my life. The prayers of my mother and unconditional love and support from brothers and cousins made my work easy. I shall all the time remain obliged to them for their support. I am indebted to my beloved father late Gh Hassan Dar (*Rahimahullah*) for teaching me two invaluable things in life- spirituality and hard work.

Mudasir

"*You can't go back and change the beginning, but you can start where you are and change the ending*" – C. S. Lewis.

Contents

CHAPTER -1

Introduction

Abstract

This chapter describes the basics of "laser direct writing (LDW)" technique and its technological perspective. LDW technique exploits nonlinear absorption processes to create embedded and/or surface structures virtually on any material. Fundamental process of femtosecond laser-matter interaction is explained. Role of pulse duration (nanosecond and femtosecond pulses) towards material processing is briefly discussed. We also discuss the formation of periodic surface structures and their historical aspect. "Laser induced periodic surface structures (LIPSS)" were written on different metals to observe the variations in periodicity in the gratings and the effect of surface plasmon bands. Choice of different metals too has been discussed.

1.1 General Introduction

Interaction of laser light can create micro- and nanoscale features on the surface of a solid material, leading to novel applications. When the first laser was built in 1960 [1], the scientific community described it as "The solution looking for a problem". Some of the extra-ordinary features of laser light are- it is highly coherent, can be focused into small area, small divergence, variable interaction time (pulsed laser with different pulse duration). Lasers have been put to use in various fields such as nano-science and technology, medicine, research, industry etc. In the field of material processing, ultrafast lasers (pulse duration < 10^{-12}s) have been used for bulk as well as surface processing, using a very simple and versatile technique- Laser Direct Writing (LDW). The basic principal is that- a laser beam is focused on the surface or inside the bulk of the material, to induce structural modification through nonlinear absorption processes. These nonlinear processes can be exploited to locally change the refractive index of the transparent material in order to create the sub-surface optical waveguide structures and 3D embedded structures [2-4]. It is possible to fabricate arbitrary waveguides within the volume of the material by simply focusing the laser beam inside the volume and translating the sample in any arbitrary direction. The size of the inscribed structures can be controlled by optimizing the laser parameters like pulse energy, repetition rate and period of the pulse. Since the refractive index is modified by nonlinear absorption processes, the size of inscribed structures can be below the diffraction limit [5].

The absorption of radiation by a material is defined by its dielectric function. Depending upon the incident energy, the photons can couple to the available electronic states through inter-band transitions, such as in semiconductors and insulators. In case of metals, having large number of free electrons, the absorption takes place through inverse bremsstrahlung process [6]. After the excitation takes place, the excited electrons transfer their energy to the lattice and thermal equilibrium is established in the system. The time it takes for the system to thermalize, depends upon the material properties and the process by which thermalization takes place. The thermalization time for metals is typically few tens of picoseconds (ps) [7]. The distance over which the temperature changes, during the laser irradiation, in the time defined by the pulse duration, is called thermal diffusion length. The heat affected zone (HAZ) is defined as the region, over which these temperature changes

occur. Material processing using femtosecond (fs) lasers is highly efficient (precise machining), because pulse width is shorter than relaxation time. This reduces HAZ in the laser irradiated region [8]. Thus, the material processing with fs laser pulses reduce the HAZ, leading to high precision processing as compared to nanosecond (ns) and longer pulses. The ns or longer pulses are incapable of micromachining precisely due to the significant melting in the HAZ during the length of the laser pulse. The ns pulse duration corresponds to lower peak powers as compared to fs laser pulse. The ns laser ablates the material by thermal processes, creating a large HAZ and leaving behind defects such as cracks and fragments. Femtosecond lasers deliver very high intensities in the focal spot size, of upto 10^{20} W cm^{-2}. Even at lower intensities of about 10^{14} W cm^{-2}, interesting phenomena take place that have both technological importance as well as effects that require good amount of fundamental research. During the interaction of fs laser pulse, the electrons can reach a local temperature of few thousands of Kelvin while as the lattice remains almost undisturbed. However, the temperature of lattice can rise rapidly during the relaxation of electrons, throwing the material into an unstable non-equilibrium state, leading to ejection of material. Therefore, a large part of absorbed energy is released during the ejection of the material, leading to smooth surface processing. This feature of precise material processing using fs lasers, improves the spatial resolution compared to the nanoscale processing, allowing ultrafast lasers to control and modify the material properties [9]. Focused fs laser beam inside the volume of a transparent material induces structural modifications through nonlinear absorption processes [10-11].

Material processing using ultrafast lasers, through LDW technique, is an important method for fabricating complex three dimensional (3D) micro-fluidic structures in substrates [12]. Fabricating 3D micro-fluidic structures is realized by a two-step process- LDW followed by etching with acid such as hydrofluoric acid. LDW technique with fs lasers, is used to fabricate different micro-optical components inside glass such as waveguides, optical couplers, micro-mirrors, Fresnel zone plates, volume Bragg gratings and binary data storage devices. Another technique that utilizes ultra-short laser pulses for the fabrication of 3D micro- and nanostructures is the two-photon polymerization (2PP) technique [13-15]. In this process, ultra-short laser pulses in the fs range initiate two-photon absorption and subsequent polymerization in the localized focal volume, thereby, resulting in the formation of 3D micro- and nano-scale structures [16].

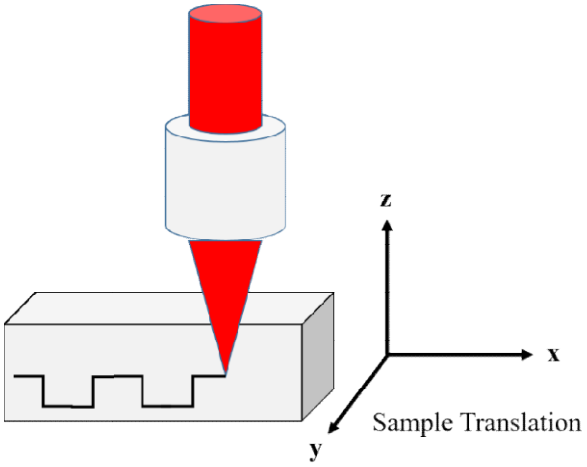

Figure 1: Schematic of LDW inside a transparent material.

Figure (1) shows the typical experimental scheme of LDW. Incident laser beam is focused on the surface of the material or deep inside. This technique can be exploited for the desired structure formation either by translating the incident laser beam or by moving the sample. Formation of periodic structures on solids, more generally known as "laser induced periodic surface structures (LIPSS)" or ripples, have been demonstrated on variety of materials like semiconductors [17-21], metals [22-29], dielectrics [30-35] and polymers [36-39] during laser irradiation. The LIPSS are characterized by the period Λ. In general, there are two types of ripples that develop during laser irradiation with wavelength λ. The ripples for which $0.4 < \Lambda/\lambda < 1$ are defined as near sub-wavelength ripples or "low spatial frequency LIPSS (LSFL)", and the ripples for which $\Lambda/\lambda < 0.4$ are defined as deep sub-wavelength ripples, also known as "high spatial frequency LIPSS (HSFL)". The formation mechanism of these ripples is usually explained by the interference phenomena, between the incident wave and the excited surface electromagnetic wave [40-43].

1.2 Femtosecond laser-matter interaction: Fundamental processes.

To remove an electron from the atom, the energy must be supplied in excess of the binding energy of that atom. When a fs laser pulse irradiates the solid surface, absorption of laser energy takes place. In metals, having large number of free electrons, the absorption process is dominated by free electrons. Free electrons below the Fermi level absorb energy

and move above the Fermi level. The intraband absorption mechanism can be described by Drude's approach [44].

$$\in(\omega) = \epsilon_c - \frac{\omega_p^2}{\omega(\omega + i\Gamma)}$$

where ϵ_c is the dielectric constant of un-irradiated material, $\omega_p = \sqrt{n_e e^2 / m_e \epsilon_0}$, the plasma frequency, determined by the density of free electrons n_e and their effective mass m_e and $\Gamma = 1/\tau$ is the electron collision frequency. Γ often taken as constant in the range of 10^{15} Hz, corresponding to the collision time in the fs range. However, Γ depends upon material parameters which change during fs laser irradiation. Interband absorption may take place in some polyvalent metals like aluminum [45]. The absorption mechanism becomes more complicated in noble metals in which d band and s band energetically coincide. Such transitions cannot be explained in the frame work of Drude model and hence need more advanced approaches [46]. In semiconductors, electrons are excited to conduction band, by absorption of photons, whose energy is greater than the band gap. During fs laser irradiation, the semiconductors change their optical properties and turn into a metallic state [47]. The absorption of laser light by free electrons can then be described by Drude formalism. In case of dielectrics, the laser light is absorbed only through nonlinear processes. Under intense fs laser irradiation, the dielectric function becomes negative and they behave as metals with high free electron density. The primary process in the laser irradiation of materials is the excitation of electrons from the equilibrium state. The excited electronic states relax through different secondary processes that eventually lead to the structural modification of the material. Structural modification using longer laser pulses with tens of picosecond pulse duration are thermal in nature and involve non-radiative relaxation processes. The energy deposition under fs-laser pulse irradiation occur in time scale shorter than any relaxation process. Hence, under fs-laser irradiation, the excited electrons and cold lattice are not in thermal equilibrium in the time duration of the pulse. Two-temperature model is generally used to explain the temperature dynamics before thermal equilibrium sets in [48, 49]. For a 100 fs laser pulse irradiation, the intensity required for the ablation of the material is 10^{13}-10^{14} W/cm^2, however, for the same material the intensity required for ablation under a 100 ns pulse is about 10^8-10^9

W/cm^2 [50]. Practically any material ionizes under fs-laser pulse irradiation of intensity 10^{13}-10^{14} W/cm^2.

1.3 Brief overview of LIPSS formation

LIPSS also known as ripples, consisting of alternate grooves and ridges, were first observed in 1965 by Birnbaum [51] on single crystal germanium surface irradiated by focused ruby laser beam. In 1973 D. C. Emmony et al observed LIPSS on germanium surface and attributed their formation to the interference of laser beam with the scattered wave [52]. Keilmann and Bai proposed that LIPSS formation takes place by the interference of incident radiation with the excited surface plasmon polaritons (SPPs) propagating along the interface [53]. Sipe and co-workers introduced the terminology LIPSS. They experimentally and theoretically analyzed the interaction of incident electromagnetic wave with the microscopically rough sample [54, 55]. They introduced the term efficacy factor (η) which represents the inhomogeneous energy distribution on a microscopically rough surface. The formation of LIPSS with period significantly smaller than the irradiating wavelength, also known as HSFL, were analyzed and explained through different mechanism [56]. Nevertheless, the formation of LIPSS on different materials gives rise to the changes in the surface properties of these materials. This leads to several applications of LIPSS. One of the applications of LIPSS is that the formed periodic structures act as diffraction gratings. The gratings generate different colors under white light illumination depending upon the periodicity of gratings and angle of incidence. Femtosecond laser induced nano-structuring can significantly change the optical properties of the metal surface [57, 58]. The control on the generation of color by LIPSS on different materials can be used for various applications like laser marking, optical data storage and decoration [59]. In addition to the changes in the optical properties of the surface under fs-laser irradiation, wetting properties of the LIPSS covered surface also change [60-63]. LIPSS formation on materials especially titanium and its alloys also show biological applications. Biological cells are grown along the length of LIPSS on titanium based materials [64, 65]. There is a correlation between the size of the LIPSS and cell spreading. LIPSS covered titanium based alloys also find applications in dental implants to increase their life span [66]. Besides many other applications, nano-structured surfaces

have been demonstrated to enhance Surface Enhanced Raman Scattering (SERS) signal by few orders of magnitude [67, 68].

1.4 Aim of the thesis

In this thesis we have used fs LDW technique to study the development of LIPSS on different metals like Ti, Mo, Ni, Fe, Ag, and Cu. We have chosen six different metals for our studies. Mo and Ti being paramagnetic in character, Ni and Fe belong to the class of ferromagnetic materials, while as Ag and Cu fall in the domain of diamagnetic materials. We started our studies with an aim, whether the magnetic character of the metals has a role in the LIPSS formation. The aim of this thesis is to achieve the control on the formation of LIPSS and their periodicity by varying parameters such as fluence, pulse number, polarization, surrounding medium, and incident laser wavelength. Based on SPP model, we calculated the SPP decay lengths for the metals under investigation. We discuss the formation of highly regular LIPSS on Mo, Ti, Fe, and Ni under 800 nm laser irradiation. Surface texturing of titanium changes the optical properties of the Ti surface. The spectral measurements show that laser processing of Ti surface greatly reduce the absolute and specular reflectance over the entire studied wavelength of 250 nm-1.8 μm as compared to the un-irradiated Ti surface. This has tremendous applications in sensitive detection systems. We have also carried out fs laser irradiation of graphite in ambient water. TEM measurements show the formation of graphene flakes and other carbon nanostructures in the form of colloids. We also record the enhancement of SERS due to colloidal solution of Graphene Quantum Dots (GQDs).

1.5 Plan of the Thesis

Chapter 1: We discuss the fs LDW technique, which we used for surface processing of different materials. We also discuss the effect of long pulse and ultrashort pulse duration on material processing. Historical perspective of LIPSS formation is also discussed.

Chapter 2: This chapter is devoted to the illustration of different experimental techniques used. Femtosecond laser direct writing setup is discussed thoroughly. Brief introduction is given about the general characterization techniques used such as FESEM, TEM, Micro-Raman spectrometer, and reflectivity measurement.

Chapter 3: In this chapter we have made a detailed study of interaction of femtosecond laser pulses with mechanically polished titanium surface, evolution of nanostructures in ambient environments of air and water. We discuss the effect of number of irradiated pulses (N), fluence (F), polarization of the incident laser pulse, surrounding dielectric medium and incident laser wavelength (λ) on the formation of periodic structures. We observed the formation of HSFL in the lower fluence regime. The HSFL can develop either parallel or orthogonal to the incident laser polarization at near normal incidence. LSFL formation is observed in the higher fluence regime. The LSFL are always oriented perpendicular to the incident laser polarization. In ambient water environment the feature size of the formed nanostructures is as small as ~λ/15 and orientated parallel to the incident laser polarization direction.

Chapter 4: This chapter describes the formation of LIPSS on different metals at 800 nm laser irradiation in ambient air and water environments. We investigated the effect of different experimental parameters on LIPSS formation. Interestingly, out of all the metals studied in this chapter, Mo shows smooth and highly regular periodic surface structure formation. However, metals like silver and copper don't show the formation of periodic structures at 800 nm irradiation in ambient air environment. The metals with large SPP decay length, doesn't sustain coherence and hence don't show the formation of regular periodic structures. The important feature observed, is the formation of nano-ripples with periodicity as small as ~λ/40 and oriented parallel to the laser polarization direction, on Mo surface in water environment.

Chapter 5: We have made an attempt to look into the applications of laser induced surface pattering. We studied the effect of nano- and micro structuring on the reflectivity of titanium surface. Spectral measurements show that laser induced surface structuring greatly suppress the absolute reflectance as well as the specular reflectance of titanium surface over the entire studied wavelength range of 250 nm-1.8 μm.

Chapter 6: Here we studied the effect of fs-laser irradiation on graphite surface in ambient air and water environments. We discuss the formation of Deep sub-wavelength nanogratings oriented orthogonal to the incident laser polarization direction. We also discuss the effect of laser irradiation on the Raman peaks of graphite, formation of graphene quantum

dots (QGDs) and carbon nanostructures under fs laser irradiation of graphite in ambient water environment.

Chapter 7: Summarizes the results and discuss the future perspective.

1.6 References

1. T. H. Maiman, Nature, 187, 493–494 (1960).
2. Somnath Ghosh, Nicholas D. Psaila, R. R. Thomson, Bishnu P. Pal, R. K. Varshney, and Ajoy K. Kar, Applied Physics Letters 100, 101102 1-4 (2012).
3. Roberto Osellame, Mirko Lobino, Nicola Chiodo, Marco Marangoni, Giulio Cerullo, Roberta Ramponi, Henry T. Bookey, Robert R. Thomson, Nicholas D. Psaila, and Ajoy K. Kar, Applied Physics Letters 90, 241107 1-3 (2007).
4. K. Miura, Jianrong Qiu, H. Inouye, T. Mitsuyu, and K. Hirao, Applied Physics Letters 71, 3329-3331 (1997).
5. Fadhil A. Umran, Yang Liao, Mazin M. Elias, Koji Sugioka, Razvan Stoian, Guanghua Cheng, and Ya Cheng, Optics Express, 21, 15259-15267 (2013).
6. B.N. Chichkov, C. Momma, S. Nolte, F. von Alvensleben, and A. Tunnermann, Appl. Phys.A Mater. Sci. Process. 63, 109-115 (1996).
7. D. Bauerle, Laser Processing and Chemistry (Springer, Berlin, 2000).
8. Carsten Momma, Boris N. Chichkov, Stefan Nolte, Ferdinand von Alvensleben, Andreas Tiinnermann, Herbert Welling, and Bernd Wellegehausen, Optics Communications 129, 134- I42 (1996).
9. Yoshiki Nakata, Tatsuo Okada, and Mitsuo Maeda, Applied Physics Letters 81, 4239-4241 (2002).
10. S. Kuper, and M. Stuke, Appl. Phys. Lett. 54, 4-6 (1989).
11. S. Kuper, and M. Stuke, Microelectron Eng. 9, 475-480 (1989).
12. Koji Sugioka and Ya Cheng, “Femtosecond Laser 3D Micromachining for Microfluidic and Optofluidic Applications” (Springer, 2012)
13. Shoji Maruo, Osamu Nakamura, and Satoshi Kawata, Optics Letters, 22, 132-134 (1997).
14. Brian H. Cumpston, Sundaravel P. Ananthavel, Stephen Barlow, Daniel L. Dyer, Jeffrey E. Ehrlich, Lael L. Erskine, Ahmed A. Heikal, Stephen M. Kuebler, I.Y. Sandy Lee, Dianne McCord-Maughon, Jinqui Qin, Harald Rockel, Mariacristina Rumi,

Xiang-Li Wu, Seth R. Marder and Joseph W. Perry, Letters to Nature, 398, 51-54 (1999).

15. Hong-Bo Sun, Shigeki Matsuo, and Hiroaki Misawa, Applied Physics Letters 74, 786-788 (1999).
16. Kotaro Obata, Ayman El-Tamer, Lothar Koch, Ulf Hinze and Boris N Chichkov, Light: Science and applications, 2, 1-4 (2013).
17. R. Kuladeep, C. Sahoo, and D. Narayana Rao, Applied Physics Letters 104, 1-4 (2014).
18. G. Miyaji, K. Miyazaki, K. Zhang, T. Yoshifuji, and J. Fujita, Optics Express 20 14848-14856 (2012).
19. G. D. Tsibidis, M. Barberoglou, P. A. Loukakos, E. Stratakis, and C. Fotakis, Physical Review B 86, 1-14 (2012).
20. R. Le Harzic, H. Schuck, D. Sauer, T. Anhut, I. Riemann, K. König, Opt. Express 13 (2005)6651–6656.
21. A. Borowiec, H.K. Haugen, Applied Physics Letters 82 (2003) 4462–4464.
22. E. V. Golosov, A. A. Ionin, Yu. R. Kolobov, S. I. Kudryashov, A. E. Ligachev, Yu. N. Novoselov, L. V. Seleznev, and D. V. Sinitsyn, Journal of Experimental and Theoretical Physics 113, 14-26 (2011).
23. Mudasir H Dar, Kuladeep R, Saikiran V and Narayana Rao D, Applied Surface Science 371 479-487 (2016).
24. Xian-Feng Li, Cheng-Yun Zhang, Hui Li, Qiao-Feng Dai, Sheng Lan, and Shao-Long Tie, Optics Express 22, 28086-28099 (2014).
25. L. Qi, K. Nishii, Y. Namba, Opt. Lett. 34 (2009) 1846–1848.
26. S. Sakabe, M. Hashida, S. Tokita, S. Namba, K. Okamuro, Phys. Rev. B: Condens. Matter 79 (2009) 033409.
27. M.S. Ahsan, Y.G. Kim, M.S. Lee, J. Laser Micro/Nanoeng. 7 (2012) 164–170.
28. J.P. Colombier, F. Garrelie, N. Faure, S. Reynaud, M. Bounhalli, E. Audouard, R. Stoian, F. Pigeon, J. Appl. Phys. 111 (2012) 024902.
29. S.R.J. Brueck, D.J. Ehrlich, Phys. Rev.Lett. 48 (1982) 1678–1681.
30. Y. Shimotsuma, P. G. Kazansky, J. Qiu, and K. Hirao, Physical Review Letters 91, 1-4 (2003).

31. Y. Yuan, L. Jiang, X. Li, C. Wang, H. Xiao, Y. Lu, and H. Tsai, Journal of Physics D: Applied Physics 45, 1-6 (2012).
32. V.R. Bhardwaj, E. Simova, P.P. Rajeev, C. Hnatovsky, R.S. Taylor, D.M. Rayner, P.B. Corkum, Phys. Rev. Lett. 96 (2006) 057404.
33. M.S. Ahsan, M.S. Lee, J. Laser Micro/Nanoeng. 7 (2012) 202–207.
34. C. Hnatovsky, R.S. Taylor, P.P. Rajeev, E. Simova, V.R. Bhardwai, D.M. Rayner,P.B. Corkum, Appl. Phys. Lett. 87 (1) (2005) 014104
35. M. Rohloff, S.K. Das, S. Höhm, R. Grunwald, A. Rosenfeld, J. Krüger, J. Bonse, J. Appl. Phys. 110 (1) (2011) 014910.
36. Susana Perez, Esther Rebollar, Mohamed Oujja, Margarita Martin, and Marta Castillejo Appl. Phys A, 110, 683-690 (2013).
37. V.T. Rathod, D. Roy Mahapatra, Anjana Jain , A. Gayathri, Sensors and Actuators A 163 (2010) 164–171.
38. Esther Rebollar, Mikel Sanz, Susana Perez, Margarita Hernandez, Ignacio Martin-Fabiani, Daniel R. Rueda, Tiberio A. Ezquerra, Concepcion Domingo and Marta Castillejo, Phys. Chem. Chem. Phys., 2012, 14, 15699–15705.
39. Marta Castillejo, Tiberio A. Ezquerra, Margarita Martin, Mohamed Oujja, Susana Perez, and Esther Rebollar, AIP Conf. Proc. 1464, 372 (2012).
40. J. E. Sipe, J. F. Young, J. S. Preston, and H. M. van Driel, Physical Review B 27, 1141–1154 (1983).
41. M. Huang, F. Zhao, Y. Cheng, N. Xu and Z. Xu, ACS Nano 3, 4062–4070 (2009).
42. G. Miyaji and K. Miyazaki, Opt. Express 16, 16265–16271 (2008).
43. J. Bonse, A. Rosenfeld, and J. Krger, J. Appl. Phys. 106, 104910 (2009).
44. Fox M, Optical Properties of Solids 2 edition (Oxford University Press) 2010.
45. Ehrenreich H, Philipp H R and Segall B, Phys. Rev. 132 1918–28 (1963).
46. Sun C-K, Vallée F, Acioli L H, Ippen E P and Fujimoto J G, , Phys. Rev. B 50 15337–44 (1994).
47. Callan J P, Kim A M-T, Roeser C A D and Mazur E, Phys. Rev. B 64 073201 (2001).
48. Chichkov B.N, Momma C, Nolte S, Von Alvensleben F, Tunnermann A, Appl. Phys. A 63, 109–115 (1996).
49. Anisimov S.I, Kapeliov B.L, Perelman T.L, Zh. Eksp. Teor. Fiz.,66, 776–781 (1974).

50. B.C. Stuart, M. D. Feit, A. M. Rubenchik, B.W. Shore, and M. D. Perry, 74, 2248 – 2251 (1995).
51. Birnbaum M, J. Appl. Phys., 36, 3688–3689 (1965).
52. D. C. Emmony, R. P. Howson, and L. J. Willis, Appl. Phys. Lett., 23, 598–600 (1973).
53. F. Keilmann and Y. H. Bai, Appl. Phys. A, 29, 9–18 (1982).
54. J. F. Young, J. S. Preston, H. M. van Driel, and J. E. Sipe, Phys. Rev. B, 27, 1155–1172, (1983).
55. J. F. Young, J. E. Sipe, and H. M. van Driel, Phys. Rev. B, 30, 2001–2015, (1984).
56. J. Reif, O. Varlamova, S. Varlamov, and M. Bestehorn, Appl. Phys. A, 104, 969–973 (2011).
57. A. Y. Vorobyev and C. Guo, Applied Physics Letters 92, 1-3 (2008).
58. Stratakis E, Zorba V, Barberoglou M,Fotakis C, and Shafeev G, Nanotechnology,20, 105303 (2009).
59. B. Dusser, Z. Sagan, H. Soder, N. Faure, J.P. Colombier, M. Jourlin and E. Audouard, Optics Express, 18, 2913 – 2924 (2010).
60. Zorba V, Persano L, Pisignano D, Athanassiou A, Stratakis E, Cingolani R, Tzanetakis P, and Fotakis C, Nanotechnology, 17, 3234–3238 (2006).
61. Baldacchini T, Carey J.E, Zhou M, and Mazur E. Langmuir, 22, 4917–4919 (2006).
62. Vorobyev A.Y. and Guo C, Laserturns silicon superwicking. Opt. Express,18, 6455–6460 (2010).
63. Vorobyev A.Y. and Guo C. Water sprints uphill on glass. J. Appl. Phys.,108, 123512 (2010).
64. Vorobyev A.Y. and Guo C, Proc. SPIE, 7203, 720300 (2009).
65. Brunette D.M, Tengvall P, Textor M, and Thomsen P, Springer, Berlin (2001).
66. A.Y. Vorobyev, and Chunlei Guo, Applied Surface Science, 253, 7272–7280 (2007).
67. Cheng-Hsiang Lin, Lan Jiang, Yen-Hsin Chai, Hai Xiao, Shean-Jen Chen1, and Hai-Lung Tsai, Optics Express, 17, 21581 – 21589 (2009).
68. V. Saikiran, Mudasir H Dar, R. Kuladeep and Narayana Rao Desai, http://journals.cambridge.org/abstract_S2059852116004680

CHAPTER – 2

Experimental setup and theoretical background

Abstract

In this chapter, we discuss the experimental layout used to carry out the femtosecond (fs) laser direct writing studies. We used femtosecond laser system (Oscillator-Amplifier Ti:Sapphire) at fundamental wavelength of 800 nm, for the surface modification. FESEM (Field Emission Scanning Electron Microscopy) is used for the characterization of the surface morphology after laser irradiation. Other characterization techniques are also briefly discussed in this chapter. We also discuss some theoretical insights about the formation of LIPSS.

2.1 Laser direct writing experimental setup

The experimental design used for the surface processing of different materials towards fabricating periodic surface structures consists of fs laser system, three nano-positioning stages, and optics for beam steering, energy control and polarization control. The fs laser source consists of a mode locked Ti:Sapphire oscillator (Mai Tai) and a regenerative amplifier (Spitfire). Mai Tai delivers a seed pulse of 1 nJ energy, 80 fs pulse duration, and 82 MHz repetition rate. The regenerative amplifier which contains the Ti:Sappire rod is pumped by Nd:YLF laser (Evolution). This pump laser delivers high power laser pulses of 532 nm wavelength, 120 ns pulse duration and 1 kHz repetition rate. The amplification takes place through chirped pulse amplification (CPA) technique. The seed pulse from Mai Tai is stretched to about ~200 picoseconds (ps). These temporally stretched pulses are then amplified in regenerative amplifier cavity, to achieve desired amplification [1]. Once the desired amplified pulse is obtained, the pulses are compressed to obtain pulses of ~ 100 fs pulse duration, 1 mJ average pulse energy at a repetition rate of 1 kHz. The output is a beam of about 9 mm diameter with central wavelength of 800 nm. Table 1 summarizes the output characteristics of the femtosecond laser system.

Particulars	**Mai Tai**	**Spitfire**
Pulse duration	82 fs	100 fs
Output pulse energy	1 nJ	1 mJ
Repetition rate	80 MHz	1 kHz
Beam diameter	3 mm	9 mm
Polarization	Horizontal	Horizontal

Table 1 Output characteristics of femtosecond laser system [2]

The laser direct experiments were carried out on a nano-positioning stage purchased from Newport, USA having horizontal and vertical adjustments with 15 nm resolution. The laser beam is incident normal to the sample surface. The laser beam is focused by a lens of focal length 5 cm (for large area nano-structuring) or by a microscopic objective with a numerical aperture of 0.25. Laser energy is controlled by using neutral density filters and a variable attenuator- which is a combination of half wave plate and polarizer. The polarizer

also controls the polarization of the incident laser pulses. The schematic diagram of the experimental setup is shown in figure (1). Laser direct writing in ambient water environment was carried out by immersing the sample in water. In all experiments incident laser beam is fixed and perpendicular to the sample surface, while the sample is scanned in horizontal direction.

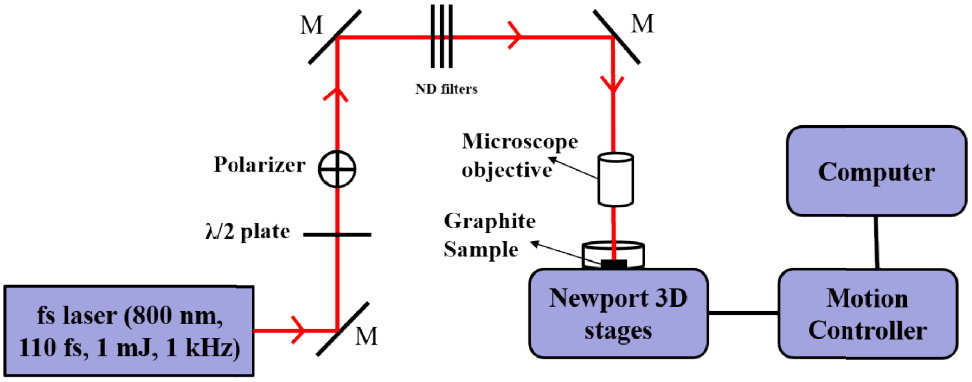

Figure 1: Experimental layout of laser direct writing technique using fs laser system.

2.2 Field emission scanning electron microscopy (FESEM)

The FESEM uses a focused electron beam that scans the sample surface and generates an image of the sample. When the focused electron beam hits the sample, the interaction process gives rise to two types of electron beams- secondary electrons (SEs) and backscattered electrons (BSEs). Specific detectors detect these signals and create an image and give information about the sample properties. Secondary electrons have low energy (less than 50 eV) and are ejected from the outer atomic shell of the sample and carry information about the surface topography. The backscattered electrons have energy greater than 50 eV and are generated by elastic scattering and carry the depth information.

The scanning electron microscopy technique is used to reveal the detailed information about the surface morphology and chemical composition of the sample. We used Zeiss Ultra-55 field emission SEM to investigate the surface morphology of the laser irradiated sample. This machine provides 1nm SEM imaging resolution. The machine is operated at an accelerating voltage of 5-10 kV.

2.3 Transmission Electron Microscopy (TEM)

TEM works on the same principle as that of light microscope. However, TEM uses electron beam instead of a light beam. The advantage is that electrons have much lower wavelength compared to light, thereby getting the resolution of several orders better than light microscope. The electron beam passes through the sample under investigation. The un-scattered electrons that pass through the specimen hit the fluorescent screen producing the shadow image with different parts displayed in varied darkness as per the density of different parts of the sample. For our TEM imaging we used TEM "(model: Tecnai 20 G2, STwin, FEI electron microscope operated at 20 kV using Gatan CCD camera)".

2.4 Reflectance measurements

We have carried the spectral reflectance measurements using JASCO ARN-731 spectrometer having wavelength range of 250 – 1800 nm. This is designed to measure the absolute reflectance of a specularly reflecting sample. This attachment consists of a detector with 60 mm-diameter integrating sphere and PbS photoconductive cell. The angle of incidence of the beam on the sample can be set by moving the position of the detector. The absolute reflectance of the sample can be measured because optical path from the center of rotation to the detector is same as that from the sample to the detector. We also recorded the relative reflectance of the sample using the reflected light from an aluminum deposited plane mirror as a reference. This was recorded with SLM-736, specular reflectance accessory available with the JASCO spectrometer.

2.5 Micro-Raman: HR 800 Horiba JobinYvon spectrometer with a charge coupled device detector has been used for the micro-Raman scattering measurements with the 633 nm as excitation wavelength.

2.6 Theoretical background

The formation of LIPSS is a common phenomena observed in almost all materials including metals, semiconductors, dielectrics and polymers [3-13]. The LIPSS appear in two forms, LSFL and HSFL, depending upon their periodicity [14, 15]. In literature LSFL are defined as ripples/nanogratings with grating period (Λ) in the range of $0.4\lambda < \Lambda < \lambda$, while HSFL are defined as ripples with period (Λ) in the range of $\Lambda < 0.4\lambda$ [3, 14], λ being the

incident laser wavelength. It is commonly accepted that, the formation mechanism of LSFL occur via the excitation of SPP and their interference with the incident laser pulse. This interaction leads to the periodic distribution of energy on the surface of the irradiated material [16-20]. We discuss the development of periodic structures during fs laser irradiation in the backdrop of SPP model. SPP is an electromagnetic excitation which propagates on a planar metal/dielectric interface. During fs laser pulse irradiation, high density of free electrons is launched on the surface of the material. The photons can couple to the oscillating electrons, thereby, giving rise to SPP. The SPP amplitude decays exponentially in the perpendicular direction into each medium from the interface [16]. The dispersion curve of SPP lies to the right of light line i.e., the free space photon wave-vector is smaller than the SPP wave vector. Hence, in order for a photon to couple to the surface plasmon, necessary momentum must be provided to the photon in the coupling direction [23]. In our experiments, this coupling is provided by the surface roughness and subsequently by the nascent grating structure so formed.

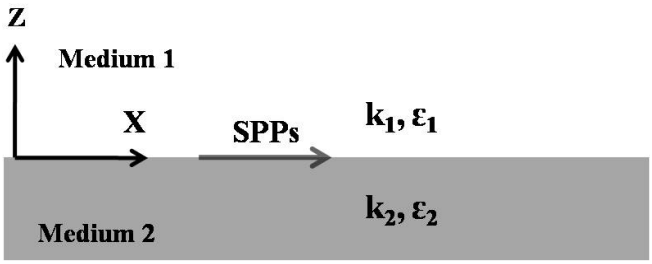

Figure 2: Interface between medium 1 and 2 at which surface Plasmon polaritons are considered.

We consider the planner interface separating two media (figure 2), at which surface plasmon polaritons are excited by the incident laser radiation. The complex dielectric permitivities are $\in_1$ and $\in_2$ and corresponding wave vectors normal to the surface are k_1 and k_2

At the interface, conservation of momentum results in the condition

$$k_{1,2}^2 = \beta^2 - k_0^2 \epsilon_{1,2} \qquad (1)$$

Where β is the SPP wavenumber, $k_0 = \frac{\omega}{c}$, the wavenumber of the incident light, ω is light angular frequency and c velocity of light in vaccum.

The boundary condition at the interface results in the equation [16, 21-23]

$$\frac{k_1}{\epsilon_1}+\frac{k_2}{\epsilon_2}=0 \quad (2)$$

This equation represents the dispersion relation of SPP at the interface.

Combining equations (1) and (2) gives the surface plasmon polariton wave number

$$\beta=\pm\frac{\omega}{c}\sqrt{\frac{\epsilon_1\epsilon_2}{\epsilon_1+\epsilon_2}} \quad (3)$$

The complex dielectric permitivities can be written as

$$\epsilon_1=\epsilon_1^{'}+i\,\epsilon_1^{''}$$

$$\epsilon_2=\epsilon_2^{'}+i\,\epsilon_2^{''}\} \quad (4)$$

Taking the positive value of equation (3) and using equation (4)

$$\beta=\frac{\omega}{c}\sqrt{\frac{(\epsilon_1^{'}+i\epsilon_1^{''})(\epsilon_2^{'}+i\epsilon_2^{''})}{(\epsilon_1^{'}+i\epsilon_1^{''})+(\epsilon_2^{'}+i\epsilon_2^{''})}} \quad (5)$$

$$\beta=\frac{\omega}{c}\sqrt{\frac{\{(\epsilon_1^{'}+i\,\epsilon_1^{''})(\epsilon_2^{'}+i\,\epsilon_2^{''})\}}{\{(\epsilon_1^{'}+i\,\epsilon_1^{''})+(\epsilon_2^{'}+i\,\epsilon_2^{''})\}}\frac{\{(\epsilon_1^{'}+i\,\epsilon_1^{''})-(\epsilon_2^{'}+i\,\epsilon_2^{''})\}}{\{(\epsilon_1^{'}+i\,\epsilon_1^{''})-(\epsilon_2^{'}+i\,\epsilon_2^{''})\}}}$$

$$\beta=\frac{\omega}{c}\sqrt{\frac{A+iB}{D}} \quad (6)$$

With

$$A=\epsilon_1^{'}\left(\epsilon_2^{'\,2}+\epsilon_2^{''\,2}\right)+\epsilon_2^{'}\left(\epsilon_1^{'\,2}+\epsilon_1^{''\,2}\right)$$

$$B=\epsilon_1^{''}\left(\epsilon_2^{'\,2}+\epsilon_2^{''\,2}\right)+\epsilon_2^{''}\left(\epsilon_1^{'\,2}+\epsilon_1^{''\,2}\right)$$

$$D=(\epsilon_1^{'}+\epsilon_2^{'})^2+(\epsilon_1^{''}+\epsilon_2^{''})^2$$

Solving equation (6) for real and imaginary parts we get

$$\mathscr{R}e(\beta)=\frac{\omega}{c\sqrt{2D}}\sqrt{A+\sqrt{A^2+B^2}} \quad (7)$$

$$Im(\beta) = \frac{\omega}{c\sqrt{2D}}\sqrt{\sqrt{A^2 + B^2} - A} \quad (8)$$

The SPP propagation length or mean free path is given by [32]

$$L_{SPP} = \frac{1}{2 \times Im(\beta)} \quad (9)$$

The spatial period Λ_{SPP} of the modulated electromagnetic field occurring from the interference of the incident laser light with excited SPP is predicted from the real part of SPP wave number as [22-26]:

$$\Lambda_{SPP} = \frac{2\pi}{\Re e(\beta)} \quad (10)$$

Interface	$\Re e(\in_{sample})$	$Im(\in_{sample})$	$Im(\beta)$ (x 10^3 /m)	Thermal conductivity (W/m K)	L_{SPP} (μm)
air/Ti	-2.85	19.12	157	22	3.2
air/Ni	-13.04	21.73	106	90	4.7
air/Ag	-29.7	0.98	3.56	427	140.4
air/Cu	-25.7	1.22	5.95	394	84.0
air/Mo	2.08	29.52	122	140	4.1
air/Fe	-6.38	20.19	139	80	3.6
water/Ti			369		1.3
water/Ni			260		1.9
water/Ag			8.65		56.2
water/Cu			15.4		33.4
water/Mo			284		1.8
water/Fe			331		1.5

Table 2: Theoretically calculated decay length of the SPPs excited on the air-metal and water-metal interface upon laser irradiation at 800 nm, the real and imaginary parts of the dielectric permittivity is taken from [27-29].

This model gives us some insights, on the formation of LIPSS and how the regularity is related with the decay length of the SPPs excited on the air-metal or water-metal interface. With the approximation that optical properties of the metal doesn't change much under laser irradiation, the regularity of LIPSS is linked and modeled through the decay length of SPP excited on the surface of irradiated metal. The dielectric function of a metal changes during fs

laser irradiation period. Using the dielectric constant of metals taken from the literature [27-29], the SPP decay lengths at the air-metal and water-metal interface under laser irradiation is summarized in table 2 for different metal/dielectric interfaces. We observed that materials with SPP decay lengths smaller than ~ 5 μm exhibit highly regular LIPSS formation. We also notice that the materials with absolute value of imaginary part greater than the absolute value of real part exhibit highest regularity of LIPSS formation. Two groups of metals can be identified based on mean free path of SPPs: (i) Metals with high optical damping, and small SPP decay length in the range of 1 to 5 μm, exhibit highly regular LIPSS at 800 nm laser irradiation. This includes metals like Ti, Mo, Ni, and Fe. (ii) Metals like Ag, Cu; with SPP mean free path longer than 5 μm exhibit low regularity LIPSS at 800 nm fs laser irradiation.

The occurrence of highly regular LIPSS on some metals upon laser irradiation can be explained on the basis of coherence of surface electromagnetic wave generated on the interface. The SPPs can be initiated by any sub-wavelength structure such as nanoparticles, sample roughness, point defects present on the surface [30, 31]. The metals having large mean free path, the SPP loses its initial coherence while propagating to long distances and interacting with different scattering centers. For the metals with small decay lengths of SPPs, the surface electromagnetic wave can preserve its initial coherence, forming a detailed periodic energy distribution pattern within the beam spot size. Our experimental observations show that metals with small SPP mean free path allow for better periodicity as against the metals having large SPP mean free path. We discuss our experimental results supporting this model in chapter 4.

2.7 References

1. Spectra-Physics Inc. operation manuals for *Mai-Tai*™ and *Spitfire*™.
2. V. N. Lugovoi and A. A. Manenkov Laser Physics. 15, 1269 (2005).
3. Iaroslav Gnilitskyi, Thibault J.Y. Derrien, Yoann Levy, Nadezhda M. Bulgakova , Tomas Mocek & Leonardo Orazi, Scientific Reports, 7, 8485 (2017).
4. P. Gregorcic et al., Appl. Surf. Sci. 387 (2016) 698–706.
5. C. Albu et al., Appl. Surf. Sci. 278 (2013) 347–351.
6. B. Tan, K. Venkatakrishnan, J. Micromech. Microeng. 16 (5) (2006) 1080–1085.
7. T.Q. Jia et al., Phys. Rev. B. 72 (12) (2005).

8. X. Ji et al., Appl. Surf. Sci. 326 (2015) 216–221.
9. Esther Rebollar, Mikel Sanz, Susana Perez, Margarita Hernandez, Ignacio Martin-Fabiani, Daniel R. Rueda, Tiberio A. Ezquerra, Concepcion Domingo and Marta Castillejo, Phys. Chem. Chem. Phys., 2012, 14, 15699–15705.
10. Marta Castillejo, Tiberio A. Ezquerra, Margarita Martin, Mohamed Oujja, Susana Perez, and Esther Rebollar, AIP Conf. Proc. 1464, 372 (2012).
11. Susana Perez, Esther Rebollar, Mohamed Oujja, Margarita Martín, and Marta Castillejo, Appl Phys A (2013) 110:683–690.
12. C. Hnatovsky, R.S. Taylor, P.P. Rajeev, E. Simova, V.R. Bhardwai, D.M. Rayner,P.B. Corkum, Appl. Phys. Lett. 87 (1) (2005) 014104
13. M. Rohloff, S.K. Das, S. Höhm, R. Grunwald, A. Rosenfeld, J. Krüger, J. Bonse, J. Appl. Phys. 110 (1) (2011) 014910.
14. M. Huang, F. Zhao, Y. Cheng, N. Xu, Z. Xu, ACS Nano 3 (2009) 4062–4070.
15. J Bonse, J., Hohm, S., Kirner, S. V., Rosenfeld, A. & Kruger, J. IEEE J. Select Topic Quant. Electron. 23 (3) (2017).
16. A. V. Zayats, I. I. Smolyaninovb, A. A. Maradudinc, Physics Reports 408, 131 (2005).
17. Sipe, J. E., Young, J. F., Preston, J. & Driel, H. V. *Phys. Rev. B* 27, 1141–1154 (1983).
18. Bonse, J., Rosenfeld, A. & Krüger, J. *J. Appl. Phys.* 106, 104910 (2009).
19. Garrelie, F. *et al*. *Opt. Express* 19, 9035–9043 (2011).
20. Derrien, T. J.-Y. *et al*. *Opt. Express* 24, 29643–29655 (2013).
21. Derrien, T. J.-Y., Itina, T. E., Torres, R., Sarnet, T. & Sentis, M. *J. Appl. Phys.* 114, 083104 (2013).
22. Maier S A 2007 Plasmonics, Fundamentals and Applications (Berlin: Springer).
23. Raether H 1986 Surface Plasmons on Smooth and Rough Surfaces and on Gratings (Berlin: Springer).
24. Derrien, T. J.-Y., Krüger, J. & Bonse, J. *J. Opt.* 18, 115007 (2016).
25. Bell, R. J., Alexander, R. W., Parks, W. F. & Kovener, G. *Opt. Commun.* 8, 147–150 (1973).
26. Ionin, A. *et al*. *Appl. Surf. Sci.* 292, 678–681 (2014).

27. Johnson, P. B. & Christy, R.-W. *Phys. Rev. B* 6, 4370–4379 (1972).
28. Ordal, M. A., Bell, R. J., Alexander, R. W., Newquist, L. A. & Querry, M. R. *Appl. Opt.* 27, 1203–1209 (1988).
29. Palik, E. D. *Handbook of Optical Constants of Solids* (Academic Press, 1985).
30. Shimizu, H., Yada, S., Obara, G. & Terakawa, M. *Opt. Express* 22, 17990–17998 (2014).
31. Barnes, W., Dereux, A. & Ebbesen, T. *Nature* 424, 824–830 (2003).
32. Andreas Hohenau, Aurelien Drezet, Matthias Weibenbacher, Franz R. Aussenegg, and Joachim R. Krenn, Physical Review B 78, 155405 (2008).

CHAPTER- 3

Investigation of sub-wavelength nanogratings on titanium surface formed during fs laser irradiation

Abstract

Here, we have studied the interaction of fs laser pulses with mechanically polished titanium surface, evolution of nanostructures in ambient air and water environments. The formation of LIPSS depends upon many factors such as pulse number, fluence, polarization, surrounding dielectric medium and incident laser wavelength. We observed the formation of HSFL in the low fluence regime. The HSFL develop either parallel or perpendicular to the incident laser polarization at near normal incidence. LSFL formation is observed in the higher fluence regime. The LSFL always develop perpendicular to the incident laser polarization. In ambient water environment, the feature size of the formed nanostructures is as small as ~λ/15 and orientated parallel to the polarization direction.

3.1 Introduction

Ultrafast laser-material interaction has been studied extensively in the past [1-4]. The periodic patterns that appear on the surface of a solid material after irradiation with certain number of laser pulses are commonly known as LIPSS [5-6]. LIPSS develop on different materials (metals, semiconductors and dielectrics) upon fs laser irradiation [7-74]. LIPSS composed of periodic or quasi-periodic surface relief features exhibit a strong dependence on incident laser wavelength and polarization. LIPSS formed during laser irradiation have various technological applications. The nanostructures formed can be used to control optical, mechanical and chemical properties of the surface.

Titanium (Ti) is a group IV transition metal, atomic number 22. The metallic Ti exhibits outstanding physical and chemical properties. Ti has excellent chemical resistance, very good fatigue strength, high melting point, crack propagation resistance, fracture toughness, highest weight-to-strength ratio compared to other metals, thereby, making it an attractive metal in biological, industrial and aerospace applications [24, 32, 49]. Femtosecond LDW technique is used to alter the material's surface properties. For example, micro and nanostructuring induced by fs laser pulses has led to the creation of materials with novel properties such as, antireflection coatings [31,35,48-50,71], colorization of metals [30], microfluidic channels [1, 3], hydrophilic−hydrophobic surfaces [24,29,52], friction control [73], and biomedical applications including reduced or enhanced cell adhesion [76-78]. Other applications include SERS effect [79], enhanced photodiode performance [80, 81], data storage [82] and X-ray generation [83].

There are numerous studies on the formation of periodic structures on the surface of Ti metal and its alloys [23-26, 32, 60, 76-79]. In this chapter, we have used LDW experimental setup to study the formation of periodic ripples on Ti surface in ambient air and de-ionized water environments under fs laser irradiation at near normal incidence. We have discussed the effect of laser parameters like fluence, number of incident pulses, wavelength, polarization and surrounding dielectric medium. We have discussed the formation of LSFL oriented orthogonal to the incident laser polarization direction and HSFL oriented parallel to the incident laser polarization direction.

3.2 Experimental procedure

Commercially available Ti wafers were used for carrying out laser direct writing experiments. Ti wafer is cut into 1cm^2 samples, mechanically polished using emery paper of grit size 80-1500. Prior to laser irradiation, the samples were sonicated in acetone for 5 minutes to remove any debris. In all our LDW experiments, the incident laser beam is fixed and incident normal to the sample, while the sample is translated. The writing was performed transverse to the direction of laser incidence. We utilized three computer controlled nano-positioning stages (Newport, USA), to translate the sample in the X, Y and Z directions. In scanning mode, the number of pulses *N* can be controlled by changing the scanning speed of the corresponding axis. The actual laser fluence at the sample surface was estimated by taking into account all the reflection losses. After laser irradiation, the samples are again sonicated in acetone to remove any loosely bound particles. After LDW experiments, detailed surface morphological characterization of the Ti sample was performed by Zeiss Ultra-55 high resolution field emission scanning electron microscope (FESEM). The FESEM instrument is operated at an accelerating voltage of 5-10 kV.

3.3 LIPSS on titanium surface under fs laser irradiation at normal incidence:

3.3.1 Effect of pulse number (N): Effect of pulse number on the formation and evolution of periodic nanostructures is carried out by translating the sample in orthogonal direction to the incident laser beam at varying scanning speeds. Figure (1) shows the morphological evolution of titanium surface after irradiation with fs laser at 800 nm wavelength in ambient air. We observed the formation of LSFL, with spatial periodicity (Λ) smaller than the incident laser wavelength (λ). The LSFL develop orthogonal to the incident laser polarization direction. At a constant laser fluence (F) of F = 0.24 J/cm^2, we studied the effect of scanning speed (number of pulses) on the formation and evolution of periodic structures. It is observed that initially first few fs laser pulses make the surface rough in the form of nanoparticles and nanocavities. The surface roughness develops into extended periodic structures with increase in the number of laser pulses. At the scanning speed of 0.8 mm/s (N = 5 pulses), it leads to the formation of random nanostructures as shown in figure 1 (a). The nano-roughness created on the metal surface by the first few pulses, can couple the free space laser light to SPPs [63].

The interference between the laser light and the excited SPPs causes a periodic spatial modulation of the energy deposition into the irradiated region. Decreasing the scanning speed to 0.6 mm/s (~7 pulses), we observed the initial traces of the formation of periodic structures within the laser irradiation spot, as shown in figure 1(b). These nascent periodic structures so formed, give rise to efficient coupling of laser light to SPPs. We

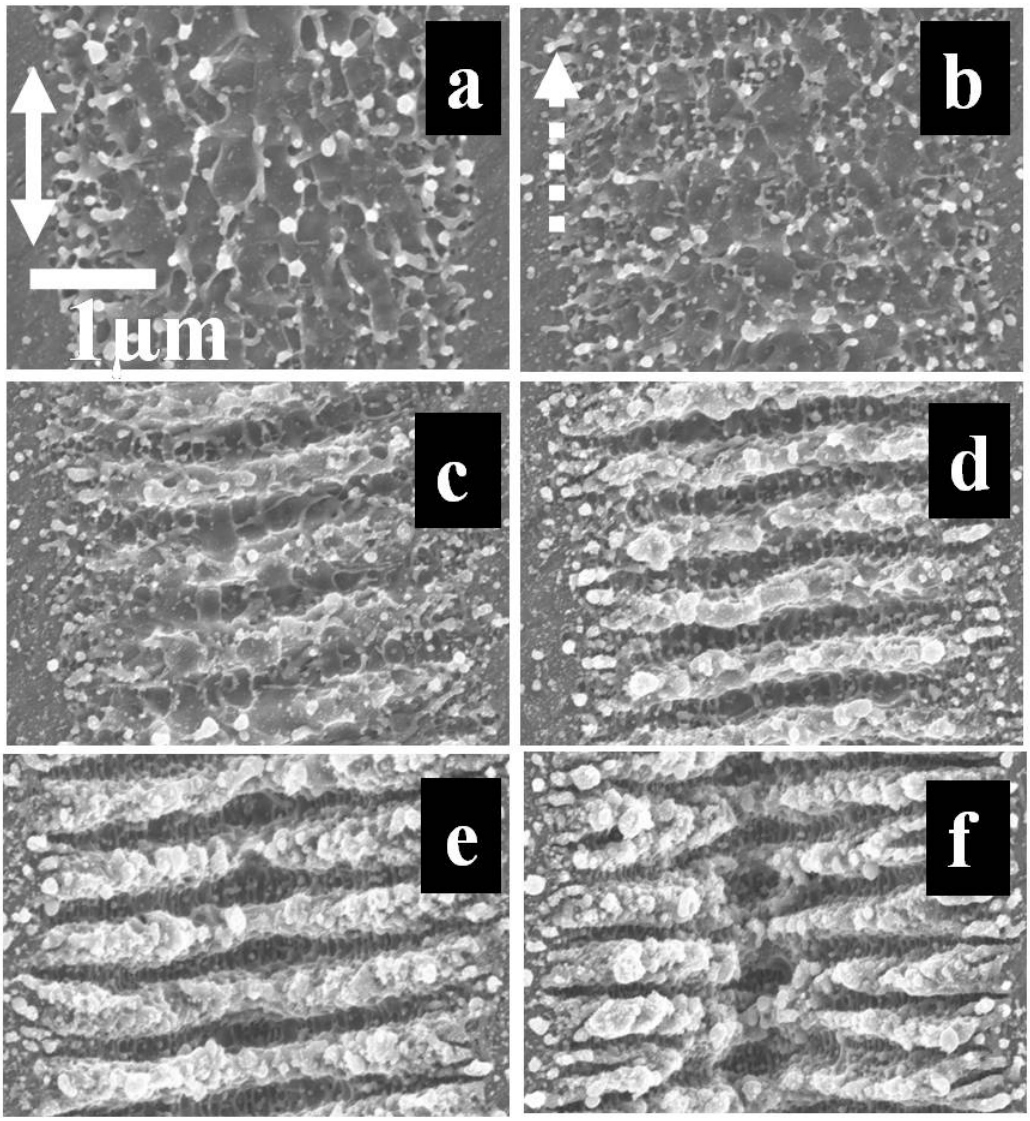

Figure 1: FESEM images show surface morphology evolved after fs laser irradiation of titanium surface in ambient air at a constant fluence of 0.24 J/cm^2. The scanning speeds are (a) 0.8 mm/s, (b) 0.6 mm/s, (c) 0.4 mm/s and (d) 0.2 mm/s, (e) 0.1 mm/s, and (f) 0.05 mm/s. Double headed arrow represents the laser polarization and dotted single headed arrow indicates the writing direction (for all). Incident wavelength is 800 nm. The scale shown in (a) is same for all.

observed the formation of LSFL when the sample is translated at a scanning speed of 0.4 mm/s (~10 pulses) as shown in the figure 1(c). The grating assisted coupling further modulates the energy deposition that leads to the formation of clear extended LIPSS at the scanning speed of 0.2 mm/s (~ 20 pulses) as shown in figure 1(d). The periodic structures continue to deepen by decreasing the scanning speed. Figure 1(e) shows the LSFL formation at the scanning speed of 0.1 mm/s (~ 40 pulses). With further decreasing the scanning speed to 0.05 mm/s (~ 80 pulses), the periodic structures gradually start to disappear from the central spot area as shown in figure 1(f). With further decrease in the scanning speed, there is not any formation of periodic structures and the material is completely removed from the ablated region.

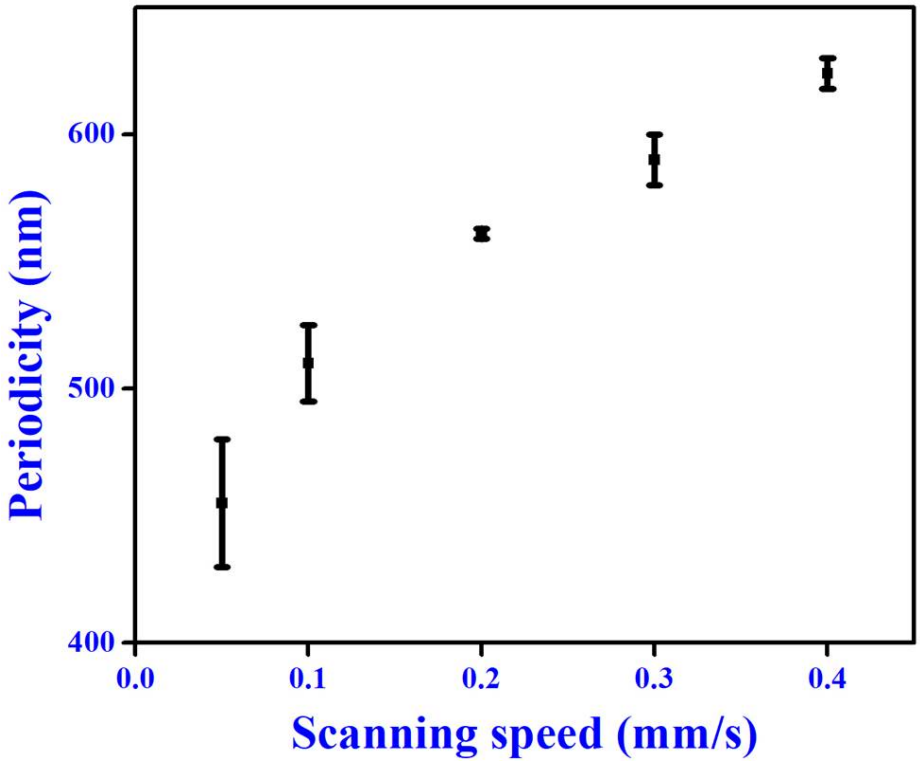

Figure 2: Shows the variation of LSFL periodicity with scanning speed (pulse number) at a constant fluence of 0.24 J/cm^2.

We observed that, at a constant fluence of 0.24 J/cm^2, periodicity of LSFL decreases from 625±10 nm to 455±25 nm with decrease in the scanning speed or increase in the number of pulses as shown in figure (2).

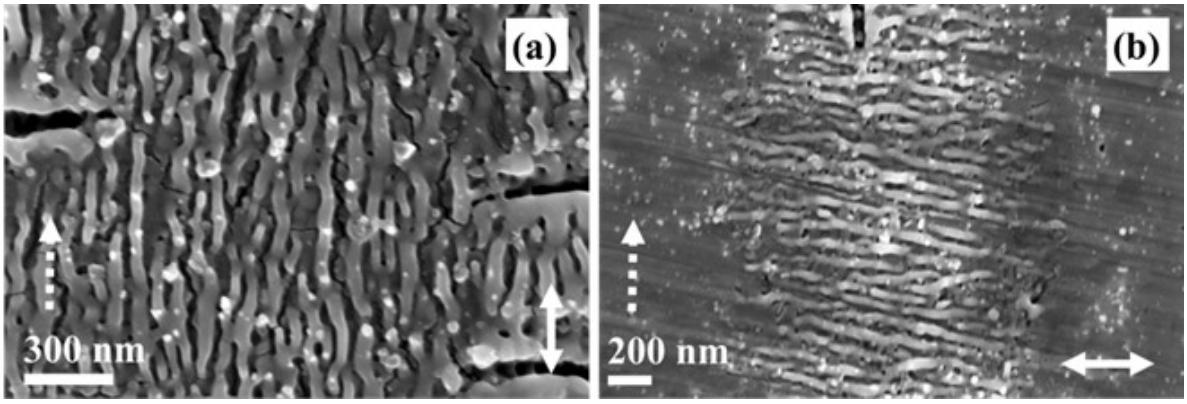

Figure 3 Morphological evolution of HSFL on Ti surface during fs laser irradiation. The fluence is 0.11 J/cm^2 and scanning speed 0.05 mm/s (~100 pulses). Double headed arrow represents the incident laser polarization and single headed dashed arrow represents the writing direction. Incident wavelength is 800 nm and Ti is irradiated in ambient air environment.

3.3.2 Effect of fluence (F): We observed the formation of HSFL oriented parallel to the laser polarization direction, at a very low fluence range of 0.06-0.12 J/cm^2, under fs laser irradiation at 800 nm wavelength in ambient air environment as shown in figure (3). By changing the incident laser polarization direction, the HSFL ripples also change and get oriented along the laser polarization direction as shown in figure 3(a) and 3(b). The spatial periodicity of HSFL ripples is found to increase from 60±15 nm to 90±20 nm as a function of fluence as shown in figure (4). The period of HSFL remains same within the error bar, in the given fluence regime. The laser fluence above this range results in the formation of LSFL ripples, which appear perpendicular to the laser polarization direction. The periodicity of LSFL is observed to decrease from 625±20 nm to 580±15 nm with increase in the fluence under 800 nm fs laser irradiation, as shown in figure (5). The scanning speed (pulse number) is constant at 0.2 mm/s (~20 pulses).

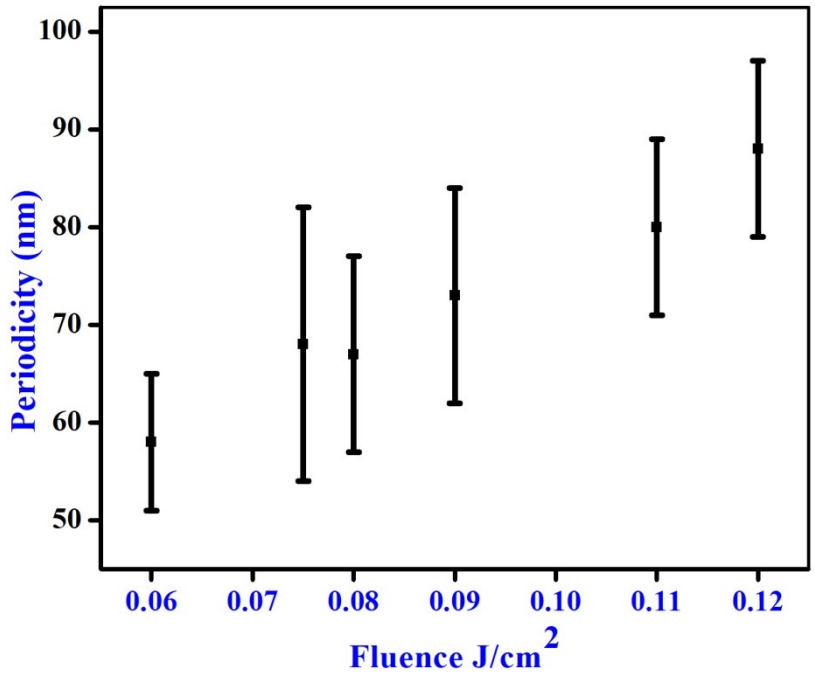

Figure 4: Variation of HSFL period with fluence at a constant scanning speed of 0.05 mm/s (~100 pulses)

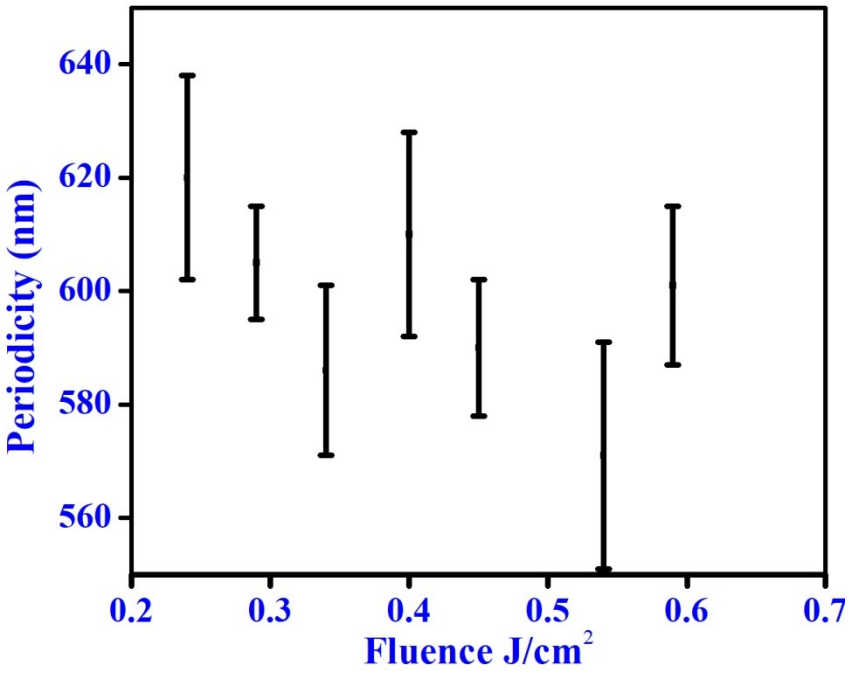

Figure 5: Variation of LSFL period with fluence at a constant scanning speed (pulse number) of 0.2 mm/s (~20 pulses).

3.3.3 Effect of surrounding medium: We study the effect of liquid environment on the LIPSS formation on Ti surface under fs laser irradiation at 800 nm wavelength. Laser direct writing pertaining to fs laser interaction with Ti surface in ambient liquid environment is carried out by immersing the sample in de-ionized water. Water is preferred, as it is most commonly used during machining and also because of its biocompatibility. The water level was ~ 2 mm above the sample surface. Figure (6) shows the surface topography of Ti evolved after laser irradiation in water, at a constant fluence of 0.23 J/cm^2. Figure 6(a) shows the morphology of the Ti surface evolved after irradiating with fs laser pulses at a scanning speed of 0.7 mm/s. We observed the formation of nano-roughness in the form of nano-cavities and spherical nano-droplets. With increase in the number of pulses or decrease in the scanning speed, the nano-roughness gets periodically structured. We observed that two types of sub-wavelength structures develop simultaneously in the laser irradiated area, as shown in figure 6(b). The structures formed orthogonal to the incident laser polarization have a spatial

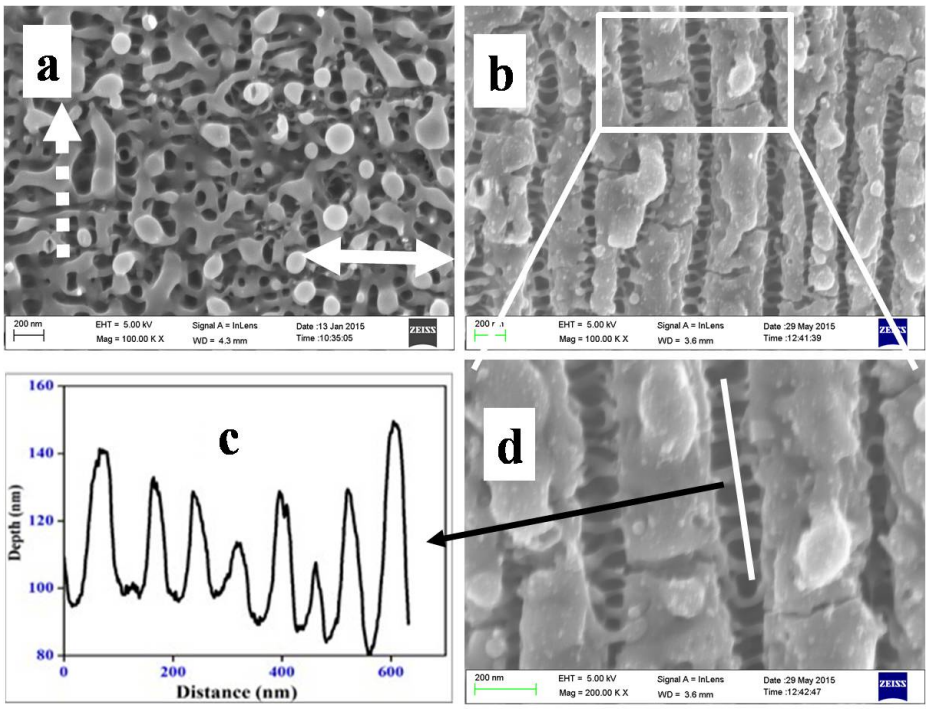

Figure 6 Evolution of surface morphology of Ti laser irradiated in water, as a function of scanning speed (number of pulses) at a constant fluence of 0.23 J/cm^2. The scanning speeds are (a) 0.7 mm/s, (b) 0.3 mm/s. Fig (d) is the magnified image of the portion marked by rectangle in fig (b). Fig(c) shows line profile of HSFL features (representing the periodicity). Double headed arrow indicates the incident laser polarization and dotted single headed arrow indicates the writing direction (for all).

periodicity of 230±20 nm and are thus assigned as HSFL. Another type of HSFL features appear parallel to incident laser polarization and are formed in the grooves of orthogonal HSFL structures as shown in the magnified image 6(d). The line profile in figure 6(c) shows the periodicity of these structures to be 80±15 nm.

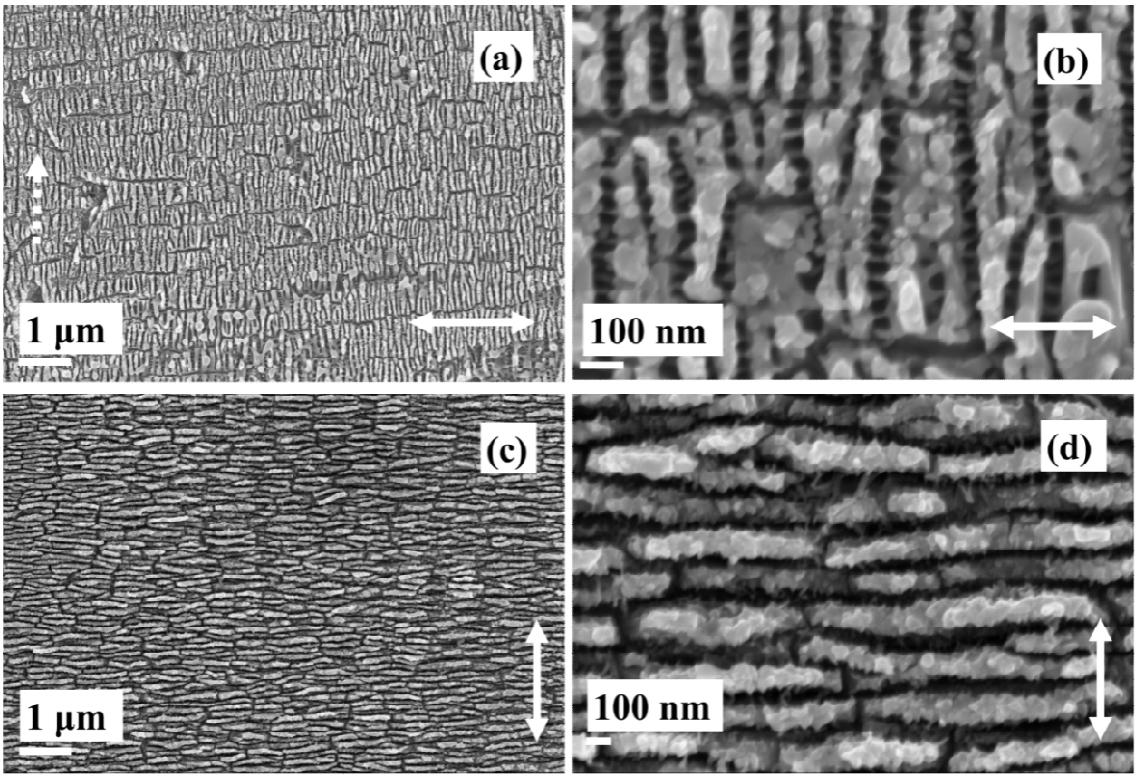

Figure 7: Polarization dependence of LIPSS formed on Ti surface after fs laser irradiation at 800 nm wavelength in water environment, at laser fluence of 0.19 J/cm^2. The sample is translated with scanning speed of (a) 0.1 mm/s and (c) 0.05 mm/s. Figures (b) and (d) are magnified images of (a) and (c) respectively. Double headed solid arrow represents the incident laser polarization and single headed dashed arrow indicates the writing direction (for all).

We observed polarization dependence of LIPSS formed during laser irradiation of Ti in water. Figure (7) shows the surface morphology of the Ti after laser irradiation, at the laser fluence of 0.19 J/cm^2. Figure 7(a) shows the FESEM image of Ti surface fabricated by fs laser irradiation at the scanning speed of 0.1 mm/s. The incident laser polarization is orthogonal to the scanning direction. As the incident laser polarization is flipped along the scanning direction, the LIPSS also get oriented perpendicular to the polarization. Figure 7(c) shows the surface topography evolved after fs laser irradiation, sample being translated at the scanning speed of 0.05 mm/s, the incident laser polarization is along the scanning direction. Magnified images of 7(a) and 7(c) are shown by figures of 7(b) and 7(d) respectively. we

observed two types of sub-wavelength structures in water around this fluence, one oriented perpendicular to laser polarization direction with periodicity of ~120±20 nm, and the other formed between the grooves and oriented parallel to the laser polarization direction corresponding to periodicity of ~50±15 nm.

3.3.4 Effect of polarization:

We observed that LSFL are always oriented orthogonal to the polarization. Figure (8) shows the effect of incident laser polarization, on the formation of periodic structures in ambient air environment. The incident laser fluence is 0.32 J/cm^2 and number of incident pulses ~ 20. Figure 8(a) shows the formation of periodic structures, when the polarization is orthogonal to the writing direction, the average periodicity observed is 520 ±20 nm. Figure 8(b) shows the evolution of periodic structures, when the polarization is parallel to the writing direction, the average periodicity is 560 ±10 nm.

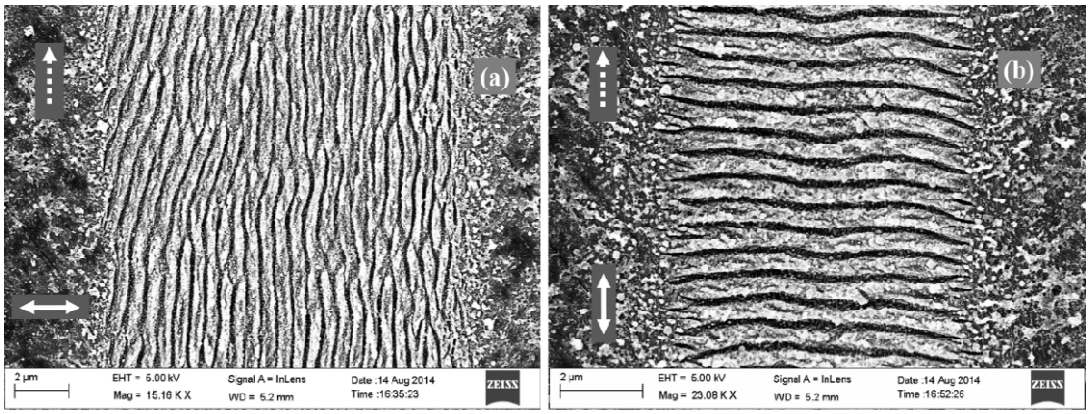

Figure 8: Shows the effect of incident laser polarization on the formation of LSFL at a constant fluence of 0.32 J/cm^2 and pulse number ~20. Double headed arrow gives the direction of incident polarization, while single headed dashed arrow gives the writing direction.

3.3.5 Effect of wavelength: We have investigated the effect of two wavelengths, the fundamental 800 nm and the second harmonic 400 nm on the formation of periodic nanostructures. Figure 9(a) shows the periodic structure formation when irradiated with 400 nm fs pulses at the incident fluence of 0.35 J/cm^2. The observed periodicity is about 240±20 nm. Figure 9(b) shows the periodic structure formation upon irradiation with 800 nm fs laser pulses at a fluence of 0.39 J/cm^2. The observed periodicity is 540±20 nm.

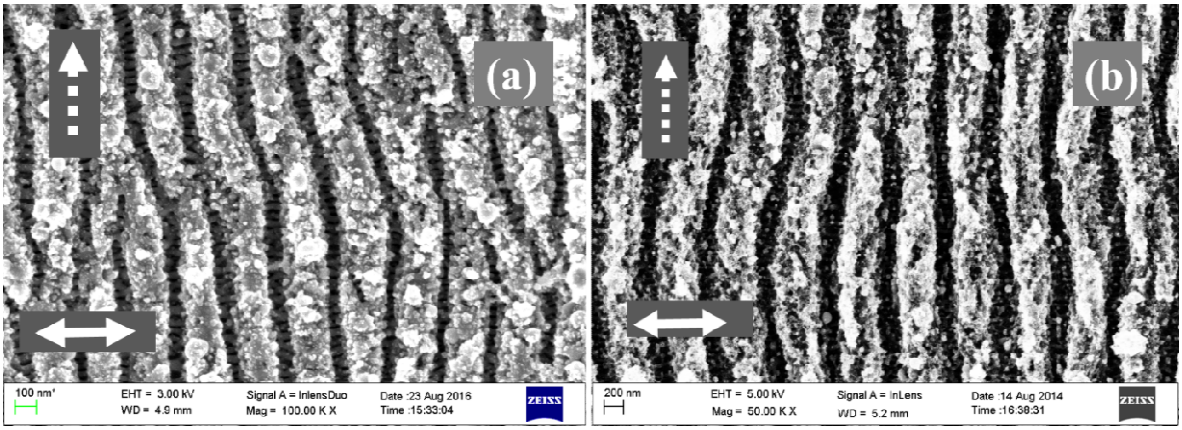

Figure 9: Shows the effect of laser wavelength on the formation of periodic structures (a) under 400 nm and fluence of 0.35 J/cm^2 (b) under 800 nm irradiation at fluence of 0.39 J/cm^2.

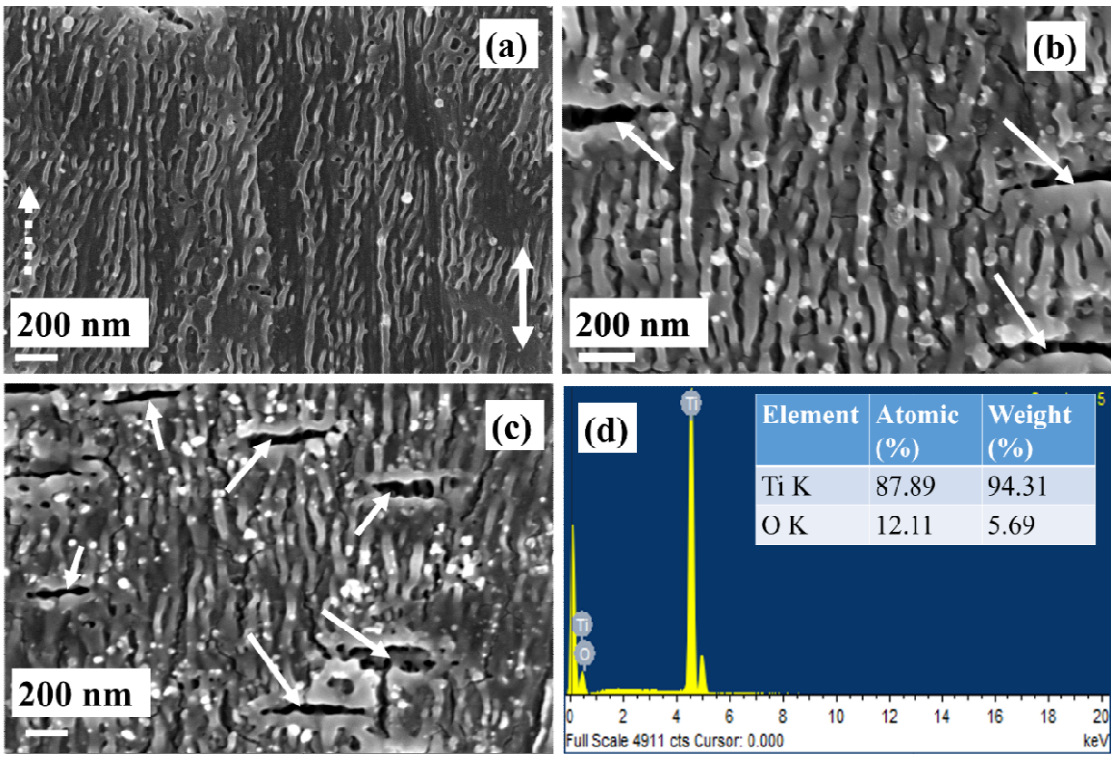

Figure 10: LIPSS formation on Ti surface in ambient air irradiated by ~100 fs laser pulses. The incident laser fluence is 0.07, 0.11 and 0.16 J/cm^2 for (a)-(c) respectively, (d) is the EDX spectra of the irradiated Ti surface. Double headed solid arrow represents the incident laser polarization direction and dotted single headed arrow represents the writing direction. Random arrows in (b) and (c) represent the trenches formed.

3.4 Discussion: Figure (10) shows the formation of HSFL under fs laser irradiation at 800 nm wavelength in ambient air environment. Figure 10(a) shows FESEM morphology of Ti surface after laser irradiation at a fluence of 0.07 J/cm^2 and the number of incident pulses ~100. Figure 10(b) shows the surface topography at incident laser fluence of 0.11 J/cm^2 (~100 pulses) and figure 10(c) shows the morphology of Ti surface evolved after laser irradiation at a fluence of 0.16 J/cm^2 (~100 pulses). When the structure formation was recorded at lower fluence, we observed the formation of HSFL structures. As we increase the fluence, we start observing the formation of trenches [indicated by arrows in figures 10(b) and 10(c)]. One can see that the direction of these trenches is perpendicular to the fine HSFL structures so formed. At still higher fluence, these isolated trenches dominate and take the shape of LSFL structures, destroying the earlier formed HSFL structures. The fluence range at which we observed the LSFL and HSFL are summarized in the table 1. This type of simultaneous formation of HSFL and LSFL features under fs laser irradiation may have a strong dependence on the surface quality [61].

	Fluence (J/cm^2)	*Periodicity (nm)*	*Scanning speed (mm/s)*	*Figure*	*Structure*
Ti in air	*0.24*	*450 to 630*	*0.8 to 0.05*	*Fig 1*	*LSFL (⊥ to the polarization)*
	0.06 to 0.12	*60 to 90*	*0.05*	*Fig 3 and Fig 10*	*HSFL(∥ to the polarization)*
Ti in water	*0.23*	*~230* *~80*	*0.3* *0.3*	*Fig 6*	*HSFL (⊥ to the polarization)* *HSFL (∥ to the polarization)*
	0.19	*~ 50* *~ 120*	*0.1, 0.05*	*Fig 7*	*Fine HSFL (∥ to the polarization)* *HSFL (⊥ to laser polarization)*

Table 1: Summary of the formation of LSFL and HSFL at different laser parameters formed on titanium surface.

Ionin et al., [65-68] had shown through numerical simulations and experiments that the non-uniform distribution of the absorbed laser pulse energy on nano-structured surface is

the main reason for the formation and evolution of the ripples under multiple pulse laser irradiation. The LSFL formation has also been explained by the interference model in earlier studies [38, 53-55].

The slow ablation rate leads to the formation of more precise and deep ripples with repetitive pulse irradiation. We recorded the absorption spectrum of Ti nanoparticles produced by fs laser ablation at 800 nm laser irradiation of Ti surface in the water medium. The observed spectrum is shown in figure 11, which shows a strong surface plasmon peak at 300 nm and very little absorption around 800 nm. Therefore to estimate the approximate ripple periodicity, we can assume that the imaginary part to be much smaller than the real part of the dielectric constant at 800 nm. However the second and third harmonic surface frequencies would be falling near the Ti nanoparticle absorption peak, where both the real and imaginary parts of the dielectric constant would play a role. Using the approach given in the reference [23], the observed fine HSFL at low fluence and LSFL at higher fluence suggest that intraband transitions could be playing a major role in the formation of the ripple structures on Ti surface. At higher energies, both the intra-band and inter-band transitions come into picture. The current results reported here show clear and periodic LSFL and HSFL over a long range on the Ti surface for a certain fluence range. ~120 nm sub-wavelength structures perpendicular to the polarization were seen with water as the dielectric medium, while we observed the HSFL parallel to the laser polarization which could possibly be due to the polarization flip of the surface plasmons. The periodicities of both these structures are different as the dielectric constants would be different in both the cases.

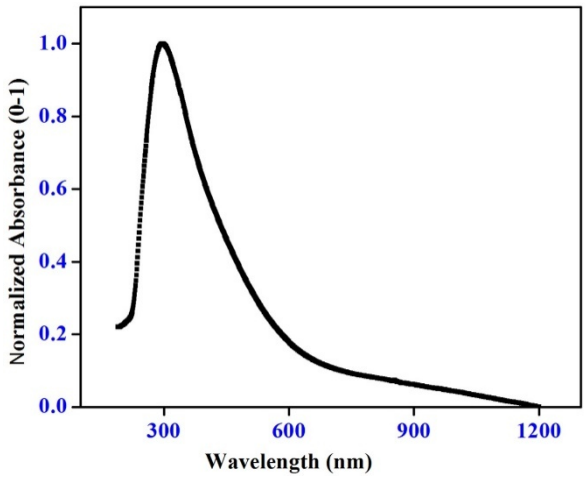

Figure 11: Absorption spectrum of Ti nanoparticles in water.

Differently polarized surface plasmons can exist on the shoulders of the surface plasmon resonance peak. It is well known that surface nonlinearities can lead to the generation of strong second harmonic and third harmonic frequencies. Excitation of the surface plasmon polaritons by the higher harmonics reduces the ripple spacing by 2 and 3 times for second harmonic and third harmonic frequencies respectively. This could explain the very fine HSFL structures observed. Li et al [26] suggested the formation of HSFL to the laser induced oxidation of the Ti surface and the generation of third harmonic frequency. Our EDX studies shown in figure 10(d) reveal the presence of traces of oxygen on the laser irradiated Ti surface. Laser induced oxidation leads to significant enhancement in third harmonic generation [68] and the excitation of SPPs by third harmonic reduces the ripple spacing.

3.5 Conclusions

We have investigated the formation of both HSFL and LSFL on Ti surface upon fs laser irradiation at near normal incidence. Surface morphology has been found to depend on different experimental parameters like fluence, number of incident pulses, laser polarization, laser wavelength, surrounding dielectric medium. The surface morphology was characterized using FESEM. The study reveals the formation of LSFL and HSFL ripples on Ti surface at a particular fluence and pulse number under fs laser irradiation in ambient air and water environments. We have demonstrated the control on LIPSS period. The LSFL period of 540 nm and 240 nm were produced on Ti surface using fundamental (800 nm) and second harmonics (400 nm) laser wavelengths. Another approach demonstrated to control the LIPSS period is by carrying laser direct writing in ambient water environment with larger refractive index than air. Number of incident laser shots also control the LIPSS period. The LSFL ripples are oriented orthogonal to incident laser polarization. However, HSFL features are oriented either parallel or orthogonal to the incident laser polarization direction. In ambient water environment the feature size of the formed nanostructures is as small as ~$\lambda/15$ and orientated parallel to the incident laser polarization direction.

3.6 References

1. Vorobyev AY, and Guo C., Laser Photon Rev, 7, 385–407 (2013).
2. Ahmmed KMT, Grambow C, and Kietzig AM, Micromachines, 5, 1219–1253 (2014).

3. Cheng J, Liu CS, Shang S, Liu D, Perrie W et al, Opt Laser Technol, 46, 88–102 (2013).
4. Li L, Hong MH, Schmidt M, Zhong ML, Malshe A et al, CIRP Ann—Manufact Technol, 60, 735–755 (2011).
5. J. Bonse, and J. Kruger, J. Appl. Phys. 108, 034903(2010).
6. P. Mannion, J. Magee, E. Coyne, G. O'Connor, and T. Glynn, Appl. Surf. Sci. 233, 275–287(2004).
7. M. Huang, F. Zhao, Y. Cheng, N. Xu, and Z. Xu, ACS Nano 3, 4062–4070 (2009).
8. S. Hohm, A. Rosenfeld, J. Kruger, and J. Bonse, Journal of Applied Physics,112, 014901-9 (2012).
9. D. Dufft, A. Rosenfeld, S.K. Das, R. Grunwald, and J. Bonse., Journal of Applied Physics 105, 034908 (2009).
10. Juan Song, Wenjun Tao, Hui Song, Min Gong, Guohong Ma, Ye Dai, Quanzhong Zhao, and Jianrong Qiu, Appl. Phys. A 122, 341 (2016).
11. George D. Tsibidis, Evangelos Skoulas, and Emmanuel Stratakis, Optics Letters, 40, 5172 – 5175 (2015).
12. W. Zhang, G. Cheng, X. D. Hui, and Q. Feng, Appl. Phys. A, 115, 1451–1455 (2014).
13. M. Barberoglou, D. Gray,1 E. Magoulakis, C. Fotakis, P. A. Loukakos, and E.Stratakis, Optics Express, 21, 18501 – 18508 (2013).
14. F. Garrelie, J. P. Colombier, F. Pigeon, S. Tonchev, N. Faure, M. Bounhalli, S. Reynaud, and O. Parriaux, Optics Express, 19, 9035 – 9043 (2011).
15. Godai Miyaji, and Kenzo Miyazaki, Optics Express, 24, 4648 – 4653 (2016).
16. Tianqing Jia, Motoyoshi Baba, Masayuki Suzuki, Rashid A. Ganeev, Hiroto Kuroda, Jianrong Qiu, Xinshun Wang, Ruxin Li, and Zhizhan Xu, Optics Express, 16, 1874 – 1878 (2008).
17. Pin Feng, Lan Jiang, Xin Li, Kaihu Zhang, Xuesong Shi, and Bo Li, Applied Surface Science 372, 52–56 (2016).
18. Roman Sajzew, Jan Schroder, Clemens Kunz, Sebastian Engel, Frank A. Muller, and Stephan Graf, Optics Letters, 40, 5734 – 5737 (2015).
19. S. Richter, M. Heinrich, S. Doring, A. Tunnermann, and S. Nolte, Appl. Phys. A, 104, 503–507 (2011).

20. Shutong He, Jijil JJ Nivas, Antonio Vecchione, Minglie Hu, and Salvatore Amoruso, Optics Express, 24, 3238 – 3247 (2016).
21. George D. Tsibidis, and Emmanuel Stratakis, Journal of Applied Physics, 121, 163106-1-12 (2017).
22. Davide Scorticati, Gert-Willem Römer, Dirk Frederik de Lange, and Bert Huis in't Veld, Journal of Nanophotonics, 6, 063528-1-11 (2012).
23. E. V. Golosov, A. A. Ionin, Yu. R. Kolobov, S. I. Kudryashov, A. E. Ligachev, Yu. N. Novoselov, L. V. Seleznev, and D. V. Sinitsyn, 113, 14-26(2011).
24. Elena Fadeeva, Vi Khanh Truong, Meike Stiesch, Boris N. Chichkov, Russell J. Crawford, James Wang, and Elena P. Ivanova, Langmuir 27, 3012-3019(2011).
25. J. Bonse, S. Hohm, A. Rosenfeld, and J. Kruger, Applied Physics A, 110, 547-551(2013).
26. Xian-Feng Li, Cheng-Yun Zhang, Hui Li, Qiao-Feng Dai, Sheng Lan, and Shao-Long Tie, Optics Express 22, 28086-28099(2014).
27. Rajamudili Kuladeep, Mudasir H. Dar, K. L. N. Deepak, and D. Narayana Rao, Journal of Applied Physics 116, 113107-1-7(2014).
28. Catalina Albu, Adrian Dinescu, Mihaela Filipescu, Magdalena Ulmeanu, and Marian Zamfirescu, Applied Surface Science 278, 347-351(2013).
29. M. Hans, F. Muller, S. Grandthyll, S. Hufner, and F. Mucklich, Applied Surface Science 263, 416-422(2012).
30. A. Y. Vorobyev, and C. Guo, Applied Physics Letters 92,041914-1-3(2008).
31. A.Y. Vorobyev, and C. Guo, Physical Review B 72,195422 1-5(2005).
32. Yang Yang, Jianjun Yang, Chunyong Liang, Hongshui Wang, Xiaonong Zhu, and Nan Zhang, Optics Express 17, 21124-21133(2009).
33. J. F. Young, J. S. Preston, H. M. van Driel, and J. E. Sipe, Physical Review B 27, 1155-1172(1983).
34. A. Y. Vorobyev, V. S. Makin, and C. Guo, Journal of Applied Physics 101, 034903-1-4, (2007).
35. L. K. Ang, Y. Y. Lau, R. M. Gilgenbach, and H. L. Spindler, Applied Physics Letters 70, 696-698 (1997).

36. M. Barberoglou, D. Gray, E. Magoulakis, C. Fotakis, P. A. Loukakos, and E. Stratakis, Optics Express 21, 18501-18508 (2013).
37. U. Chakravarty, R. A. Ganeev, P. A. Naik, J. A. Chakera, M. Babu, and P. D. Gupta, Journal of Applied Physics. 109 084347-1-8 (2011).
38. G. Miyaji, K. Miyazaki, K. Zhang, T. Yoshifuji, and J. Fujita, Optics Express 20, 14848-14856 (2012).
39. R. Kuladeep, C. Sahoo, and D. Narayana Rao, Applied Physics Letters 104, 222103-1-4 (2014).
40. M. Barberoglou, G. D. Tsibidis, D. Gray, E. Magoulakis, C. Fotakis, E. Stratakis, and P. A. Loukakos, Applied Physics A 113, 273-283 (2013).
41. G. D. Tsibidis, M. Barberoglou, P. A. Loukakos, E. Stratakis, and C. Fotakis, Physical Review B 86, 115316, 1-14 (2012).
42. U. Chakravarty, P. A. Naik, J. A. Chakera, A. Upadhyay, and P. D. Gupta, Applied Physics A 115, 1457-1467 (2014).
43. Y. Shimotsuma, P. G. Kazansky, J. Qiu, and K. Hirao, Physical Review Letters 91, 247405, 1-4 (2003).
44. Y. Yuan, L. Jiang, X. Li, C. Wang, H. Xiao, Y. Lu, and H. Tsai, Journal of Physics D: Applied Physics 45, 175301, 1-6 (2012).
45. G. Miyaji, and K. Miyazaki, Optics Express 16, 16265-16271 (2008).
46. M. K. Kuntumalla, K. Rajamudili, N. R. Desai, and V. V. S. S. Srikanth, Applied. Physics Letters 104, 161607, 1-4 (2014).
47. M. Shinoda, R. R. Gattass, and E. Mazur, Journal of Applied Physics 105, 053102, 1-4 (2009).
48. A. Y. Vorobyev, and ChunleiGuo, Optics Express 19,1031-1036(2011).
49. B. Hopp, T. Smausz, T. Csizmadia, C. Vass, C. Tapai, B. Kiss, M. Ehrhardt, P. Lorenz, and K. Zimmer, Applied Physics A 113, 291-296 (2013).
50. H. Tao, J. Lin, Z. Hao, X. Gao, X. Song, C. Sun, and X. Tan, Applied. Physics Letters, 100, 201111, 1-3 (2012).
51. T. Baldacchini, J. E. Carey, M. Zhou, and E. Mazur, Langmuir 22,4917–9(2006).
52. A. Y. Vorobyev, and Chunlei Guo, Optics Express 18 6455-6460 (2010).

53. J. E. Sipe, J. F. Young, J. S. Preston, and H. M. van Driel, Physical Review B 27,1141–1154 (1983).
54. J. F. Young, J. E. Sipe, and H. M. van Driel, Physical Review B 30,2001–2015 (1984).
55. M. Huang, F. Zhao, Y. Cheng, N. Xu, and Z. Xu, ACS Nano 3, 4062–4070 (2009).
56. J. Reif, F. Costache, M. Henyk, and S. V. Pandelov, Applied Surface Science 197, 891–895 (2002).
57. D. Dufft, A. Rosenfeld, S. K. Das, R. Grunwald, and J. Bonse, Journal of Applied Physics 105,034908, 1-9 (2009).
58. R. Le Harzic, D. Dorr, D. Sauer, M. Neumeier, M. Epple, H. Zimmermann, and F. Stracke, Optics Letters 36, 229-231 (2011).
59. A. A. Ionin, S. I. Kudryashov, A. E. Ligachev, S. V. Makarov, L. V. Seleznev, and D. V. Sinitsyn, Journal of Experimental and Theoretical Physics Letters, 94,266–269 (2011).
60. A. A. Ionin, S. I. Kudryashov, S. V. Makarov, L. V. Seleznev, D. V. Sinitsyn, A. E. Ligachev, E. V. Golosov, and Yu. R. Kolobov, Laser Physics Letters 10056004, 1-5 (2013).
61. Chandra S.R. Nathala, Ali Ajami, Andrey A. Ionin, Sergey I. Kudryashov, SergeyV Makarov, Thomas Ganz, Andreas Assion, and Wolfgang Husinsky, Optics Express 23, 5915-5929 (2015).
62. Taek Yong Hwang, and Chunlei Guo, Journal of Applied Physics 108, 073523, 1-4 (2010).
63. A.V. Zayats, and I. I. Smolyaninov, Journal of Optics A: Pure and Applied Optics 5,S16-S50(2003).
64. C. G. Granqvist, and O. Hunderi, Physics Review B 16,3513-3534(1977).
65. A. A. Ionin, S. I. Kudryashov, S. V. Makarov, A. A. Rudenko, S. V. Seleznev, D. V. Sinitsyn, T. P. Kaminskaya, and V. V. Popov, JEPT letters 101, 350-357 (2015).
66. E. V. Golosov, V. I. Emelyanov, A. A. Ionin, Yu. R. Kolobov, S. I. Kudryashov, A. E. Ligachev, Yu. N. Novoselov, L. V. Seleznev, and D. V. Sinitsyn, JEPT Letters 90, 107-110 (2009).

67. A. A. Ionin, Sergey I Kudryashov, Sergey V Makarov, Andrey A Rudenko, Leonid V Seleznev, Dmitry V Sinitsyn, and Vladimir I Emel'yanov, Laser Physics Letters 12, 025902, 1-6 (2015).
68. Andrey A Ionin, Sergey I Kudryashov, Sergey V Makarov, Alexey O Levchenko, Andrey A Rudenko, Irina N Saraeva, Dmitry A Zayarny, Chandra R Nathala,and Wolfgang Husinsky, Laser Phys. Lett. 13,025603, 1-8 (2016).
69. A. A. Ionin, Y. M. Klimachev, A. Y. Kozlov, S. I. Kudryashov, A. E. Ligachev, S. V. Makarov, L. V. Seleznev, D. V. Sinitsyn, A. A. Rudenko, and R. A. Khmelnitsky, Applied Phys. B 111, 419-423 (2013).
70. V. P. Korolkov, A. A. Ionin, S. I. Kudryashov, L. V. Seleznev, D. V. Sinitsyn, R. V. Samsonov, A. I. Masliy, A. Zh. Medvedev, and B.G. Goldenberg, Quantum Electronics 41, 387-392 (2011).
71. H. Long, A. Chen, G. Yang, Y. Li, and P. Lu, Thin Solid Films 517, 5601–5604 (2009).
72. R.J. Bell, R.W. Alexander Jr., W.F. Parks and G. Kovener, Optics Communications 8, 147-150 (1973).
73. J. Eichstadt, G.R.B.E. Romer, and A.J.H. in't Veld, Phys. Procedia 12 7–15 (2011).
74. Liang C.Y, Wang H.S, Yang J.J, Li B, Yang Y, and Li H.P, Appl. Surf. Sci., 261, 337–342 (2012).
75. Yang, Y, Yang J.J, Liang C.Y, Wang H.S, Zhu X.N and Zhang N, Opt. Expr., 17, 21124–21133 (2009).
76. Fadeeva E, Schlie S, Koch J,and Chichkov B.N, J. Adhes. Sci. Technol., 24, 2257–2270 (2010).
77. Fadeeva E, Truong V.K, Stiesch M, Chichkov B.N, Crawford R.J, Wang J,and Ivanova E.P, Langmuir, 27, 3012–3019 (2011).
78. Liang F, Lehr J, Danielczak L, Leask R,and Kietzig A.M. Int. J. Mol. Sci., 15, 13681–13696 (2014).
79. Truong S.L, Levi G, Bozon-Verduraz F, Petrovskaya A.V, Simakin A.V, and Shafeev G.A, Appl. Surf. Sci., 254, 1236–1239 (2007).
80. Carey J.E, Crouch C.H, Shen M.Y,and Mazur E *Opt. Lett.*, *30*, 1773–1775 (2005).

81. Myers R.A, Farrell R, Karger A.M, Carey J.E, and Mazur E, *Appl. Opt.*, *45*, 8825–8831(2006).
82. Barmina E.V, Barberoglou M, Zorba V, Simakin A.V, Stratakis E, Fotakis C, and Shafeev G.A, *J. Optoelectron. Adv. Mater.*, *12*, 495–499 (2010).
83. Volkov R.V, Golishnikov D.M, Gordienko V.M, and Savel'ev A.B, *JETP Lett.*, *77*, 473–476 (2003).

CHAPTER- 4

Highly regular LIPSS and their origin of regularity

Abstract

This chapter describes the formation of LIPSS on different metals at 800 nm laser irradiation in ambient air and water environments. We investigated the effect of different experimental parameters on LIPSS formation. Interestingly, out of all the metals studied in this chapter, Mo shows smooth and highly regular periodic surface structure formation. However, metals like Silver and Copper don't show the formation of prominent periodic structures at 800 nm irradiation in ambient air environment. We link the formation of regular periodic structures with decay lengths of the excited SPPs on the irradiated metal interface. The metals with large SPP decay length, doesn't sustain coherence and hence don't show the formation of regular periodic structures. The important feature observed between the grooves of LSFL in Mo, is the formation of nano-ripples with periodicity as small as ~λ/40 and oriented parallel to the polarization direction.

4.1 Introduction

Surface texturing of materials is important for various scientific, biomedical and industrial applications [1-3]. There are various methods used for the fabrication of nano-structured surfaces such as chemical vapor deposition, sputtering, chemical and plasma etching, optical and physical lithography [4-6]. Most commonly used techniques are electron beam lithography and photolithography that provides high precision nanostructuring. However, these methods involve multistep processes and thus prove costly and time consuming.

Ultrafast laser direct writing technique (LDW) is robust and cheaper alternative to lithography for surface structuring of various materials [7]. LDW technique for material processing involves a mask free, single step process and is considered as bottom-up approach [8]. LIPSS represent a periodic surface relief which appear in two main forms referred to as LSFL and HSFL depending up on the periodicity [9]. Laser induced surface structuring both at nano and micro scales has been studied extensively owing to its tremendous applications in various fields. Femtosecond laser pulse surface structuring is effective for material processing due to minimal thermal and mechanical damage. Ultrafast laser pulses have been utilized to produce LIPSS on a variety of materials including semiconductors, metals, dielectrics and polymers [10-27]. This field of nanoscale fabrication has stimulated lot of research activities to understand the physics behind it. Furthermore, this field of surface processing has potential applications in nano-science and technology [28-34].

In this chapter, we study the interaction of fs laser at 800 nm wavelength on different metals like Mo, Ni, Fe, Ag, and Cu towards the formation of LIPSS. Among the metals studied, LIPSS could be obtained only on Mo, Ni, Fe and Ti (discussed in chapter 3). On Ag and Cu, we couldn't achieve highly regular LIPSS. We explain this observation based on SPP decay lengths.

4.2 Experimental details

The laser direct experiments were carried out on a nano-positioning stage purchased from Newport, USA having horizontal and vertical adjustments. The incident laser beam is fixed, while the sample is scanned in horizontal direction. Laser energy is controlled by using

neutral density filters and a variable attenuator- which is a combination of half wave plate and polarizer. The polarizer also controls the polarization of the incident laser pulses. Detailed morphological characterization of the Ti surface after irradiation, was performed by Zeiss Ultra55 high resolution field emission scanning electron microscope (FESEM) operated at an accelerating voltage of 5-10kV. The detailed experimental procedure is discussed in chapter 3.

4.3 Results on Molybdenum

We have carried out femtosecond LDW experiments on Mo surface. Figure 1(a)-(b) shows the FESEM images of Mo surface, evolved after fs-laser irradiation at 800 nm

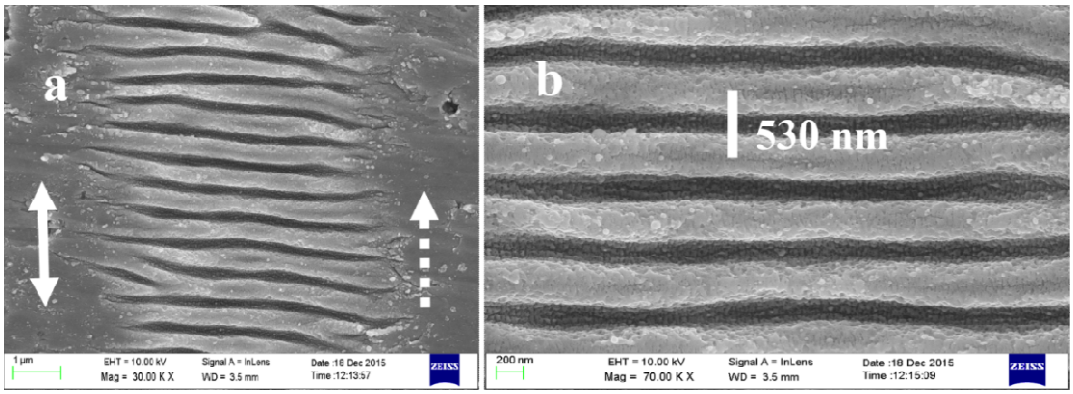

Figure 1: FESEM image showing the formation of periodic structures on molybdenum surface after fs-laser irradiation at 800 nm wavelength under normal incidence in ambient air environment. Laser fluence is 0.33 J/cm^2 and scanning speed 0.07 mm/s. Double headed solid arrow represents incident laser polarization, single headed doted arrow represents writing direction. (b) is the magnified image of (a)

wavelength in ambient air environment. The fluence is 0.33 J/cm^2 and scanning speed 0.07 mm/s. Figure 1(b) is the magnified image of figure 1(a). Surface morphology reveals the formation of highly regular LSFL oriented orthogonal to the incident laser polarization direction. The regular and continuous formed ripples show a period of approximately 530 ± 10 nm. These periodic ripples are assigned as near sub-wavelength ripples (NSRs) or low spatial frequency LIPSS (LSFL) with grating period (Λ) ~0.66λ.

Effect of surrounding dielectric medium is carried out by immersing the sample in water. Figure 2 shows the surface morphology of Mo, evolved after fs-laser irradiation at 800 nm wavelength at normal incidence in ambient water environment. The fluence is 0.08 J/cm^2 and scanning speed 0.02 mm/s. We observed the formation of two types of periodic

nanostructures under fs laser irradiation on Mo surface in ambient water environment. The ripple periodicity observed is about 340 ± 20 nm for the periodic structures oriented orthogonal to the polarization direction as shown in figure 2 (a).These are assigned as LSFL, as the feature size is greater than 0.4λ. The interesting observation is the formation of ~ 20 nm ripples in the grooves of LSFL as shown in figure 2 (b). These ripples are oriented parallel to the incident laser polarization direction.

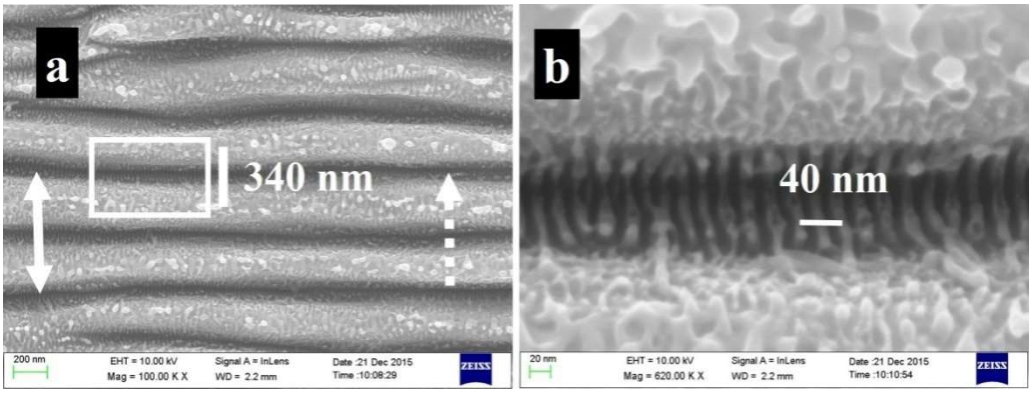

Figure 2: Evolution of surface topography of molybdenum after fs-laser irradiation in water environment. The fluence is 0.08 J/cm^2 and scanning speed 0.02 mm/s.(b) is the magnified image of the area shown by rectangle in (a).

To study the dependence of LSFL periodicity on laser wavelength, we carried out the experiments with both fundamental (800 nm) and second harmonic (400 nm) fs laser pulses of the Ti:Sapphire laser system. Figure 3 shows the topography of the Mo surface upon fs-laser irradiation at the 400 nm wavelength in ambient air environment. The incident laser fluence is 0.17 J/cm^2 and scanning speed 0.07 mm/s. The observed period of these ripples is about 260 nm, and oriented perpendicular to the incident laser polarization.

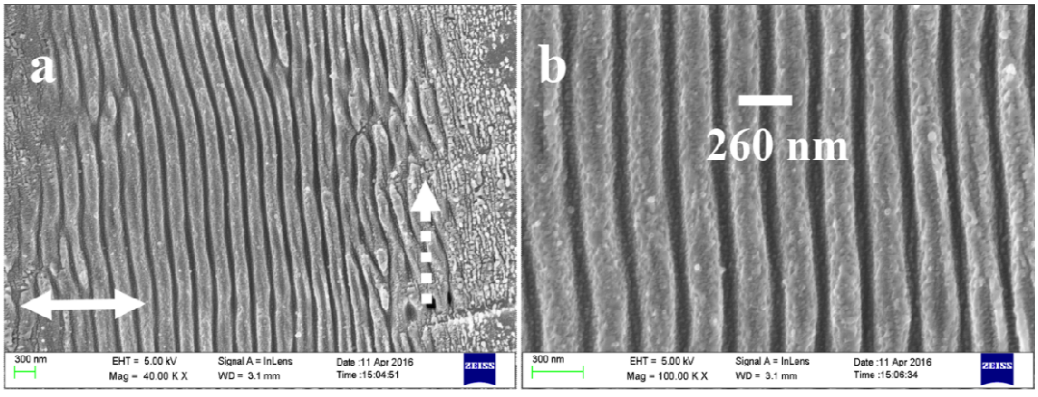

Figure 3: Evolution of surface topography of molybdenum after fs-laser irradiation of second harmonic radiation at the 400 nm wavelength. The fluence is 0.17 J/cm^2 and scanning speed 0.07 mm/s. (b) is the magnified image of (a). Double headed arrow represents polarization and single headed arrow writing direction.

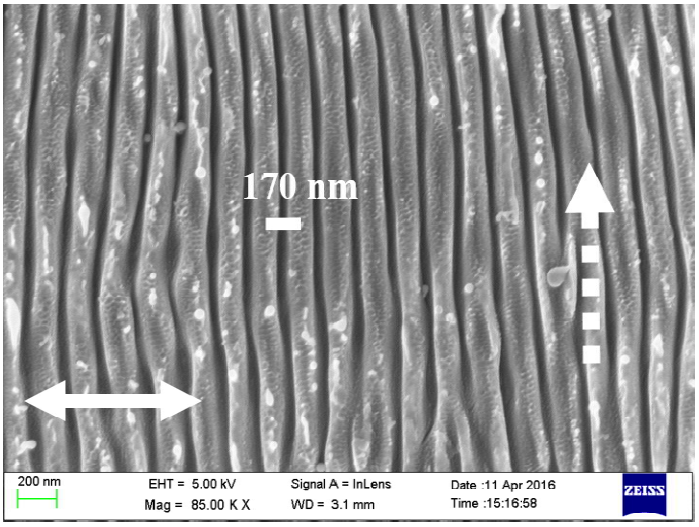

Figure 4: Surface morphology of molybdenum sample after irradiating with 400 nm fs-laser pulses in ambient water environment. The laser fluence is 0.09 J/cm^2 and scanning speed 0.01 mm/s. Double headed solid arrow represents incident laser polarization, single headed doted arrow represents writing direction.

Figure 4 shows the LIPSS formation on molybdenum surface under fs-laser irradiation at 400 nm wavelength in ambient water environment. Incident laser fluence is 0.09 J/cm^2 and scanning speed 0.01 mm/s. The figure shows the formation of periodic ripples oriented perpendicular to the incident laser polarization direction. The spatial period observed is about 170 nm. We demonstrate that LSFL period on Mo surface can be controlled more easily by the choice of wavelength and the surrounding medium.

4.4 LIPSS formation on different metals during fs laser irradiation at 800 nm.

We studied the interaction of fs laser at 800 nm wavelength on 6 different metals which include Mo, Ti, Fe, Ni, Ag, and Cu. Figure 5 shows the formation of highly regular LIPSS on Mo, Ti, Fe, and Ni. Figure 5(a) shows the formation of LSFL on Mo surface when irradiated with 800 nm fs laser pulses in ambient air environment at the fluence of 0.33 J/cm^2 and scanning speed 0.07 mm/s. The spot size of the incident laser beam on the sample is ~ 8 µm. The average periodicity of LSFL on Mo surface is ~ 520 nm. The detailed discussion of LIPSS formation on Mo surface is given in section 6.3. Figure 5(b) shows the morphology of Ni surface after irradiated with fs laser pulses at 800 nm wavelength in ambient air at the fluence of 0.32 J/cm^2 and scanning speed 0.04 mm/s. The average periodicity of LSFL on Ni

surface is ~ 450 nm. Figure 5(c) shows the formation of LSFL on Ti surface when irradiated with 800 nm fs laser pulses in ambient air environment at the laser fluence of 0.21 J/cm^2 and scanning speed 0.1 mm/s. The average periodicity of LSFL on Ti surface is ~ 510 nm. We have given a detailed description of LIPSS formation on titanium in chapter 3. Figure 5(d) shows the surface morphology of Fe irradiated with fs laser pulses at 800 nm wavelength in ambient air at the fluence of 0.15 J/cm^2 and scanning speed 0.2 mm/s. The average periodicity of LSFL fabricated on Fe surface, oriented perpendicular to incident laser polarization direction, is ~ 560 nm. The results on different metals are summarized in table 1. All these 4 metals Mo, Ni, Fe, and Ti show the formation of periodic structures under appropriate laser irradiation conditions. Furthermore, figure (5) also shows us the polarization controlled LIPSS formation on these metals. However, metals like Ag and Cu don't show the formation of good and deep periodic surface structures when irradiated with 800 nm fs laser pulses in ambient air environment.

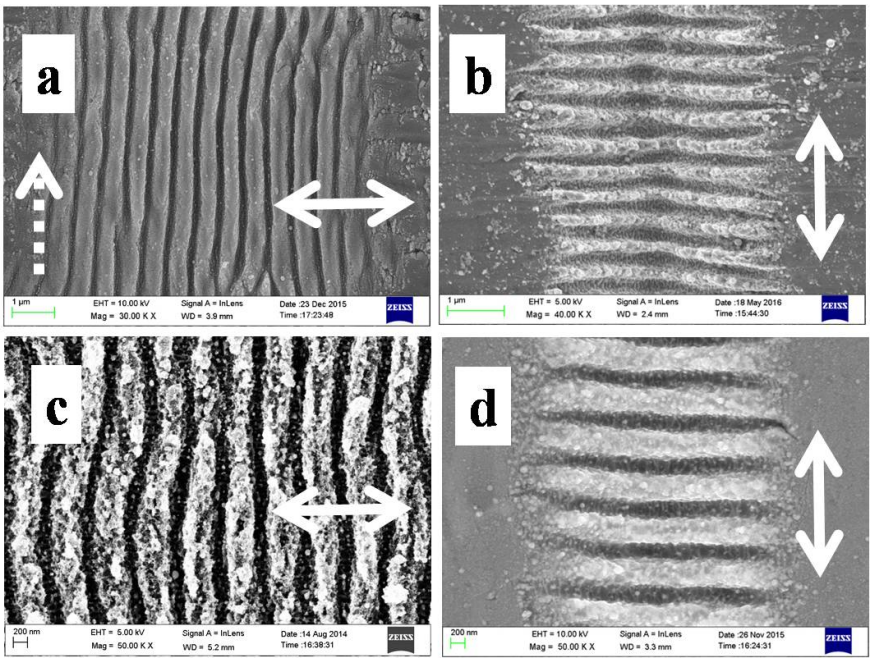

Figure 5: Surface morphology of (a) Mo, (b) Ni, (c) Ti, (d) Fe, evolved after fs laser irradiation at 800 nm wavelength in ambient air environment. Dashed single headed arrow shows writing direction for all. Double headed arrow represents the incident laser polarization.

Figure 6(a) shows the surface morphology of Ag after irradiating with 800 nm fs laser in ambient air at the laser fluence of 0.28 J/cm^2 and scanning speed 0.1mm/s. Figure 6(c) shows the surface morphology of Ag after irradiating with 800 nm fs laser in ambient water

environment at the laser fluence of 0.35 J/cm^2 and scanning speed 0.05 mm/s. We didn't observe the formation of LIPSS on Ag surface in air by varying the available experimental parameters of fluence and pulse number. However when irradiated in water the periodic structures start appearing, though not prominent.

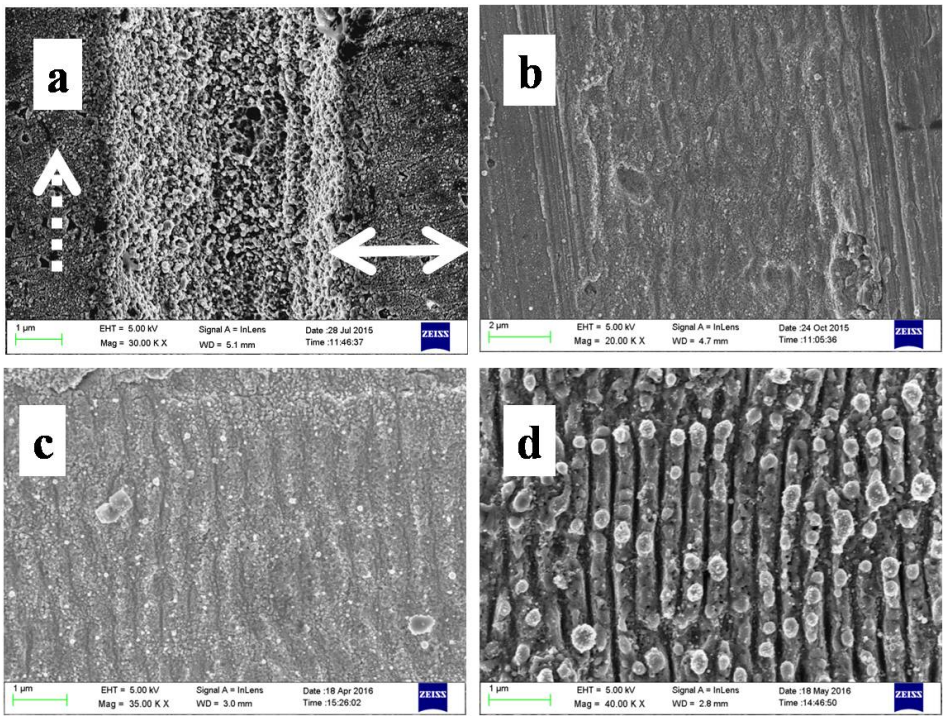

Figure 6: FESEM imaged surface morphology of (a) Ag in air (b) Cu in air (c) Ag in water (d) Cu in water. Single headed dashed arrow represents writing direction and double headed solid arrow represents incident laser polarization (for all).

Figure 6(b) shows the formation of LSFL on Cu surface, when irradiated with 800 nm fs laser pulses in ambient air environment, at the fluence of 0.24 J/cm^2 and scanning speed 0.2 mm/s. Here again, we didn't observe the formation of prominent periodic structures. Figure 6 (d) shows the formation of LSFL on Cu surface, when irradiated with 800 nm fs laser pulses in ambient water environment, at the laser fluence of 0.32 J/cm^2 and scanning speed 0.05 mm/s. we observed LIPSS formation with an average periodicity of ~360 nm. This could be due to high thermal conductivity of silver and copper in comparison to the other metals. When the thermal conductivity is high, the localized energy may quickly distribute to the neighboring areas leading to a weak formation of the ripples in the medium. With water as the surrounding medium, it is quite likely that the thermal energy gets trapped leading to a localized material trapping. Further studies however are needed to confirm this possibility.

Experimental observations show that highly regular structures are formed on 4 metals Mo, Ti, Ni, and Fe, during fs laser irradiation in ambient air environment at 800 nm wavelength, shown in figure (5). Out of these 4 metals, Mo surface shows the best quality LIPSS formation. All these metals give rise to short SPP decay lengths at 800 nm wavelength as discussed in table 1 of chapter 2.

With the approximation that dielectric function of metals doesn't change much during irradiation, we have calculated decay lengths of the SPPs excited on the surface of the irradiated metal using equation 9 in chapter 2. During fs laser irradiation on air/Ag interface at 800 nm wavelength, it gives rise to SPP with decay length of 140.4 μm. The observed surface morphology is shown in figure 6(a). There is not any prominent formation of LIPSS structures. However, when the fs laser irradiation is carried on water/Ag interface at 800 nm wavelength, SPP decay length reduces to 56.2 μm; traces of periodic structures begin to appear as shown by the surface morphology in figure 6(c). Similarly we observed in copper, under fs laser irradiation on air/Cu interface at 800 nm wavelength, the mean free path of the SPP excited on the Cu surface is 84 μm. FESEM reveals the morphology as shown in figure 6(b). Here also, we didn't observe any conspicuous formation of LIPSS. However, during fs laser irradiation on water/Cu interface at 800 nm wavelength, SPP decay length reduce to 33.4 μm. Surface morphology reveals the formation of LIPSS as shown in figure 6(d).

We predicted from the theoretical calculations in chapter 2 that the interface which give rise to SPP decay lengths of < 5 μm at 800 nm fs laser irradiation lead to the formation of highly regular LIPSS. This is observed to be the case in 4 metals Mo, Ni, Fe and Ti. However, larger SPP decay lengths don't give rise to the formation of periodic surface structures. We also observed that the materials with absolute value of imaginary part greater than the absolute value of real part exhibit highest regularity of LIPSS formation. Two groups of metals can be identified based on mean free path of SPPs: (i) Metals with high optical damping, and small SPP decay length in the range of 1 to 5 μm, exhibit highly regular LIPSS at 800 nm laser irradiation. This includes metals like Ti, Mo, Ni, and Fe. (ii) Metals like Ag,

Cu; with SPP mean free path larger than 5 μm exhibit low regularity LIPSS at 800 nm fs laser irradiation.

4.5 Conclusion

Our experimental results are consistent with the predication that short SPP decays lengths give rise to highly regular periodic structures. Among all the metals studied, Mo shows smooth and highly periodic structures. This model based on the evaluation of SPP decay lengths from the knowledge of real and imaginary parts of dielectric function, helps us to select materials that exhibit highly regular LIPSS under suitable irradiation conditions. Some metals that are identified as the candidates for the fabrication of highly regular periodic structures under proper irradiation conditions include Mo, Ti, Ni and Fe while as Ag, and Cu belong to the group of low regularity LIPSS at 800 nm wavelength.

4.6 References

1. Pease, R. F. & Chou, S. Y. *Proc. IEEE* **96**, 248–270 (2008).
2. Pimpin, A. & Srituravanich, W. *Engineering J.* **16**, 37–56 (2011).
3. Seisyan, R. Nanolithography in microelectronics: A review. *Technical Phys.* **56**, 1061–1073 (2011).
4. Imboden, M. & Bishop, D. *Phys. Today* **67**, 45–50 (2014).
5. Aksu, S. *et al*. *Nano Lett.* **10**, 2511–2518 (2010).
6. Fujii, T. Focused ion beam system as a multifunctional tool for nanotechnology (Cambridge University Press, 2007).
7. Bonse, J., Krüger, J., Höhm, S. & Rosenfeld, A. *J. Laser Appl.* **24**, 042006 (2012).
8. Borowiec A and Haugen H K 2003 *Appl. Phys. Lett.* **82** 4462–4
9. Bonse, J., Hohm, S., Kirner, S. V., Rosenfeld, A. & Kruger, J. *IEEE J. Sel. Top. Quantum Electron.* **23**, 9000615 (2017).
10. V.T. Rathod, D. Roy Mahapatra, Anjana Jain , A. Gayathri, Sensors and Actuators A 163 (2010) 164–171.
11. Esther Rebollar, Mikel Sanz, Susana Perez, Margarita Hernandez, Ignacio Martin-Fabiani, Daniel R. Rueda, Tiberio A. Ezquerra, Concepcion Domingo and Marta Castillejo, Phys. Chem. Chem. Phys., 2012, 14, 15699–15705.

12. Marta Castillejo, Tiberio A. Ezquerra, Margarita Martin, Mohamed Oujja, Susana Perez, and Esther Rebollar, AIP Conf. Proc. 1464, 372 (2012).
13. Susana Perez, Esther Rebollar, Mohamed Oujja, Margarita Martín, and Marta Castillejo, Appl Phys A (2013) 110:683–690.
14. R. Le Harzic, H. Schuck, D. Sauer, T. Anhut, I. Riemann, K. König, Opt. Express 13 (2005)6651–6656.
15. A. Borowiec, H.K. Haugen, Applied Physics Letters 82 (2003) 4462–4464.
16. Y. Shimotsuma, P.G. Kazansky, J. Qiu, K. Hirao, Phys. Rev. Lett. 91 (2003) 247405.
17. V.R. Bhardwaj, E. Simova, P.P. Rajeev, C. Hnatovsky, R.S. Taylor, D.M. Rayner, P.B. Corkum, Phys. Rev. Lett. 96 (2006) 057404.
18. M.S. Ahsan, M.S. Lee, J. Laser Micro/Nanoeng. 7 (2012) 202–207.
19. C. Hnatovsky, R.S. Taylor, P.P. Rajeev, E. Simova, V.R. Bhardwai, D.M. Rayner,P.B. Corkum, Appl. Phys. Lett. 87 (1) (2005) 014104
20. M. Rohloff, S.K. Das, S. Höhm, R. Grunwald, A. Rosenfeld, J. Krüger, J. Bonse, J. Appl. Phys. 110 (1) (2011) 014910.
21. L. Qi, K. Nishii, Y. Namba, Opt. Lett. 34 (2009) 1846–1848.
22. S. Sakabe, M. Hashida, S. Tokita, S. Namba, K. Okamuro, Phys. Rev. B: Condens. Matter 79 (2009) 033409.
23. M.S. Ahsan, Y.G. Kim, M.S. Lee, J. Laser Micro/Nanoeng. 7 (2012) 164–170.
24. J.P. Colombier, F. Garrelie, N. Faure, S. Reynaud, M. Bounhalli, E. Audouard, R. Stoian, F. Pigeon, J. Appl. Phys. 111 (2012) 024902.
25. S.R.J. Brueck, D.J. Ehrlich, Phys. Rev.Lett. 48 (1982) 1678–1681.
26. M.H. Dar, N. Momen, C. Sahoo, S.R.G. Naraharisetty, D.N. Rao, Laser Phys. Lett. 14 (2017) 2.
27. Dar M H, Kuladeep R, Saikiran V and Narayana Rao D, Appl. *Surf. Sci.* **371** 479–87 (2016).
28. Yang Y, Yang J, Liang C and Wang H 2008 *Opt. Express* **16** 11259–65.
29. Zhang C-Y, Yao J-W, Liu H-Y, Dai Q-F, Wu L-J, Lan S, Trofimov V A and Lysak T M 2012 *Opt. Lett.* **37** 1106–8
30. Hopp B, Smausz T, Csizmadia T, Vass C, Tapai C, Kiss B, Ehrhardt M, Lorenz P and Zimmer K 2013 *Appl. Phys.* A **113** 291–6

31. Lin C-H, Jiang L, Chai Y-H, Xiao H, Chen S-J and Tsai H-L 2009 *Opt. Express* **17** 21581–9.
32. Diebold E D, Mack N H, Doorn S K and Mazur E 2009 *Langmuir* **25** 1790–4.
33. Lin C H, Jiang L, Xiao H, Chen S J and Tsai H L 2010 *Opt. Lett.* **35** 2937–9.
34. Vorobyev A Y and Guo C 2011 *Opt. Express* **19** 1031–6

CHAPTER - 5

Fabrication of low-reflective titanium surface upon femtosecond laser irradiation

Abstract

Laser direct writing technique can be utilized to create micro/nano structures on the surface, which can reduce light reflection. The fs laser induced nano-structured surface show unique optical properties and many interesting phenomena. We studied the reflectivity of titanium surface after fs laser irradiation. Surface reflectivity of the Ti sample can be controlled by varying parameters such as fluence, pulse number (scanning speed) and the surrounding dielectric medium during the irradiation process. Spectral measurements show that laser induced surface structuring greatly suppress the specular reflectance of Ti surface over the wavelength range of 250-1800 nm.

5.1 Introduction

The properties of matter can be understood by the interaction with the surface surrounding the matter. Scientific community used different methods from time to time to understand the surface properties of matter. With the advancement in science and technology new methods and sophisticated instruments were used to study the surface properties of matter. Laser-surface interaction became an important area of optics both from the fundamental research point of view as well as from the technological perspective. The laser intensity becomes the defining parameter from application point of view. The pulsed lasers with intensities ranging from 10^{11} to 10^{22} W/cm^2 are used for many scientific applications such as medicine, cleaning of artifacts, driving chemical processes, surface processing etc. When the incident laser intensity is around the melting threshold of the material, many interesting phenomena take place such as formation of periodic nanoripples. These periodic structures form in material like metals, semiconductors, polymers and dielectrics [1-18]. Surface processing of materials is increasingly used to control the physical, chemical and biological properties of surfaces. Femtosecond LDW has become an important technique for high precision material processing. The important advantage of using ultrafast lasers for micromachining is essentially due to minimal thermal damage to the bulk of the material. Furthermore, surface texturing using ultrashort laser pulses is fast and environmental friendly. LDW has demonstrated the ability to produce nano and microstructures on the surface of various metals [19-21]. One of the important prospects of these laser induced surface textures is that they exhibit modified optical properties [22-24]. Spectroscopic studies reveal that highly reflective metals may become almost completely absorptive over a broad wavelength range due to nanostructuring of the surface. Potential applications of these broadband absorptive metal surfaces involve every field which requires efficient light harvesting and manipulation techniques such as antireflection coatings, optical/optoelectronic devices, metal colorization, and solar light absorbers [25-27].

Nano-structuring of metals leads to the modification of their optical properties [28, 29]. A polished metal surface can reflect 98% of the incident light, however nano-structuring of metal surface lead to strong absorption of incident light. It is now well understood that the inconsistency in the reflection spectrum from metallic gratings observed by Wood [30], occur

due to excitation of SPs on the metallic surface [31-34]. Excitation of SPs induces a strong field enhancement at the metal surface. This field has attracted scientific community towards light-matter interaction. Absorption of light by the nano-structured surface has many applications in photovoltaic [35-37], and SERS [38-40].

5.2 Experimental details

Commercially available Ti target of 1 mm thickness and purity of 99.7% purchased from Sigma Aldrich have been used in the experiments. LDW technique is used for the fabrication of micro/nanostructures. Surface texturing using fs laser was carried out over an area of 1 cm^2. The incident laser source is Ti:Sapphire oscillator amplifier system, producing laser pulses of ~ 110 fs pulse duration and repetition rate of 1 kHz at 800 nm central wavelength. Surface topography is characterized by Zeiss Ultra-55 high resolution field FESEM operating at an accelerating voltage of 5 kV. The laser irradiated sample was cleaned thoroughly by ultrasonication in ethanol for 15 minutes. Series of experiments were carried out at different processing parameters (fluence, scanning speed and surrounding dielectric medium) to investigate the reduction in the reflectance measurements. The absolute reflectance of the fs laser treated sample was carried out using JASCO spectrometer having 60 mm integrating sphere (ARN-731 model). The specular reflectance measurements were carried out at the fixed angle of incidence 5^0 using specular reflectance accessory (SLM-736).

5.3 Spectral measurements on fs laser irradiated titanium surface

We study the effect of fs laser induced surface nano-structuring on the reflectivity of the Ti surface. The samples of titanium were fabricated at different laser parameters and processing conditions. For taking the spectral measurements, laser induced surface texturing was carried out on area of 10 mm^2. The spectral measurements were done using SLM-736 specular reflectance accessory attached to JASCO spectrometer. This instrument measures the relative reflectance of the sample, having aluminum deposited plane mirror as the reference. We observed that laser induced surface modifications were found to suppress the specular reflectance of Ti surface over the entire studied wavelength range of 250-1800 nm to a great extent. Figure (1) show the percentage specular reflectance of the nano-structured Ti surface

fabricated with different processing parameters such as fluence, scanning speed (pulse number) and surrounding environment. Curve A shows the percentage specular reflectance of the surface of titanium sample processed under 800 nm fs-laser irradiation. The incident laser fluence is F = 0.9 J/cm^2 and translation stage carrying the sample is moving with speed of 0.2 mm/s. The laser irradiation on Ti surface is carried out in ambient water environment. The surface morphology so formed is shown in figure 2(a). Curve B shows the percentage specular reflectance of titanium surface irradiated with fs-laser at the processing conditions of fluence F = 1.2 J/cm^2 and scanning speed of 0.05 mm/s. The sample is processed in ambient water environment and the corresponding surface morphology is shown in figure 2(b). The curve shows that percentage specular reflectance reduced to < 1% in the UV-Vis region of the wavelength spectrum. However, at the wavelength of 1.8 μm, the percentage specular reflectance is about 20%. Curve C shows the spectral measurement of titanium surface after fs-laser irradiation. The processing parameters are, fluence F = 1.2 J/cm^2 and a scanning speed of 0.005 mm/s. The sample surface is irradiated in ambient water environment and the corresponding FESEM image is shown in figure 2(c). The spectral measurement shows that the percentage specular reflectance reduces to < 1% in the wavelength range of 250 – 1100 nm, the percentage reflectance is about 10% at 1.8 μm wavelength. We observed that the percentage specular reflectance reduces to < 1% in the entire wavelength range of 250 nm – 1.8 μm as shown in curve D. This is observed when the surface processing is carried out at the fluence of F = 1.6 J/cm^2 and scanning speed of 0.2 mm/s in ambient air environment. For comparison, Curve E shows the percentage specular reflectance of the mechanically polished untreated titanium surface. The percentage specular reflectance is about 11% at the wavelength of 250 nm. The percentage reflectance increases to 50% at the wavelength of 1.8 μm.

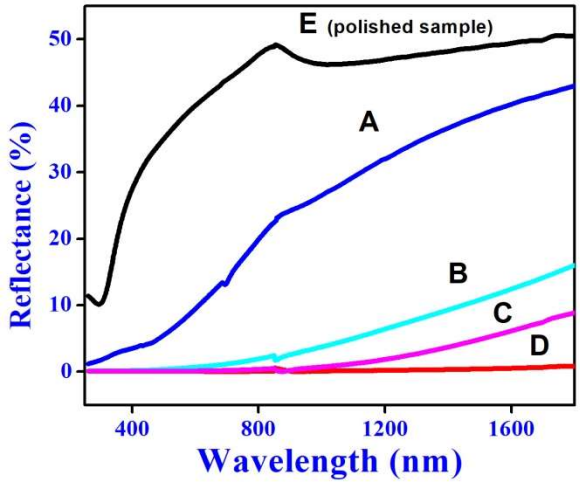

Figure 1: Graph depicts the specular reflection spectra of the nano-structured Ti samples over a wavelength range of 250-1800 nm.

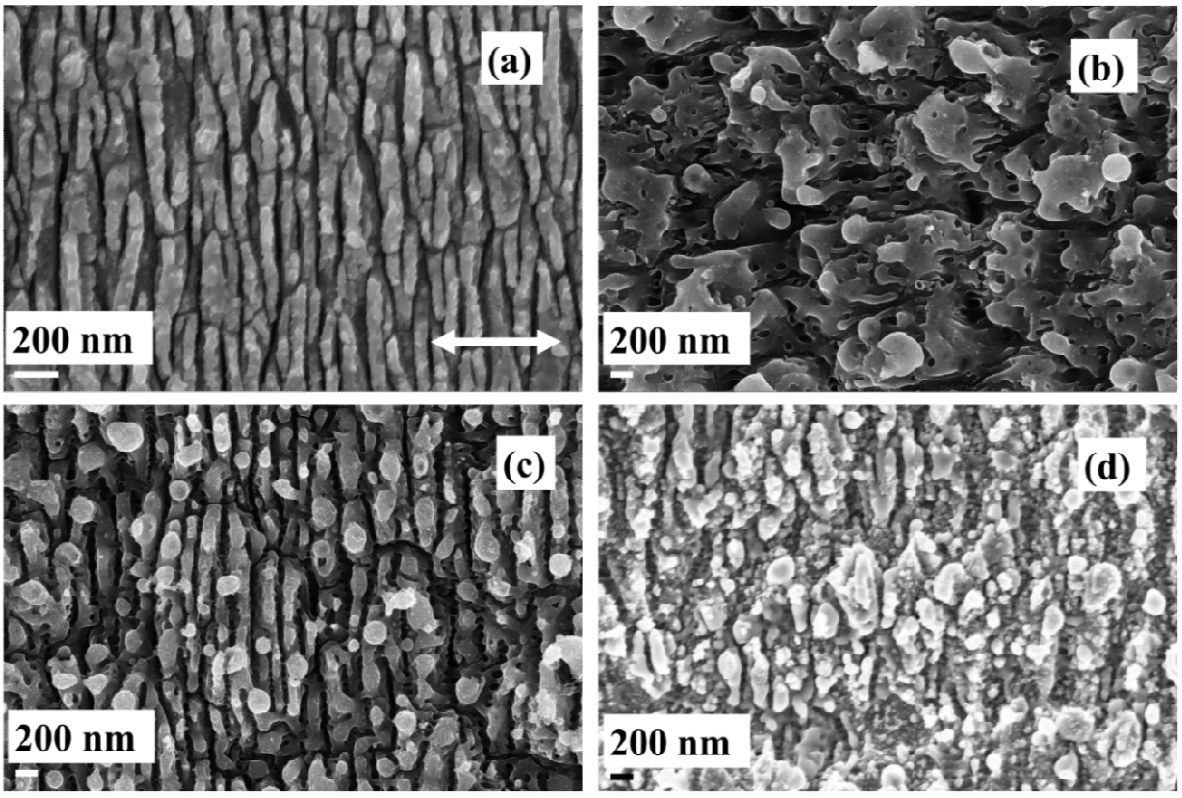

Figure 2: FESEM surface morphologies of the fs laser fabricated Ti surface (a) 0.9 J/cm^2 and scanning speed 0.2 mm/s (b) 1.2 J/cm^2 and scanning speed 0.05mm/s (c) 1.2 J/cm^2 and scanning speed of 0.005 mm/s (d) 1.6 J/cm^{2}and scanning speed 0.2 mm/s. a, b, c shows the morphology under irradiation in water while d shows the morphology under laser irradiation in air.

Figure 2(a) shows the FESEM image of the titanium metal surface processed by fs-laser irradiation with fluence of F = 0.9 J/cm^2 and scanning speed of 0.2 mm/s in ambient water environment. As can be seen, the surface mostly consists of quasi-periodic nano-gratings and nanostructures on the ridges of nano-gratings. These nanostructures and nano-gratings increase the surface area of the metal which leads to the increase in scattering and multiple reflections. The specular reflectance measurements in the wavelength range of 250 nm – 1.8 μm is depicted in curve A of figure 1. This surface shows a specular reflectance of < 5 % in the ultraviolet region of electromagnetic spectrum and about 40 % reflectance at the wavelength of 1.8 μm. The periodic ripple is oriented at right angles to the polarization direction. The average periodicity (Λ) measured is about $\Lambda\sim$ 200 nm. If $\Lambda < \lambda$, it has been established/demonstrated that sub-wavelength gratings ($\Lambda < \lambda$) have antireflection effect and only zero order diffraction effect exists, while higher order diffraction effects are evanescent. The effect of sub-wavelength gratings (SWGs) can be described by effective medium theory [41-44]. When the grating period $\Lambda > \lambda$, the light trapping effect is described in the realm of geometrical optics. For $\Lambda \sim \lambda$, in this regime strong diffraction effects occur and surface gratings exhibit antireflection behavior [45, 46]. Figure 2 (b) shows the FESEM image of titanium surface processed under 800 nm fs-laser irradiation with a fluence of F = 1.2 J/cm^2 and scanning speed of 0.05 mm/s in ambient water environment. At these processing parameters, we observed the formation of coral-like surface structures- consisting of random micro-protrusions, nanocavities and nanoparticles. These coral-like structures increase the surface area of the metal surface and act as light absorbers. The spectral measurement of this surface is depicted in curve B of figure (1). We can see that these fs-laser induced coral-like structures show a reflectance of < 1 % in the UV-Vis region of electromagnetic spectrum and reflectance of 15 % in the infrared region at around 1.8 μm. Figure 2 (c) shows the surface morphology of titanium after fs-laser irradiation with fluence of F = 1.2 J/cm^2 and a scanning speed of 0.005 mm/s. The laser irradiation is carried in ambient water environment. The FESEM image shows the formation of periodic ripples covered with nanostructures in the form of nanoparticles and nanocavities. The nanogratings are oriented orthogonal to the laser polarization direction and have average periodicity of Λ ~230 nm. The nanostructure covered gratings show a reflectance of < 1 % in the wavelength range of 250 – 1100 nm. These structures show a reflectance of about 10 % at 1.8 μm wavelength, as depicted in the curve C

of figure (1). Again the low reflectance is attributed to the grating effect and the formation of nanostructures. The interesting modification of the titanium metal surface was achieved by processing the titanium surface in ambient air environment with the incident laser fluence of F = 1.6 J/cm^2 and scanning speed of 0.2 mm/s. Figure 2(d) shows the FESEM surface morphology of titanium after fs-laser irradiation. As can be seen from the figure, the laser treated surface is completely covered with nanoparticles or cluster of nanoparticles with varying size. The spectral measurement shows < 1 % reflectance in the entire studied wavelength range of 250 nm to 1.8 μm. Since the laser irradiation is carried out in ambient air environment, the surface is entirely covered with nanoparticles.

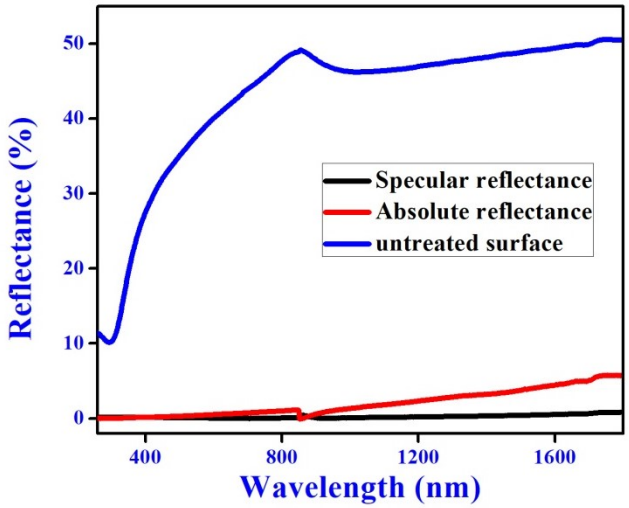

Figure 3: Absolute reflectance and specular reflectance from laser irradiated titanium surface (sample with surface morphology shown in figure 2(d)). For comparison, reflectance of untreated surface is also shown.

Figure (3) shows the comparison of specular reflectance and absolute reflectance of Ti surface of the sample shown in figure 2(d). The absolute reflectance was carried out using 60 mm integrating sphere. We observe that laser induced surface structures have a considerable reflectivity drop over the wavelength range (250 – 1800 nm). The most significant decrease is observed in the range of 250 – 800 nm.

The fs laser induced nanostructures fabricated on the surface of a material affect the reflectance of the surface compared to that of the polished surface. Ionin et al. [47] fabricated large area nano-gratings on GaAs surface under fs laser irradiation, with an average spatial

period of 650 nm and these nano-gratings were found to show a decrease in the specular reflectance of about 42% at a wavelength of ~2.5 μm. In our studies, we observed the formation of periodic surface structures in the form of nanoparticles, nanogrooves, nanocavities and nano-gratings during fs laser irradiation of Ti surface at 800 nm wavelength. All these laser induced structures contribute to the decrease in the surface reflectance of the sample. Surface roughness created by laser irradiation can enhance the absorption of light by multiple reflections and multiple absorptions compared to that of a perfectly flat surface [48]. A.Y. Vorobyev et al. [49] attributed the enhanced absorption to the combined effect of nano-structural and micro-structural surface modifications. Korolkov et al. [50] demonstrated that femtosecond laser induced nanostructures on metals can be used to produce antireflective coatings on polymer replicas. When laser irradiation is carried out in the air environment, the ablated fragments get re-deposited and solidify on the laser processed region, which might have also contributed to the reduction in the reflectivity.

5.4 Conclusion

Exploiting the ability of fs lasers to modify the surface properties of materials, we fabricated different structures on titanium surface in the form of periodic gratings, coral-like structures and nanoparticles. The spectroscopic measurements reveal that reflectance of titanium surface is greatly reduced due to these surface structures. We observed the reflectance of < 1 % in the wavelength range of 250 nm to 1.8 μm, when the surface structuring is carried in ambient air environment with fluence of F = 1.6 J/cm^2 and scanning speed of 0.2 mm/s.

5.5 References

1. Iaroslav Gnilitskyi, Thibault J.Y. Derrien, Yoann Levy, Nadezhda M. Bulgakova , Tomáš Mocek & Leonardo Orazi, Scientific Reports, 7, 8485 (2017).
2. P. Gregorcic et al., Appl. Surf. Sci. 387 (2016) 698–706.
3. C. Albu et al., Appl. Surf. Sci. 278 (2013) 347–351.
4. B. Tan, K. Venkatakrishnan, J. Micromech. Microeng. 16 (5) (2006) 1080–1085.
5. T.Q. Jia et al., Phys. Rev. B. 72 (12) (2005).
6. X. Ji et al., Appl. Surf. Sci. 326 (2015) 216–221.

7. M. Huang, F. Zhao, Y. Cheng, N. Xu, Z. Xu, ACS Nano 3 (2009) 4062–4070.
8. V.T. Rathod, D. Roy Mahapatra, Anjana Jain , A. Gayathri, Sensors and Actuators A 163 (2010) 164–171.
9. Esther Rebollar, Mikel Sanz, Susana Perez, Margarita Hernandez, Ignacio Martin-Fabiani, Daniel R. Rueda, Tiberio A. Ezquerra, Concepcion Domingo and Marta Castillejo, Phys. Chem. Chem. Phys., 2012, 14, 15699–15705.
10. Marta Castillejo, Tiberio A. Ezquerra, Margarita Martin, Mohamed Oujja, Susana Perez, and Esther Rebollar, AIP Conf. Proc. 1464, 372 (2012).
11. Susana Perez, Esther Rebollar, Mohamed Oujja, Margarita Martín, and Marta Castillejo, Appl Phys A (2013) 110:683–690.
12. Y. Shimotsuma, P.G. Kazansky, J. Qiu, K. Hirao, Phys. Rev. Lett. 91 (2003) 247405.
13. V.R. Bhardwaj, E. Simova, P.P. Rajeev, C. Hnatovsky, R.S. Taylor, D.M. Rayner, P.B. Corkum, Phys. Rev. Lett. 96 (2006) 057404.
14. M.S. Ahsan, M.S. Lee, J. Laser Micro/Nanoeng. 7 (2012) 202–207.
15. C. Hnatovsky, R.S. Taylor, P.P. Rajeev, E. Simova, V.R. Bhardwai, D.M. Rayner,P.B. Corkum, Appl. Phys. Lett. 87 (1) (2005) 014104
16. M. Rohloff, S.K. Das, S. Höhm, R. Grunwald, A. Rosenfeld, J. Krüger, J. Bonse, J. Appl. Phys. 110 (1) (2011) 014910.
17. R. Le Harzic, H. Schuck, D. Sauer, T. Anhut, I. Riemann, K. König, Opt. Express 13 (2005)6651–6656.
18. A. Borowiec, H.K. Haugen, Applied Physics Letters 82 (2003) 4462–4464.
19. A.Y. Vorobyev, C. Guo, Laser Photon. Rev. 7 (2013) 385–407.
20. A.Y. Vorobyev, C. Guo, Opt. Express 14 (2006) 2164–2169.
21. A.Y. Vorobyev, C. Guo, Adv. Mech. Eng. 2010 (2010) 1–4.
22. M.S. Ahsan, F. Ahmed, Y.G. Kim, M.S. Lee, M.B.G. Jun, Appl. Surf. Sci. 257 (2011) 7771–7777.
23. A.Y. Vorobyev, C. Guo, Opt. Photonics News 19 (2008), 30-30.
24. A.Y. Vorobyev, C. Guo, Appl. Phys. Lett. 92 (2008) 041914.
25. V.V. Iyengar, B.K. Nayak, K.L. More, H.M. Meyer, M.D. Biegalski, J.V. Li, et al., Sol. Energy Mater. Sol. Cells. 95 (2011) 2745–2751.

26. R. Torres, V. Vervisch, M. Halbwax, T. Sarnet, P. Delaporte, M. Sentis, J. Optoelectron. Adv. Mater. 12 (2010) 621–625.
27. T. Sarnet, M. Halbwax, R. Torres, P. Delaporte, M. Sentis, S. Martinuzzi, et al., Proc. of SPIE 6881 (2008), 688119.1-688119.15.
28. W. A. Murray and W. L. Barnes, Adv. Mater.(Weinheim, Ger.) 19, 3771 (2007).
29. J. B. Pendry, L. Martin-Moreno, and F. J. Garcia-Vidal, Science 305, 847 (2004).
30. R. W. Wood, Philos. Mag. 4, 396 (1902).
31. J. Le Perchec, P. Quémerais, A. Barbara, and T. López-Rios, Phys. Rev. Lett. 100, 066408 (2008).
32. M. C. Hutley and D. Maystre, Opt. Commun. 19, 431(1976).
33. Hessel and A. A. Oliner, Appl. Opt. 4, 1275 (1965).
34. D. Maystre, in Electromagnetic Surface Modes, A. D. Boardman, ed. (Wiley, 1982), Chap. 17.
35. V.V. Iyengar, B.K. Nayak, K.L. More, H.M. Meyer, M.D. Biegalski, J.V. Li, et al., Sol. EnergyMater. Sol. Cells. 95 (2011) 2745–2751.
36. R. Torres, V. Vervisch, M. Halbwax, T. Sarnet, P. Delaporte, M. Sentis, J. Optoelectron. Adv. Mater. 12 (2010) 621–625.
37. T. Sarnet, M. Halbwax, R. Torres, P. Delaporte, M. Sentis, S. Martinuzzi, et al., Proc. of SPIE 6881(2008), 688119.1-688119.15.
38. L. Chen, H. K. Seo, Z. Mao, Y. M. Jung , B. Zhao , *Anal. Methods* 2011, *3*, 1622.
39. J. Yin , Y. S. Zang , C. Yue , Z. M. Wu , S. T. Wu , J. Li , Z. H. Wu , *J. Mater. Chem.* 2012, *22*, 7902.
40. X.-D. Lin, V. Uzayisenga, J.-F. Li, P.-P. Fang, D.-Y. Wu, B. Ren, Z.-Q. Tian, *J. Raman Spectrosc.* 2012, *43*, 40.
41. E. N. Glytsis and T. K. Gaylord, Appl. Opt. **31**(22), 4459–4470 (1992).
42. D. H. Raguin and G. M. Morris, Appl. Opt. **32**(14), 2582–2598 (1993).
43. Y.-F. Huang, S. Chattopadhyay, Y.-J. Jen, C.-Y. Peng, T.-A. Liu, Y.-K. Hsu, C.-L. Pan, H.-C. Lo, C.-H. Hsu, Y.-H. Chang, C.-S. Lee, K.-H. Chen, and L.-C. Chen, Nat. Nanotechnol. **2**(12), 770–774 (2007).
44. D. L. Brundrett, T. K. Gaylord, and E. N. Glytsis, Appl. Opt. **37**(13), 2534–2541 (1998).

45. R. E. Smith, M. E. Warren, J. R. Wendt, and G. A. Vawter, Opt. Lett. **21**(15), 1201–1203 (1996).
46. D. H. Raguin and G. M. Morris, Appl. Opt. **32**(14), 2582–2598 (1993).
47. A. A. Ionin, Y. M. Klimachev, A. Y. Kozlov, S. I. Kudryashov, A. E. Ligachev, S. V. Makarov, L. V. Seleznev, D. V. Sinitsyn, A. A. Rudenko, R. A. Khmelnitsky, Applied Phys. B 111 (2013) 419-423.
48. L. K. Ang, Y. Y. Lau, R. M. Gilgenbach, H. L. Spindler, Applied Physics Letters 70 (1997) 696-698.
49. A.Y. Vorobyev, C. Guo, Physical Review B 72(2005) 195422 1-5.
50. V. P. Korolkov, A. A. Ionin, S. I. Kudryashov, L. V. Seleznev, D. V. Sinitsyn, R. V. Samsonov, A. I. Masliy, A. Zh. Medvedev, B.G. Goldenberg, Quantum Electronics 41 (2011) 387-392.

CHAPTER-6

Femtosecond laser induced quasi-periodic nano-ripples on graphite surface and formation of novel carbon nano-structures

Abstract

Here, we studied the effect of fs-laser irradiation on graphite surface in ambient air and water environments at 800 nm wavelength. Surface morphology characterized through FESEM reveal the formation of Deep sub-wavelength nanogratings oriented orthogonal to the polarization direction with ripple period Λ = 130, 150, 200, and 230 nm in ambient air environment. Analysis of aqueous solution through TEM imaging, reveal the formation of graphene quantum dots (GQDs) and graphitic flakes during fs-laser irradiation. We also discuss the effect of laser irradiation on the Raman peaks of graphite, formation of different carbon nanostructures under fs laser irradiation of graphite in ambient water environment.

6.1 Introduction

Material processing with ultrashort lasers has become an active area of research. Scientists are interested to understand the basic mechanism of interaction between high intense lasers and materials. Apart from the fundamental research, lasers have many applications in industry (cutting, drilling etc), surface processing and chemical processing. Nano-structuring of materials using lasers have found lot of applications in photonics, optical bio-sensing, nanofluidics, biomedicine etc. many of these applications involve surface processing of materials to modify the optical, mechanical or chemical properties of the surface. Many studies have shown LIPSS can be produced using fs laser pulses on semiconductors [1-2], dielectrics [3-7], metals [8-12] and polymers [13-16].

Material ablation and subsequent removal from solid surface upon laser irradiation started in 1960, just after the invention of first laser [17]. Thereafter, the technique of "pulsed laser ablation (PLA)" has been used for deposition of thin films and clusters, nanoparticle synthesis, micromachining of materials and cleaning of surfaces. PLA of solid target immersed in liquid environment, involves a simple experimental arrangement compared to other methods used for fabrication of nanomaterials [18-19]. However, the reactions involved at solid-liquid interface under laser ablation are complex in nature. This makes the technique less exploited for theoretical and simulation modelling. Laser ablation under liquid confinement involves the formation of plasma, plasma expansion under liquid confinement, reaction between the different plasma species so formed with the liquid environment and finally condensation to form nanomaterials [20-22]. The NPs produced by PLA in liquids can conjugate almost five times more number of bio-molecules on the surface compared to the NPs produced by chemical methods [23-24]. NPs and aggregates synthesized through laser ablation in liquids provide comparatively higher signal to noise ratio when used as SERS substrates [25-26].

Carbon based nano-structures such as carbon nanotubes, graphene quantum dots (GQDs), etc have become very important materials in nanotechnology [27-31]. There are methods to transfer one form of nanocarbon to another form, which involves either the use of tedious chemical procedures or high-end instrumentation [32, 33]. Thus, there is an important

need for easy and feasible fabrication methods. Femtosecond laser irradiation of a target material in liquid environment has proved to be one such method. Hu et al, reported the synthesis of sp-bonded carbon chain on graphite surface under fs laser irradiation in liquid environment [34]. Russo et al, demonstrated the synthesis of GQDs by fs laser ablation of graphite target in ambient water environment [35].

We demonstrate a simple and green approach for the synthesis of different carbon nanostructures such as GQDs, nano-graphitic sheets by single step fs laser irradiation of graphite surface in ambient water environment. Nano-carbon based materials have become popular in many areas that include drug delivery, hydrogen storage, nano-catalysis, etc.

Here, we discuss the formation of LIPSS on graphite surface under fs-laser irradiation at 800 nm in ambient air. We discuss the formation of graphene quantum dots, porous graphene and other nano-graphitic flakes, formed during fs laser irradiation of graphite target immersed in water environment. We also discuss the difference in micro Raman spectra on laser irradiated graphite and un-irradiated graphite surface.

6.2 Results and discussion:

6.2.1 HSFL or deep sub-wavelength nano-gratings on graphite surface:

We discuss the formation of quasi-periodic nanogratings on the graphite surface under appropriate irradiation conditions of fluence (F) and pulse number (N). Figure (1) shows the surface morphology of the graphite surface, evolved after fs-laser irradiation with 800 nm wavelength in ambient air. The number of pulses irradiated on the sample is N ~ 3000 pulses at the fluence F = 1.33 J/cm^2. The FESEM image reveals that surface topography evolved after fs laser irradiation is uneven and contains certain depressed and low-lying regions as shown by the circles. It appears that some parts of the parent ripple get broken and fly off randomly. The rectangles in figure (1) show some of these broken ridges. The detaching of the ridges from the parent ripple implies that a strong localized shock may exist in the grooves during the ablation process. The nano-ripples are quasi-periodic in nature and oriented orthogonal to the incident laser polarization direction. The double headed solid arrow represents the incident laser polarization and single headed dashed arrow represents the writing direction.

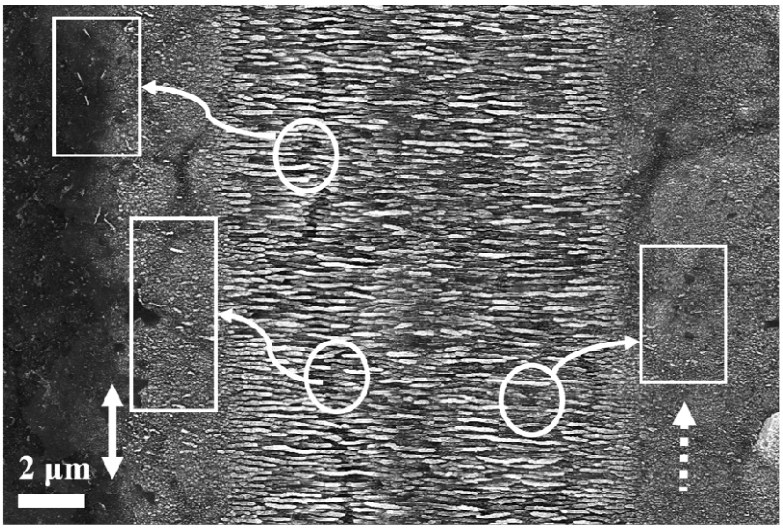

Figure 1: Surface morphology of graphite surface irradiated by linearly polarized 800 nm fs laser pulses. The incident laser fluence is F=1.33 J/cm^2 and pulse number N ~3000. Double headed solid arrow represents the polarization and single headed dashed arrow represents the writing direction.

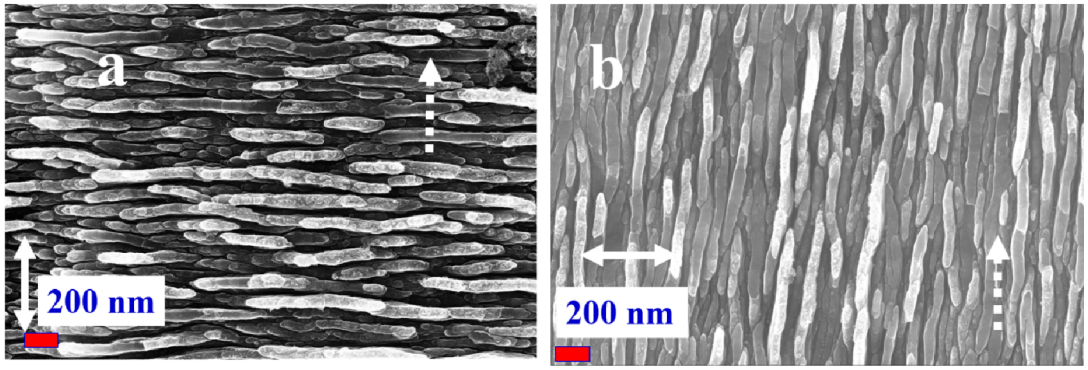

Figure 2: FESEM image reveals the polarization dependence of nanograting formation on the graphite surface irradiated with fs laser pulses at 800 nm wavelength in ambient air environment, F=1.33 J/cm^2 and N =3000. Incident laser polarization shown by double headed arrow (a) along the writing direction (b) perpendicular to the writing direction.

We observed that the nanograting formation on graphite depend upon polarization and oriented orthogonal to the incident laser polarization direction. Figure (2) shows the surface morphology of graphite evolved after irradiating with fs laser pulses at 800 nm wavelength, N = 3000 and F = 1.33 J/cm^2. In figure 2(a) the incident laser polarization is parallel to the writing direction. In figure 2(b) the incident laser polarization is perpendicular to the writing direction. One interesting feature we observed on graphite surface under fs laser irradiation is the formation of quasi-periodic nano-gratings with variable grating period as shown in figure

3. The observed grating period varies from 130 nm to 230 nm. Since the grating period is much smaller than the incident laser wavelength, they are assigned as HSFL or deep sub-wavelength quasi-periodic nano-gratings.

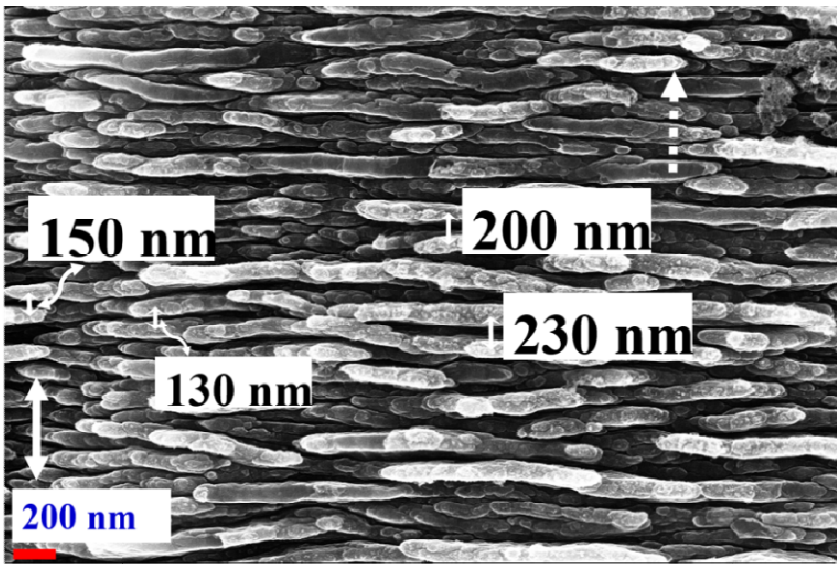

Figure 3: Surface morphology of graphite irradiated at 800 nm wavelength fs laser pulses with F = 1.33 J/cm^2 and N = 3000. FESEM image reveals the formation of quasi-periodic nanogratings with variable periodicities within the irradiated region.

Figure (4) shows the surface morphology of graphite evolved after irradiating with linearly polarized fs laser pulses at 800 nm wavelength in the water environment. We observed the formation of conical nanostructures on graphite surface, at the laser fluence of 0.93 J/cm^2 and pulse number N ~ 2000. The graphite target is immersed in water and then laser irradiated. The liquid after laser irradiation, is collected and analyzed through TEM, PL, FESEM and Raman spectroscopy.

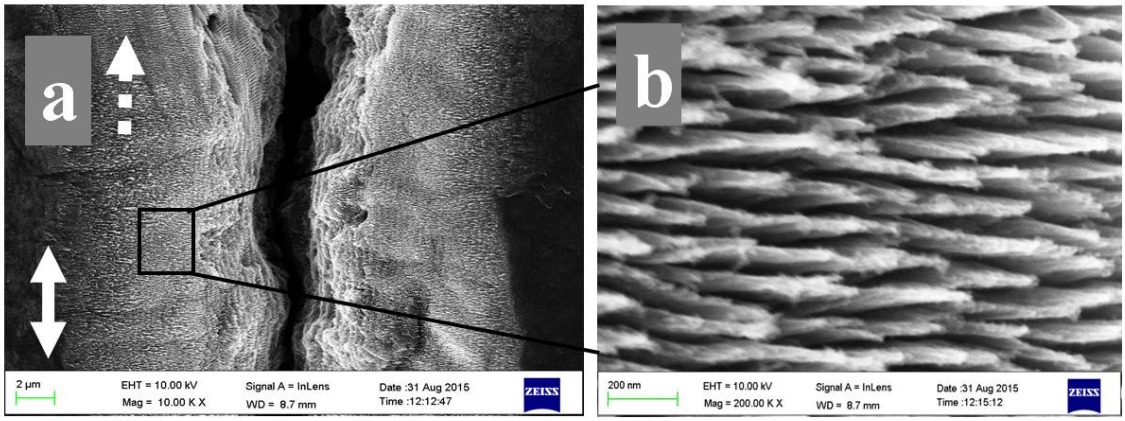

Figure 4: FESEM image showing surface morphology evolved after fs laser irradiation of graphite target in water environment, at the laser fluence of 0.93 J/cm^{2}and pulse number ~2000. (b) is the magnified image of (a) showing the formation of conical nanostructures. Double headed solid arrow represents the polarization direction and single headed dashed arrow represents the writing direction.

6.2.2 Raman studies:

Raman spectroscopy is an important spectroscopic tool to probe the defects in graphite and other related samples through the changes in the defect induced Raman peaks such as D and D′ modes. There are also Raman peaks G and 2D (G′) that are related to the vibrational modes of carbon. In general, G band arises due to the in-plane vibrations of the sp^2 bonded carbon atoms. D band arises due to the disorder or defects in the sp^2 bonded carbon atoms [36, 37]. Figure (5) shows the comparison of Raman spectra of the fs laser irradiated graphite surface and un-irradiated graphite surface. From the Raman spectra of the irradiated graphite it is clearly observed that the G band intensity reduces, which indicates that the sp^2 carbon atoms reduce in the irradiated region and at the same time an increase in the disorder is seen as observed from the increase in the D band intensity. The sp^2 crystallinity of the graphite is destroyed at the irradiated region due to high intensity of incident laser pulse. For un-irradiated sample, the value of the disorder parameter defined by the ratio of intensities of the D mode with that of the G mode is 0.03, where as for the fs laser irradiated sample it becomes 4.05, this indicates the formation of defects at the irradiated site. According to this value the defects formed may be like vacancy type defects or SP^3 bonded chains on the graphite surface [38]. The G and D band vibrations of the graphene are observed as shown in Figure (5). On

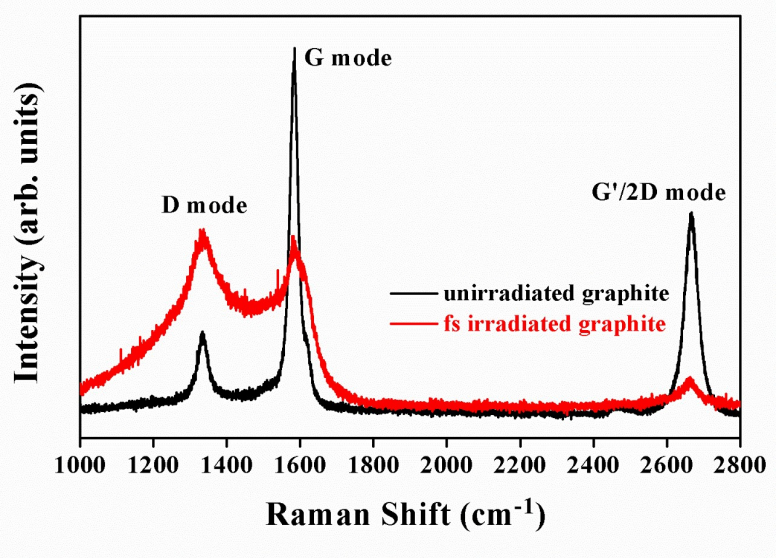

Figure 5: Micro Raman spectra of the fs laser irradiated graphite surface at the irradiation conditions (F=1.33 J/cm^2 and N =3000) compared to that of the un-irradiated graphite surface.

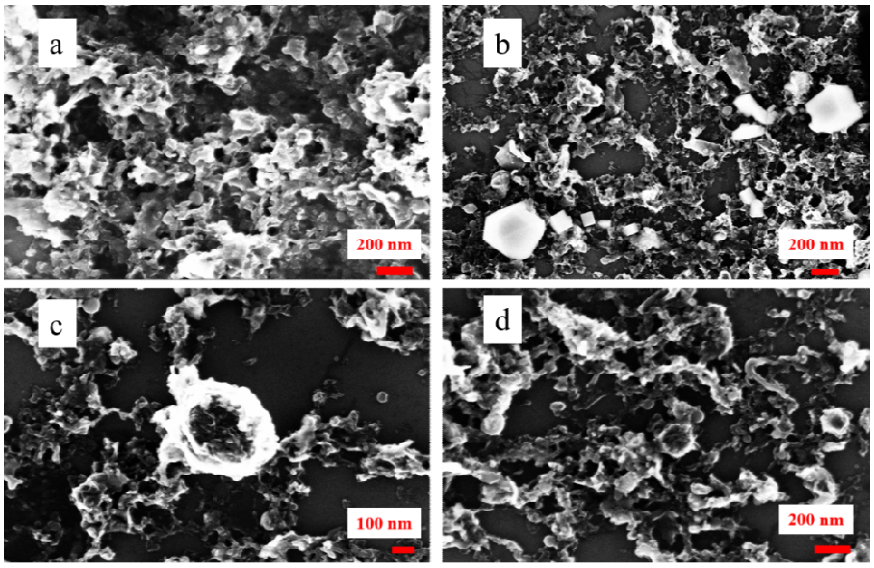

Figure 6: FESEM image of the debris collected on a glass plate after laser irradiation shows the graphene flakes and graphitic carbon structures. (a) shows the porous structures, (b) shows the cubic and other diamond like structures, (c) and (d) represents the other different nano graphitic flakes and forms.

the other hand, with the increase in laser fluence, initially the G band shows high intensity and with the increase in fluence it is observed that the intensity of the D band is more than that of the G band. The evolution of the D band in the irradiated graphite indicates that the edge defects are dominating at the high irradiation fluence. Figure (6) shows the morphology of the

debris collected on a glass plate after laser irradiation of graphite surface. FESEM images show the formation of different forms of the nanographite structures, such as porous graphite (Figure 6(a)), cubic and diamond like carbon nanostructures (figure 6(b)) have been formed as a result of fs laser irradiation.

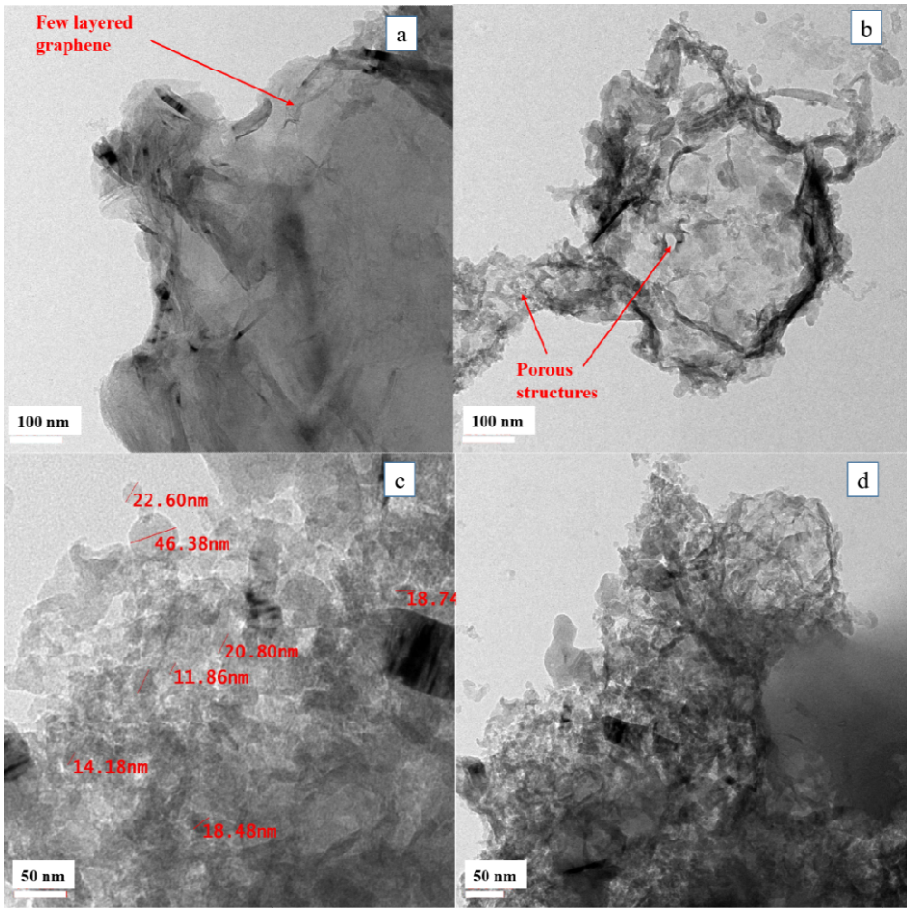

Figure 7: TEM image shows the formation of (a) graphene flakes and (b) porous graphene, (c) and (d) the porous network and nano-graphene related structure after fs laser irradiation of graphite surface.

Figure (7) show the TEM images of the debris collected on TEM grids after laser irradiation of graphite surface. The images show the layers detached from the graphite due to laser irradiation. These isolated layers exhibit a corrugated surface. Moreover, the layers also exhibited a discontinuous surface where some holes were detected, as clearly seen in the higher magnification and show the presence of suspended layers of the graphene, porous graphene and NPs.

6.2.3 Synthesis of carbon nanostructures by laser irradiation of graphite target in ambient water environment:

We observed the formation of novel carbon nanostructures when the fs laser irradiation is done on graphite target immersed in water medium. The observed carbon nanostructures include GQDs and other graphene related nano-carbon products such as few layered graphene etc. Under fs laser irradiation of graphite target in ambient water environment, the surface of graphite is evaporated by the incident laser pulses and in turn produces plasma plume on the surface of the graphite. The plasma plume expands and then condenses thereby generating nanoparticles of graphite, nano-graphene, graphene quantum dots. The properties of these generated nanostructures depend on laser irradiation parameters. Figure 8(a) shows the absorption spectra of the colloidal solution of GQDs. It shows two absorption bands at 260 and 400 nm. The peak at 260 nm is generally observed for smaller sized GQDs in the solution and is generally attributed to π-π* transition of electrons and it matches well with the reported values [39, 40]. The observed peak at 400 nm may be due to larger sized structures formed in the solution when irradiated with fs laser pulses. The photoluminescence (PL) spectrum of GQDs is shown in figure 8(b). The GQDs show a strong blue luminescence as seen in the figure. The PL emission from the GQDs can be tailored with their size [41]. The reason for this emission from nano-sized carbon materials which include GQDs and other nano-carbon structures, may be due to the optical confinement of quantum

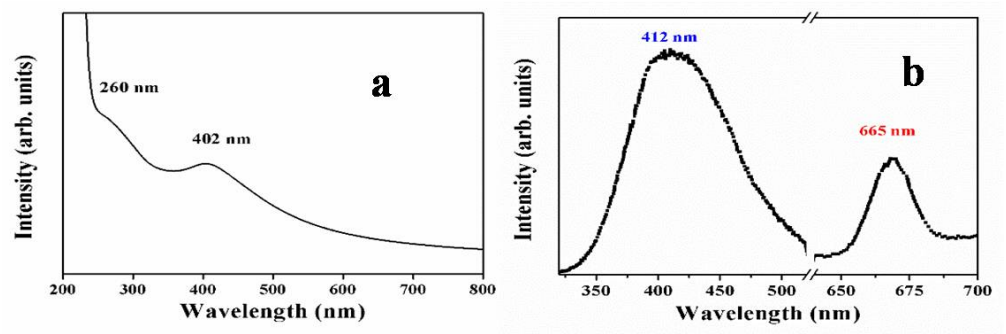

Figure 8: Shows the absorption spectrum of GQDs and strong luminescence from the GQDs in water.

sizes and defects present in the GQDs [42]. Apart from the blue luminescence centered at 412 nm we have also observed slightly weaker luminescence band at around 660 nm (red), which may be due to the larger sized NPs formed in the laser irradiation process. In the TEM images, we have observed such larger sized particles.

6.2.4 TEM studies:

Transmission electron microscopy (TEM) has been used to study the size distribution of GQDs and to observe the formation of different nano-carbon products, formed after laser irradiation of graphite in water environment. For recording the TEM images, the colloidal solution was drop casted onto copper grid. Figure (9) shows the TEM images of the GQDs. We observed the average size to be around 2-4 nm. These GQDs are observed to form over a graphitic layer and at some places they are embedded within it. Figure (10) shows the TEM images of the graphene flakes, few layered graphene along with the formation of porous graphene.

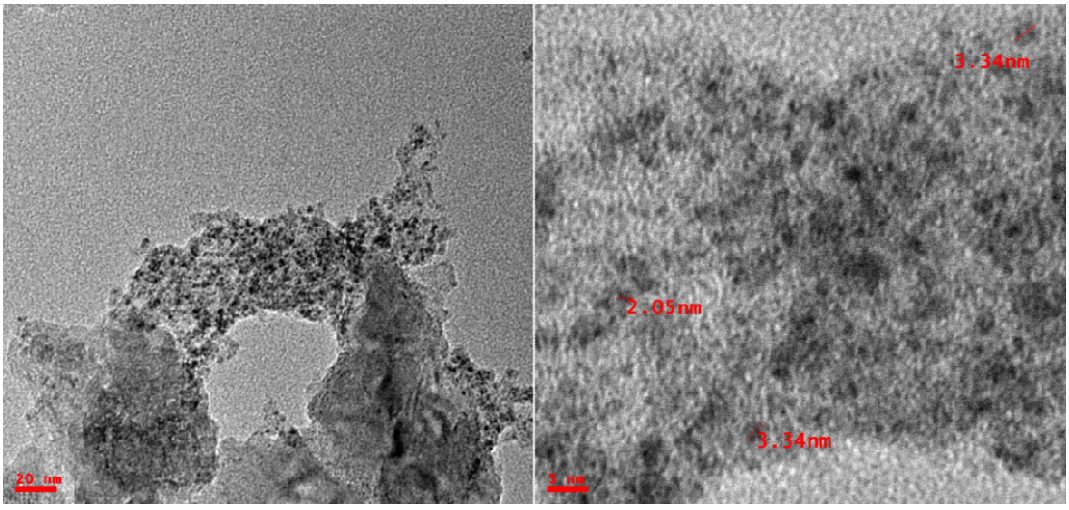

Figure 9: TEM images show the formation of graphene quantum dots under fs laser irradiation of graphite target in water environment.

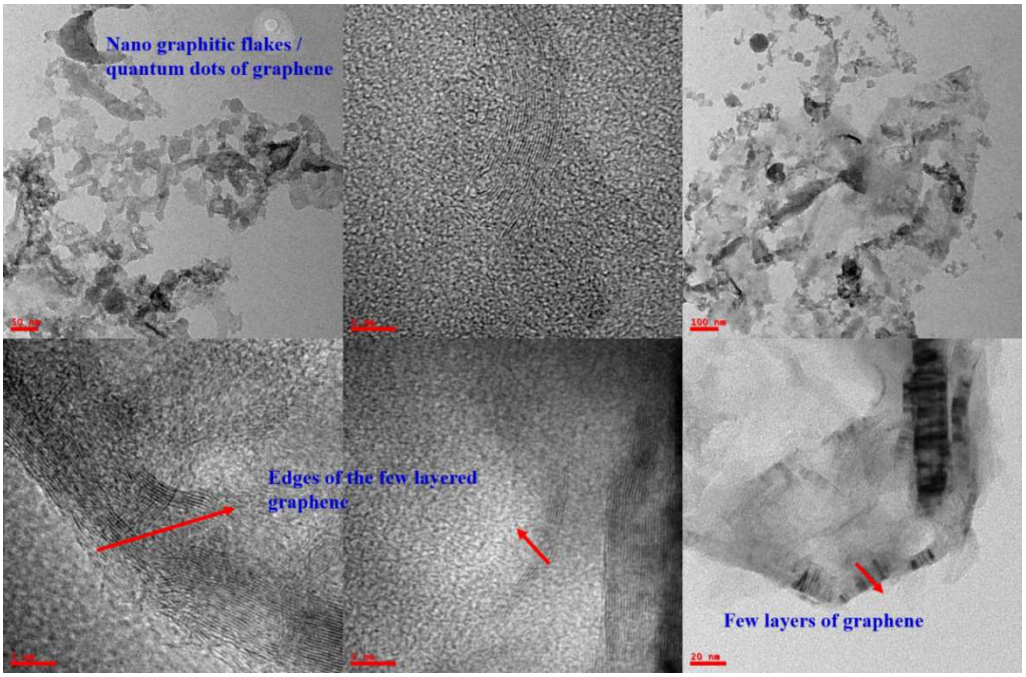

Figure 10: TEM micrograph shows the folded graphene flakes and the few layered graphene edges formed after laser irradiation of graphite target immersed in water.

6.2.5 Micro Raman studies:

Raman spectroscopy is an important spectroscopic tool for studying the properties of carbon based compounds. The general features of the Raman spectra of the graphite consist of major peaks at 1580 cm^{-1} (G Band), 1330 cm^{-1} (D Band) and 2690 cm^{-1} (2D Band). We observed that drop casted colloidal solution has shown all these important micro Raman peaks

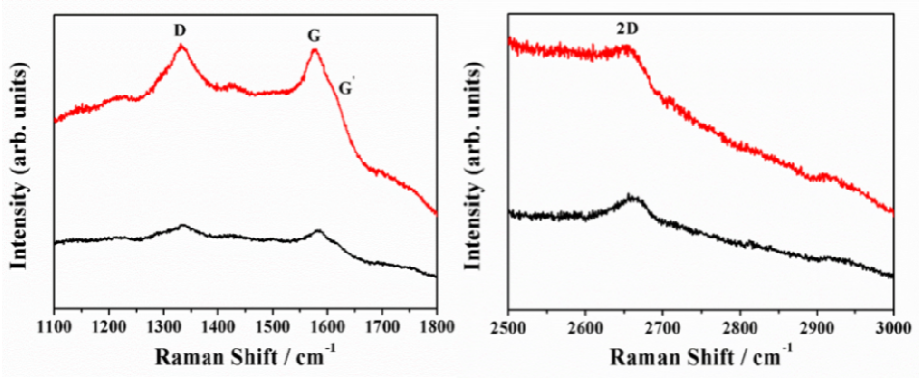

Figure 11: Raman spectra of the colloidal solution drop casted on a cover-slip, showing the presence of GQDs with D, G, 2D modes.

related to GQDs, formed in the water under fs irradiation at 800 nm wavelength. The Raman spectrum is shown in Figure (11). It is observed that Raman peaks are very weak in intensity and the spectra are broad, so to see the Raman modes of vibration clearly, we have coated the glass plate with Au NP colloids and then drop casted the colloidal solution containing GQDs and other carbon nano-structures on the top (a schematic is shown in the inset of figure 12). The surface enhanced Raman scattering due the presence of Au NPs enhances the Raman spectra of colloids containing GQDs, the respective SERS spectra is shown in Figure 12. Here we have observed more peaks in the Raman spectra apart from the regular D and G modes of the graphite related compounds with good resolution and high enhancement. The additional peaks are observed at 1140 cm^{-1}, 1212 cm^{-1}, 1305 cm^{-1}, 1450 cm^{-1}, and 1530 cm^{-1}, along with the regular D and G modes at 1340 cm^{-1} and 1580 cm^{-1}. We observed an increase in intensity of all these peaks because of the influence of surface plasmonic enhancement, due

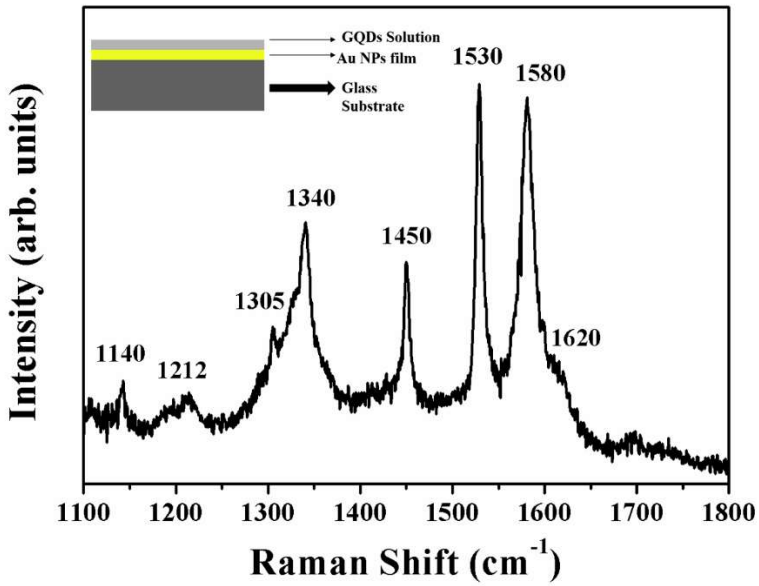

Figure 12: SERS spectra of the colloidal solution drop casted on cover slip containing Au NPs. The inset shows the schematic of the SERS measurements.

to the addition of Au NPs [43-45]. The peak existing at 1140 cm^{-1} usually present in the samples containing few nm sized carbon nanoclusters of sp^2-sp^3 bonded carbon atoms. In some cases, it was reported that, this peak may appear at slightly lower wavenumbers of 1120 cm^{-1} due to sp^3 bonded carbon nano-clusters. In general, this occurs because of few nm sized

carbon clusters due to the C-C bond stretching modes of vibration and it appears mostly in the polyene like structures and nanocrystalline diamond samples [46-48]. The peak present at 1450 cm^{-1} confirms the existence of the trans-polyacetylene [trans-(CH)x] chains with different CH chain lengths [49, 50]. This peak generally appears in the trans-(CH)x molecules due to the sum and difference combinations of stretching in the C=C chain and wagging in CH vibrational modes [51]. The peak observed at 1530 cm^{-1} appears in general due to phenyl ring stretching of neutral poly (p phenylene vinylene) molecule [52, 53]. The peaks at 1305 cm^{-1} and 1340 cm^{-1} normally indicate the disorder induced peaks [54]. Overall, we have observed that the fabrication of different carbon related nanostructures under the fs laser irradiation of graphite surface at 800 nm wavelength in air and water environments. The formation of these cabon nano-structures purely depend on laser irradiation parameters such as fluence and surrounding environment. Different kinds of carbon species such as carbyne and trans-polyacetylene chains have been observed along with the formation of nano-porous graphene and GQDs.

6.3 Conclusion

Polarization controlled quasi-periodic nano-gratings have been observed on graphite surface when irradiated with fs laser pulses in ambient air. FESEM reveal the formation of ripples with grating period 130-230 nm. We observed the formation of carbon nano-structures such as GQDs and graphitic flakes dispersed in solution under fs laser irradiation of graphite target in ambient water environment. Blue luminescent GQDs have been observed in water with average dimensions of 2-4 nm.

6.4 References

1. R. Le Harzic, H. Schuck, D. Sauer, T. Anhut, I. Riemann, K. König, Opt. Express 13 (2005)6651–6656.
2. A. Borowiec, H.K. Haugen, Applied Physics Letters 82 (2003) 4462–4464.
3. Y. Shimotsuma, P.G. Kazansky, J. Qiu, K. Hirao, Phys. Rev. Lett. 91 (2003) 247405.
4. V.R. Bhardwaj, E. Simova, P.P. Rajeev, C. Hnatovsky, R.S. Taylor, D.M. Rayner, P.B. Corkum, Phys. Rev. Lett. 96 (2006) 057404.
5. M.S. Ahsan, M.S. Lee, J. Laser Micro/Nanoeng. 7 (2012) 202–207.

6. C. Hnatovsky, R.S. Taylor, P.P. Rajeev, E. Simova, V.R. Bhardwai, D.M. Rayner,P.B. Corkum, Appl. Phys. Lett. 87 (1) (2005) 014104
7. M. Rohloff, S.K. Das, S. Höhm, R. Grunwald, A. Rosenfeld, J. Krüger, J. Bonse, J. Appl. Phys. 110 (1) (2011) 014910.
8. L. Qi, K. Nishii, Y. Namba, Opt. Lett. 34 (2009) 1846–1848.
9. S. Sakabe, M. Hashida, S. Tokita, S. Namba, K. Okamuro, Phys. Rev. B: Condens. Matter 79 (2009) 033409.
10. M.S. Ahsan, Y.G. Kim, M.S. Lee, J. Laser Micro/Nanoeng. 7 (2012) 164–170.
11. J.P. Colombier, F. Garrelie, N. Faure, S. Reynaud, M. Bounhalli, E. Audouard, R. Stoian, F. Pigeon, J. Appl. Phys. 111 (2012) 024902.
12. S.R.J. Brueck, D.J. Ehrlich, Phys. Rev.Lett. 48 (1982) 1678–1681.
13. V.T. Rathod, D. Roy Mahapatra, Anjana Jain , A. Gayathri, Sensors and Actuators A 163 (2010) 164–171.
14. Esther Rebollar, Mikel Sanz, Susana Perez, Margarita Hernandez, Ignacio Martin-Fabiani, Daniel R. Rueda, Tiberio A. Ezquerra, Concepcion Domingo and Marta Castillejo, Phys. Chem. Chem. Phys., 2012, 14, 15699–15705.
15. Marta Castillejo, Tiberio A. Ezquerra, Margarita Martin, Mohamed Oujja, Susana Perez, and Esther Rebollar, AIP Conf. Proc. 1464, 372 (2012).
16. Susana Perez, Esther Rebollar, Mohamed Oujja, Margarita Martín, and Marta Castillejo, Appl Phys A (2013) 110:683–690.
17. T. H. Maiman, Nature, 187, 493-494 (1960).
18. P. P. Patil, D. M. Phase, S. A. Kulkarni, S. V. Ghaisas, S. K. Kulkarni, S. M. Kanetkar, and S. B. Ogale, Physical Review Letters, 58, 238-241 (1987).
19. Qi Chen and Z. John Zhang, Applied Physics Letters, 73, 3156-3158 (1998).
20. OguzYavas and Paul Leiderer, Physical Review Letters, 72, 2021-2024 (1994).
21. O. Yavas, P. Leiderer, H. K. Park, C. P. Grigoropoulos, C. C. Poon, W. P. Leung, N. Do, A. C. Tam, Appl. Phys. A, 58, 407-415 (1994).
22. Hee K. Park and Costas P. Grigoropoulos, Appl. Phys. Lett. 68, 596-598 (1996).
23. A. V. Simakin, V. V. Voronov, N. A. Kirichenko and G. A. Shafeev, Appl. Phys. A, 79, 1127–1132 (2004).
24. Savas Georgiou and AntonisKoubenakis, Chem. Rev., 103, 349−393 (2003).

25. G. X. Chen, M. H. Hong, T. S. Ong, M. Lam, W. Z. Chen, H. I. Elim, W. Ji, and T. C. Chong, Carbon 42, 2735–2737 (2004).
26. Douglas B. Chrisey and Graham K. Hubler, Pulsed Laser Deposition of Thin Films, Wiley-Interscience, New York (1994).
27. P. Avouris, Z. Chen, V. Perebeinos, Nat. Nanotechnol. 2 (2007) 605–615.
28. L.S. Li, X. Yan, J. Phys. Chem. Lett. 1 (2010) 2572–2576.
29. J.J. Adjizian, R. Leghrib, A.A. Koos, I. Suarez-Martinez, A. Crossley, et al., Carbon 66 (2014) 662–673.
30. H. Sun, L. Wu, W. Wei, X. Qu, Mater. Today 16 (2013) 433–442.
31. D.V. Kosynkin, A.L. Higginbotham, A. Sinitskii, J.R. Lomeda, A. Dimiev, B.K. Price, et al., Nature 458 (2009) 872–876.
32. X. Yan, X. Cui, L.S. Li, J. Am. Chem. Soc 132 (2010) 5944–5945.
33. J. Lu, P.S. E.Yeo, C.K. Gan, P. Wu, K.P. Loh, Nat. Nanotechnol. 6 (2011) 247–252.
34. A. Hu, M. Rybachuk, Q.-B. Lu, W.W. Duley, Appl. Phys. Lett. 91 (2007) 131906.
35. P. Russo, A. Hu, G. Compagnini, W.W. Duleyd, Y.Zhoua Norman, Nanoscale 6 (2014) 2381–2389.
36. K. Narendra, A.A. Sagade, G.U. Kulkarni, Adv. Funct. Mater. 21 (2011) 3836–3842.
37. Denis A. Sokolov, C.M. Rouleauc, D.B. Geoheganc, T.M. Orlando, Carbon 53 (2013) 81–89.
38. Zijie Yan, B. Douglas Chrisey, J. Photochem. Photobiol. C: Photochem. Rev. 13 (2012) 204–223.
39. V. Thongpool, A. Phunpueok, V. Piriyawong, S. Limsuwan, P. Limsuwan, Energy Procedia. 34 (2013) 610–616.
40. A. De Giacomo, A. De Bonis, M. Dell'Aglio, O. De Pascale, R. Gaudiuso, S. Orlando, A. Santagata, G.S. Senesi, F. Taccogna, R. Teghil, J. Phys. Chem. C 115 (2011) 5123–5130.
41. S.I. Kudryashov, S.V. Makarov, A.A. Ionin, C.S.R. Nathala, A. Ajami, T. Ganz, A. Assion, W. Husinsky, Opt. Lett. 40 (2015) 4967–4970.
42. M.H. Dar, N. Momen, C. Sahoo, S.R.G. Naraharisetty, D.N. Rao, Laser Phys. Lett. 14 (2017) 2.
43. A.C. Ferrari, Solid State Commun. 143 (2007) 47–57.

44. A.C. Ferrari, J. Robertson, Phys. Rev. B 64 (2001) (075414-1-13).
45. A. Eckmann, A. Felten, A. Mishchenko, L. Britnell, R. Krupke, K.S. Novoselov, et al., Nano Lett. 12 (2012) 3925–3930.
46. J. Zhou, C. Booker, R. Li, X. Zhou, T.-K. Sham, X. Sun, et al., J. Am. Chem. Soc. 129 (2007) 744–745.
47. E. Blanco, G. Blanco, J.M. Gonzalez-Leal, M.C. Barrera, M. Domı´ınguez, M. Ramirez-del-Solar, J. Nanopart. Res. 17 (2015) 214.
48. S. Sarkar, D. Gandla, Y. Venkatesh, P.R. Bangal, S. Ghosh, Y. Yang, S Misra Phys. Chem. Chem. Phys. 18 (2016) 21278–21287.
49. W. Zhang, Y. Liu, X. Meng, T. Ding, Y. Xu, Hao Xu, et al., Phys. Chem. Chem. Phys. 17 (2015) 22361–22366.
50. D. Tan, Y. Yamada, S. Zhou, Y. Shimotsuma, K. Miura, J. Qiu, Nanoscale 5 (2013) 12092–12097.
51. L. Polavarapu, Qing-Hua Xu, Langmuir 24 (2008) 10608–10611.
52. L. Vigderman, E.R. Zubarev, Langmuir 28 (2012) 9034–9040.
53. X.N. He, Y. Gao, M. Mahjouri-Samani, P.N. Black, J. Allen, M. Mitchell, et al., Nanotechnology 23 (2012) 205702.
54. H. Ishida, H. Fukuda, G. Katagiri, A. Ishitani, Appl. Spectrosc. 40 (1986) 322–330.

CHAPTER - 7

Summary and future perspective

In this thesis, our focus is the formation of highly regular LIPSS and their control, on different metals, using a simple and single step experimental technique of laser direct writing (LDW). Our aim is to look for candidates suitable for the formation of LIPSS and achieve control on the period of the LIPSS formed under appropriate irradiation conditions. We have also demonstrated the application of laser induced surface structuring towards fabrication of low reflective surfaces and SERS substrate.

We studied the interaction of linearly polarized fs laser pulses (800 nm wavelength, 110 fs pulse duration, 1kHz repetition rate) with different metals like Ti, Mo, Ni, Fe, Ag and Cu in ambient air and water environments, at near normal incidence, around the ablation threshold. In our experiments, the incident laser beam is fixed while the sample is scanned in the horizontal direction. Our aim is to produce periodic nano-gratings by varying the available experimental parameters. Formation of periodic surface structures is found to vary with fluence, number of pulses, polarization, wavelength, surrounding environment and the material chosen. Surface morphology characterized by FESEM reveals that LSFL for which $0.4 < \Lambda/\lambda < 1$, are always oriented perpendicular to the incident laser polarization, Λ being the ripple period and λ the incident laser wavelength. FESEM also reveals the formation HSFL under appropriate irradiation conditions, characterized by $\Lambda/\lambda < 0.4$, sometimes also known as deep sub-wavelength structures. In case of laser irradiation of Mo surface at 800 nm wavelength in ambient water environment, we observed that between the grooves of LSFL, is the formation of nano-ripples with periodicity as small as $\sim\lambda/40$ and oriented parallel to the laser polarization direction. We have carried out laser induced nano-structuring on Ti surface towards fabrication of low reflective surface. Spectral measurements carried out using JASCO spectrometer with a 60 mm diameter integrating sphere show that laser induced surface nanostructures modify the optical properties of the surface. Surface structuring of titanium is found to suppress the absolute and specular reflectance over the entire studied wavelength range of 250-1800 nm. Polarization controlled quasi-periodic nano-gratings are formed on

graphite surface when irradiated with fs laser at 800 nm wavelength in ambient air environment. Under laser irradiation of graphite target in water environment, we observed the formation of carbon nanostructures such as GQDs and graphitic flakes dispersed in solution. Blue luminescent GQDs have been observed in water with average dimensions of 2-4 nm.

We discuss the formation of highly regular LSFL in the backdrop of SPP excitation and its interaction. We theoretically calculated the SPP decay lengths from the knowledge of real and imaginary parts of the dielectric function of the un-irradiated metal surface at 800 nm wavelength. Though the dielectric function of a metal changes during fs laser irradiation period, we have used the dielectric constant of metals taken from the literature, and then calculated SPP decay length of Mo as ~ 5 μm at air/Mo interface. However, this number could vary a lot during the pulse irradiation period as it produces high density electron plasma. The SPP decay length for air/Ni is ~ 4.5 μm, and for Ti/air interface, it comes out to be ~ 3 μm. The SPP decay length of Ag and Cu is calculated to be ~140 μm and ~ 84 μm respectively in ambient air at wavelength of 800 nm. Out of all the metals studied, Mo shows smooth and highly regular periodic structures. We also find that the materials with absolute value of imaginary part greater than the absolute value of real part exhibit highest regularity of LIPSS formation. Ag and Cu don't show the formation of LSFL at 800 nm fs laser irradiation. It is believed that, for the metals with large SPP decay length, the SPP loses its initial coherence while propagating to long distances and interacting with different scattering centers. Thus, we don't observe highly regular LSFL on these metals at 800 nm laser wavelength. The formation mechanism of HSFL oriented parallel to the laser polarization direction, with period of < 100 nm, could be due to the generation of higher harmonics at interfaces and their interaction with the surface plasmon polaritons. We therefore explain the observation of the HSFL, that are formed between the grooves (prominent in Mo) with period of ~ 20 nm, as due to the generation of higher harmonics of exciting fundamental λ at the interface of the molten state and the bulk metal during the length of the laser pulse. The harmonic, which has its polarization perpendicular to that of the fundamental, would thus lead to the formation of HSFL. Hence, the HSFL are formed perpendicular to the higher harmonics generated at the interface (within the grooves) at the bottom. Independent theoretical studies are planned in this direction to prove our explanation.

We conclude that, out of all the metals studied Ti, Mo, Fe, and Ni are the candidates that give rise to highly regular periodic surface structures at 800 nm laser irradiation under appropriate conditions of fluence and pulse number. We are able to control the LSFL period by change in the incident wavelength, number of pulses, fluence and surrounding medium. The fabrication of LIPSS has got lot of potential applications. Surface nano/micro-structuring of titanium is found to suppress the total and specular reflectance over the entire studied wavelength range of 250-1800 nm. Thus, by fs laser surface processing, it is possible to obtain highly absorptive surfaces without the need of surface coatings or chemical modifications of the material surface. This has got tremendous applications in optical/opto-electronic devices. Different grating structures can also be prepared very easily on any given medium. Preliminary studies have also indicated their application to prepare hydrophobic surfaces with very high contact angles.

List of publications

Related to the thesis work:

1. "Femtosecond laser nanostructuring of titanium metal towards fabrication of low-reflective surfaces over broad wavelength range", **Mudasir H. Dar**, R. Kuladeep, V. Saikiran, Narayana Rao D, Applied Surface Science 371 (2016) 479–487.
2. "Ultrafast laser induced reproducible nano-gratings on molybdenum surface", **Mudasir H Dar**, Nabil A Saad, Chakradhar Sahoo, Sri Ram G Naraharisetty and Narayana Rao Desai, Laser Phys. Lett. 14 (2017) 026101.
3. "Femtosecond laser induced nanostructuring of graphite for the fabrication of quasi-periodic nanogratings and novel carbon nanostructures", V. Saikiran, **Mudasir H. Dar**, D. Narayana Rao, Applied Surface Science 428 (2018) 177–185.

Publications not included in the thesis:

4. "Ultrafast laser induced periodic sub-wavelength aluminum surface structures and nanoparticles in air and liquids", Rajamudili Kuladeep, **Mudasir H. Dar**, K. L. N. Deepak, and D. Narayana Rao, Journal of Applied Physics 116, 113107 (2014).
5. "Investigations on the growth, linear, nonlinear, dielectric tensor and thermal properties of an acidic molecule: diphenylacetic acid single crystal", RO. MU. Jauhar, **Mudasir H. Dar**, P. Vivek, D. Narayana Rao,P. Murugakoothan, Journal of Optics DOI 10.1007/s12596-017-0418-x (2017).
6. "Ultrafast Laser Induced Subwavelength Periodic Surface Structures on Semiconductors/Metals and Application to SERS Studies" V. Saikiran, **Mudasir H Dar**, R. Kuladeep and Narayana Rao Desai, , MRS Advances, June 2016, pp 1 – 11.
7. "Saturable and reverse saturable absorption of a Cu_2O-Ag nanoheterostructure". Nabil A. Saad, **Mudasir H. Dar**, E. Ramya, Sri Ram G. Naraharisetty, and D. Narayana Rao, Journal of Materials Science. https://doi.org/10.1007/s10853-018-2811-5.

Femtosecond laser induced periodic surface structures on metals and graphite: Fabrication of low reflective surface and SERS substrates

by Mudasir Hassan Dar

Submission date: 31-Jan-2019 03:49PM (UTC+0530)
Submission ID: 1071012231
File name: library_plagiarism.pdf (14.08M)
Word count: 17127
Character count: 90590

Femtosecond laser induced periodic surface structures on metals and graphite: Fabrication of low reflective surface and SERS substrates

ORIGINALITY REPORT

26%	1%	26%	1%
SIMILARITY INDEX	INTERNET SOURCES	PUBLICATIONS	STUDENT PAPERS

PRIMARY SOURCES

1	V. Saikiran, Mudasir H. Dar, D. Narayana Rao. "Femtosecond laser induced nanostructuring of graphite for the fabrication of quasi-periodic nanogratings and novel carbon nanostructures", Applied Surface Science, 2018 Publication	11%
2	Mudasir H. Dar, R. Kuladeep, V. Saikiran, Narayana Rao D.. "Femtosecond laser nanostructuring of titanium metal towards fabrication of low-reflective surfaces over broad wavelength range", Applied Surface Science, 2016 Publication	10%
3	Dar, Mudasir H., R. Kuladeep, V. Saikiran, and Narayana Rao D.. "Femtosecond laser nanostructuring of titanium metal towards fabrication of low-reflective surfaces over broad wavelength range", Applied Surface	1%

Science, 2016.
Publication

4	www.jlps.gr.jp Internet Source	1%
5	Iaroslav Gnilitskyi, Thibault J.-Y. Derrien, Yoann Levy, Nadezhda M. Bulgakova, Tomáš Mocek, Leonardo Orazi. "High-speed manufacturing of highly regular femtosecond laser-induced periodic surface structures: physical origin of regularity", Scientific Reports, 2017 Publication	1%
6	Rajamudili Kuladeep, Mudasir H. Dar, K. L. N. Deepak, D. Narayana Rao. "Ultrafast laser induced periodic sub-wavelength aluminum surface structures and nanoparticles in air and liquids", Journal of Applied Physics, 2014 Publication	<1%
7	Qiumei Bian, Shouyuan Chen, Byung-Tai Kim, Nicholas Leventis, Hongbing Lu, Zenghu Chang, Shuting Lei. "Micromachining of polyurea aerogel using femtosecond laser pulses", Journal of Non-Crystalline Solids, 2011 Publication	<1%
8	Stratakis, Emmanuel, Ekaterina Barmina, Panagiotis Loukakos, Georgy Shafeev, and Costas Fotakis. "Ultrafast Laser-Assisted	<1%

Surface Micro- and Nanostructuring", Ultrafast Laser Processing From Micro- to Nanoscale, 2013.
Publication

---

9 Martsinovsky, G. A., G. D. Shandybina, D. S. Smirnov, S. V. Zabotnov, L. A. Golovan, V. Yu. Timoshenko, and P. K. Kashkarov. "", Proceedings of SPIE, 2008. <1%
Publication

---

10 V. Saikiran, Mudasir H Dar, R. Kuladeep, Narayana Rao Desai. "Ultrafast Laser Induced Subwavelength Periodic Surface Structures on Semiconductors/Metals and Application to SERS Studies", MRS Advances, 2016 <1%
Publication

---

11 Submitted to University of Hyderabad, Hyderabad <1%
Student Paper

---

12 K. K. Anoop, Nancy Verma, Nithin Joy, S. S. Harilal, Reji Philip. "Enhancement of optical emission and ion currents in a laser produced silicon plasma by femtosecond laser-induced periodic surface structuring", Physics of Plasmas, 2018 <1%
Publication

---

13 Min Huang, Fuli Zhao, Ya Cheng, Ningsheng Xu, Zhizhan Xu. "Origin of Laser-Induced Near- <1%

Subwavelength Ripples: Interference between Surface Plasmons and Incident Laser", ACS Nano, 2009
Publication

---

14 Mincuzzi, G., L. Gemini, M. Faucon, and R. Kling. "Extending ultra-short pulse laser texturing over large area", Applied Surface Science, 2016. <1%
Publication

---

15 M. Sundar. "Laser removal of TiN from coated carbide substrate", The International Journal of Advanced Manufacturing Technology, 04/28/2009 <1%
Publication

---

16 Haidong He, Ningsong Qu, Yongbin Zeng. "Lotus-leaf-like microstructures on tungsten surface induced by one-step nanosecond laser irradiation", Surface and Coatings Technology, 2016 <1%
Publication

---

17 Rajamudili Kuladeep, Chakradhar Sahoo, Desai Narayana Rao. "Direct writing of continuous and discontinuous sub-wavelength periodic surface structures on single-crystalline silicon using femtosecond laser", Applied Physics Letters, 2014 <1%
Publication

18	Yunxia Ye, Miao Wu, Xudong Ren, Jianzhong Zhou, Lin Li. "Hole-like surface morphologies on the stainless steel surface through laser surface texturing underwater", Applied Surface Science, 2018 Publication	<1%
19	V. Oliveira, S.P. Sharma, M.F.S.F. de Moura, R.D.F. Moreira, R. Vilar. "Surface treatment of CFRP composites using femtosecond laser radiation", Optics and Lasers in Engineering, 2017 Publication	<1%
20	Gamaly, E.G.. "The physics of ultra-short laser interaction with solids at non-relativistic intensities", Physics Reports, 201111 Publication	<1%
21	Koji Sugioka, Ya Cheng. "Femtosecond Laser 3D Micromachining for Microfluidic and Optofluidic Applications", Springer Nature America, Inc, 2014 Publication	<1%
22	C. C. Chirilă. "Effect of dressing on high-order harmonic generation in vibrating H_{2} molecules", Physical Review A, 04/2008 Publication	<1%

Exclude quotes	On	Exclude matches	< 14 words
Exclude bibliography	On		

SCHOOL OF PHYSICS
UNIVERSITY OF HYDERABAD
HYDERABAD 500046, INDIA

Prof. D. Narayana Rao

Dr. V. S. Ashoka

Feb 04, 2019

To whom it may concern

This is to certify that the thesis titled "Femtosecond laser induced periodic surface structures on metals and graphite: Fabrication of low reflective surface and SERS substrates" submitted by Mr. Mudasir Hassan Dar (Reg No. 13PHPH16) is based on his research work done under our guidance. This thesis has been screened by Turnitin software at the library of University of Hyderabad. The software shows a similarity index of 26%. Out of this 22% is from the published papers of Mr. Mudasir Hassan Dar as either the lead author or co-author. A thorough look at the report shows that the major part of the remaining 4% might have come from other articles and use of some standard technical terms. Therefore, this thesis is free from plagiarism.

Yours sincerely

Prof. D. Narayana Rao Dr. V. S. Ashoka